CAPITAL UNIVERSITY OF SCIENCE AND TECHNOLOGY, ISLAMABAD

Investigation of Unsteady Williamson Hybrid Nanofluid Flow using the Cattaneo-Christov Heat Flux, Magnetic Field, Forchheimer Flow and Chemical Reaction

by

Madiha Tariq

A thesis submitted in partial fulfillment for the degree of Master of Philosophy

in the

Faculty of Computing
Department of Mathematics

2024

This thesis is dedicated to my cherished parents, whose boundless love, unwavering support and belief in my abilities have been the driving force behind my academic journey. Their sacrifices, encouragement, and constant presence have inspired me to persevere and reach for excellence. I am forever grateful for the values and guidance they have instilled in me, which have shaped my character and ambitions. This work is a testament to their selfless dedication and the profound impact they have had on my life. I am privileged to have such remarkable parents who have always stood by me with unwavering love and care.

CERTIFICATE OF APPROVAL

Investigation of Unsteady Williamson Hybrid Nanofluid Flow using the Cattaneo-Christov Heat Flux, Magnetic Field, Forchheimer Flow and Chemical Reaction.

by

Madiha Tariq

(MMT221016)

THESIS EXAMINING COMMITTEE

(a)	External Examiner	Dr. Yasir Mehmood	UOL, Sargodha
(b)	Internal Examiner	Dr. Muhammad Afzal	CUST, Islamabad
(c)	Supervisor	Dr. Muhammad Sagheer	CUST, Islamabad

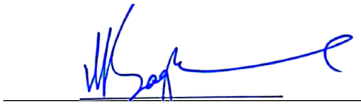

Dr. Muhammad Sagheer
Thesis Supervisor
September, 2024

Dr. Muhammad Sagheer
Head
Dept. of Mathematics
September, 2024

Dr. M. Abdul Qadir
Dean
Faculty of Computing
September, 2024

Author's Declaration

I, **Madiha Tariq** hereby state that my MPhil thesis titled "**Investigation of Unsteady Williamson Hybrid Nanofluid Flow using the Cattaneo-Christov Heat Flux, Magnetic Field, Forchheimer Flow and Chemical Reaction.**" is my own work and has not been submitted previously by me for taking any degree from Capital University of Science and Technology, Islamabad or anywhere else in the country/abroad.

At any time if my statement is found to be incorrect even after my graduation, the University has the right to withdraw my MPhil Degree.

(Madiha Tariq)

Registration No: MMT221016

Plagiarism Undertaking

I solemnly declare that research work presented in this thesis titled "**Investigation of Unsteady Williamson Hybrid Nanofluid Flow using the Cattaneo-Christov Heat Flux, Magnetic Field, Forchheimer Flow and Chemical Reaction**" is solely my research work with no significant contribution from any other person. Small contribution/help wherever taken has been dully acknowledged and that complete thesis has been written by me.

I understand the zero tolerance policy of the HEC and Capital University of Science and Technology towards plagiarism. Therefore, I as an author of the above titled thesis declare that no portion of my thesis has been plagiarized and any material used as reference is properly referred/cited.

I undertake that if I am found guilty of any formal plagiarism in the above titled thesis even after award of MPhil Degree, the University reserves the right to withdraw/revoke my MPhil degree and that HEC and the University have the right to publish my name on the HEC/University website on which names of students are placed who submitted plagiarized work.

(Madiha Tariq)

Registration No: MMT221016

Acknowledgement

I wish to convey my sincere gratitude and admiration to everyone who has helped me to successfully finish this thesis.Above all, I want to express my sincere gratitude to Dr. Muhammad Sagheer, my supervisor, for his constant leadership, inspiration, and assistance during this research project. The direction and caliber of this work have been greatly influenced by his knowledge and insightful observations.In addition, I am incredibly appreciative of my friend and sister's constant support, love, and faith in me. Their unwavering patience and support have been a source of courage during this academic journey's trying times. Their selflessness and supportive remarks have sustained my drive and concentration.

A particular thank you to my parents whose support and selflessness have been the cornerstone of my academic career. My accomplishments have been fueled by their persistent faith in me, and I will always be appreciative of their counsel and insight.In conclusion, without the combined efforts of everyone listed above, this thesis would not have been feasible.

(Madiha Tariq)

Registration No: MMT221016

Abstract

The purpose of this research is to examine in depth, the Unsteady Williamson hybrid nanofluid flow of $(GO - Cu/SA)$ along a stretching sheet. Cattaneo-Christov diffusion model has been incorporated . The resistance to the flow and measure of heat transfer rate have been analyzed subjected to some crucial effects like Forchheimer flow, magnetic field, thermal radiation, diffusion, and chemical reaction parameter. The nonlinear ordinary differential equations extracted from the partial differential equations governing the aforementioned flow, through the similarity transformations and are solved using the shooting approach in the computational framework of MATLAB. Notably, the study identifies the significant role of Cattaneo-Christov heat flux and magnetic field effects in enhancing heat transfer efficiency, thereby improving thermal diffusion within the system. Furthermore, the inclusion of diffusion and Forchheimer flow led to noticeably effect the velocity, temperature and concentration profiles and and their rates of change. The study also reveals initial uncertain behavior observed in nanoparticle concentration before reaching stable values for certain parameter combinations. This transient behavior is crucial to understand the dynamics of nanofluid flow and its practical implications in engineering applications. The drag force, heat and mass transfer rate are calculated numerically. Plots and tables are used to show the numerical results. From the conclusion of the current work, it is important to mention that the Forchheimer parameter and the schmidt number respectively animate to scale down the fluid velocity.

Contents

List of Figures

List of Tables

Abbreviations

BCs	Boundary conditions
HNF	Hybrid Nano Fluid
IVPs	Initial value problem
MHD	Magnetohydrodynamics
NF	Nano Fluid
ODEs	Ordinary differential equation
PDEs	Partial differential equation
RK-4	Range kutta order 4

Symbols

G_1	x-component of fluid velocity
G_2	y-component of fluid velocity
V_w	Porosity of the encompassing plate
N_w	Slip length
μ	Viscosity
ν	Kinematic viscosity
ρ	Density
K	Thermal conductivity
α	Thermal diffisuitivity
σ	Electrical conductivity
B_t	Magnetic field strength
T_w	Temperature of the wall
T_∞	Ambient temperature of the nanofluid
T	Temperature
C_w	Concentration of nanoparticles at the stretching surface
C_∞	Ambient concentration of the hybrid nanofluid
C	Concentration
ρ_f	Density of the fluid
μ_f	Viscosity of the fluid
ν_f	Kinematic viscosity of the base fluid
ρ_{nf}	Density of the nanofluid
μ_{nf}	Viscosity of the nanofluid
q_r	Radiative heat flux
σ^*	Stefan Boltzmann constant

k^*	Absorption coefficient
ψ	Stream function
χ	Similarity variable
C_f	Skin friction coefficient
Nu	Nusselt number
Nu_x	Local Nusselt number
Sh	Sherwood number
Sh_x	Local Sherwood number
Nn_x	Density of motile micro-organisms
Re	Reynolds number
Re_x	Local Reynolds number
ϕ	Nanoparticle volume fraction
λ	Williamson parameter
A	Unsteadiness parameter
K	Porous medium parameter
Λ	Velocity slip parameter
Nr	Thermal radiation parameter
M	Magnetic parameter
Ec	Eckert number
Pr	Prandtl number
S	Suction/injection parameter
Br	Brinkman number
Re	Reynold number
Fr	Forchheimer flow
β	Cattaneo Christov parameter
Bi	Biot number
Sc	Schmidt number
Kc	Chemical reaction parameter
Nt	Thermoporesis parameter
Nb	Brownian motion parameter
Ω	Microorganism Parameter
ρ_{hnf}	Density of the hybrid nanofluid

ρ_f	Density of the pure fluid
μ_{hnf}	Viscosity of the hybrid nanofluid
μ_f	Viscosity of the base fluid
$(\rho C_p)_{hnf}$	Heat capacitance of hybrid nanofluid
$(\rho C_p)_f$	Heat capacitance of base fluid
σ_{hnf}	Electrical conductivity of the hybrid nanofluid
σ_f	Electrical conductivity of the base fluid (Engine Oil)
K_{hnf}	Thermal conductivity of the hybrid nanofluid
K_f	Thermal conductivity of the base fluid
f	Dimensionless velocity
θ	Dimensionless temperature
ϕ	Dimensionless concentration

Subscripts

p	Nanoparticle
nf	Nanofluid
hnf	Hybrid nanofluid

Chapter 1

Introduction

1.1 Background

The phase of matter referred to as a fluid responds to external forces by deforming or flowing. There are three types of fluids, including liquids, gases, and plasma [1], characterized by a vanishing shear modulus, making them unable to withstand shear forces. As an essential component of daily life, fluids play vital role in natural processes. Fluid dynamics, a branch of fluid mechanics, analyzes fluid flow, its causes, and the impact of forces, offering insights into phenomena like stellar evolution, ocean currents, tectonic plate movement, and blood flow [2]. Fluid dynamics is used in everything from air conditioning systems and rocket engines to wind turbines and oil pipelines [3]. The study of fluid mechanics dates back to the early fifteenth century, encompassing Newtonian and non-Newtonian fluids, the latter displaying non-linear relationships between stress and strain. Archimedes' principle, addressing the motion of objects in fluids, remains foundational in fluid dynamics. The relationship between shear stress and the rate of deformation defines Newton's viscosity law. Fluids that deviate from this law are termed as non-Newtonian, such as ketchup, paint, blood etc. These non-Newtonian fluids find extensive applications across diverse fields like material processing, nuclear and chemical industries, bio-engineering, and geophysics. Their flow behavior is simulated mathematically, with implications for the petroleum extraction, oil recovery, filtration, polymer engineering, and ceramics industries. The significance of non-Newtonian fluids extends to

nuclear waste removal, solid matrix design, geothermal energy production, and petroleum reservoir management.

The Williamson fluid flow model is a non-Newtonian fluid model that was introduced by John A. Williamson in 1929 [4]. This model describes the behavior of certain viscoelastic fluids. It defines the stress tensor as a combination of the rate of strain tensor and the relaxation time tensor, making it suitable for studying viscoelastic fluids that exhibit both elastic and viscous behavior. Since its introduction, the Williamson fluid flow model has been extensively studied and applied in various fields of engineering and science. A number of researchers have also conducted comprehensive reviews on the Williamson fluid, including works by Shaheen et al. [5], Jangid et al. [6], and Taj and Salahuddin [7].

The main source of heat from the sun is solar energy, which drives photovoltaic cells, solar power plates, and other devices. Currently, Hussain et al. [8] are looking into how to use solar radiation and nanotechnology to improve avionics efficiency. Many factors, including solar heat radiation, a skewed magnetic field, and viscous dissipation, are taken into consideration in their research. Using the Keller box approach, the momentum and energy terms were numerically solved. Numerous control parameters are thoroughly examined, including temperature, shear stress, velocity, frictional element, and Nusselt number [8].

Heat transfer is used in many sectors. With a greater heat exponent than nanofluids, a novel class of nanofluids called hybrid nanofluid is being used to increase the heat transfer capacity of conventional fluids. Jamshed et al. [9] examine the features of thermal transport and steady hybrid nanofluid moving across a slippery surface. They are thoroughly examined, taking into account the effects of radiative flux, heat source, porosity material, viscous dissipative flow, and nanosolid particle morphologies. A domain of partial differential equations (PDEs) is created, and its dominating flow equations are derived. The Keller-box computational procedure finds the self-similar solution for formulas that are correctly transformed into ordinary-differential equations (ODEs). Han and Shihao [10] presented a study on the coupled flow and heat transfer of an upper-convected Maxwell fluid across a stretching plate with a velocity slip barrier. In contrast to the majority of classical research, the newly proposed Christov heat flow model is employed. The Homotopy analysis method yields analytical solutions (HAM). In their investigation, they also

contrast the Cattaneo-Christov heat flux model with Fourier's Law.

Using numerical simulations, Ali et al. [11] studied the rotational flow of two hybrid nanofluids over a horizontally elongated planar sheet: ($MOS_2 - Ag/C_2H_6O_2 - H_2O$ and $MOS_2 - Go/C_2H_6O_2 - H_2O$). To solve the resulting set of equations, they used the Fi-nite Element Method (PDEs). Ali and Mahesha [12] investigated the MHD flow and heat transmission from a horizontal stretched surface to a laminar liquid layer. The flow of a thin fluid film and the subsequent heat transfer from the stretching surface are studied using similarity transformation. They used a successful shooting technique to determine the numerical solution of the resulting non-linear differential equations.

Nanofluids' flow are a mixture of metal, polymeric or non-metallic nano-sized strengths with base fluid (water, oil, milke tc). To speed up the transfer of heat, they are used in a variety of applications. Bhatti and Rashidi [13] investigated the combined effects of thermal radiation and thermo-diffusion on Williamson nanofluid over a porous stretched sheet. The solute, concentration of nanoparticles, energy, and motion regulating equations have all been described using similarity transformation variables. The resulting coupled ordinary nonlinear differential equations are solved by the Chebyshev spectral collocation method (CSC) and the successive linearization method (SLM). As an example instance for our investigation, the skin friction coefficient and the local Nusselt number have also been numerically compared. All of the important parameters—the radiation parameter, the modified Dufour parameter, the Brownian motion parameter, the thermophoresis parameter, the nano-Lewis number, and the Williamson fluid parameter are physically discussed using graphs. In [13], numerical results for the Sherwood number and local Nusselt number are also presented using tables.

Hussain et al. [14] examined the effects of thermal radiation on electrically conducting, viscous, and incompressible magneto-nanofluids free convective flow in the presence of an inclined magnetic field. To determine the precise solution of the mathematical form in closed form, apply the Laplace transform technique. In their work [15], Reddy et al. examined how biological systems lose energy due to entropy formation. Entropy formation of gold-blood pseudoplastic nanofluid flow in a microchannel with electrokinetic force and electro-conductive heating is demonstrated numerically. The dimensional form of the momentum and temperature equations is converted into the dimensionless form by

assuming long wavelengths and low Reynolds numbers. The effect of thermal radiation on the viscous dissipative boundary layer flow o f a heat-absorbing m agneto-nanofluid across a permeable exponentially stretched sheet with Navier's velocity and thermal slips was investigated by Hussain et al. [16]. With the proper similarity variables, the dominating mathematical equations are converted into nonlinear ordinary differential equations. These equations are then numerically solved with the help of the shooting strategy and the fourth-order Runge-Kutta scheme. Mishra et al. [17] investigate the transient free convective boundary layer stream of an electrically leading, viscous, and incompressible magneto-nanofluid across an incautiously moving vertical sloping temperature plate.

The impact of heat radiation on the magnetohydrodynamic electrically conducting free convective flow of incompressible and viscous nanofluids across an exponentially accelerated moving ramping temperature plate was studied by Hussain et al. [18]. In order to account for an angled magnetic field, Sharma et al. [19] investigated the effects of Soret and Dufour on the typical convective and heat-retaining stream of a viscoelastic radiative nanofluid driven by a directly extended sheet. The differential equations are solved using the Galerkin finite element method (GFEM). The momentum and thermal slip conditions of a hydromagnetic dissipative and radiative graphene Maxwell nanofluid moving across a linearly stretched sheet were examined in the work by Hussain et al. [20].

The goal of Sharma et al.'s study [21] was to clarify the impact of various real boundaries on the evo-lution of the graphene Maxwell nanofluid along a linearly expanded sheet. The magnetic field, the heat absorption, the thermal radiation, the viscosity and Joule dissipations, momentum, and thermal slip conditions were some of these boundaries. By employing similarity vari-ables, mathematical problems are transformed into extremely nonlinear coupled ordinary differential equations (ODE), which are then numerically solved by the use of the shooting procedure.

Hussain et al. [22] investigate the impact of Navier's slip condition on the mixed convective flow of Casson-nanofluid across a vertically heated Riga plate. We looked at heat radiation, velocity slip, convective boundary conditions, and a changing magnetic field. Hamid et al. [23] investigated the effects of velocity slip, thermal radiation, and variable magnetic field convective boundary conditions. The characteristics of induced magnetic field and nonlinear radiation on forced convective Falkner-Skan flow of water nanofluid

and diamond-ethylene glycol (EG) and Single-Walled Carbon NanoHorn (SWCNH) over a wedge, plate, and stagnation point are investigated by Basha et al. [24]. Khan et al. [25] examined the assumption of constant viscosity under thermal investigation of non-Newtonian materials. Applications of activation energy and nonlinear thermal radiation are perceived as a novel influence. To ensure correct use of the shooting technique, a numerical presentation of the defined collection of linked and nonlinear flow problems is provided. Basha et al. studied blood flow inside the circulatory system in [26]. Due to the fact that many non-Newtonian fluid models, such as Powell-Eyring fluid, Herschel Buckley fluid, Williamson fluid, etc., incorporate characteristics of blood. Their work aims to characterize the effects of gyrotactic microorganisms and an induced magnetic field on the tangent hyperbolic nanofluid flow over a plate, including the wedge and stagnation of the plate. The fluid transport equations are transformed into ordinary differential equations using the relevant self-similarity variables, and these equations are then solved by the Runge-Kutta-Fehlberg (RKF) method. Moreover, [27]- [28] investigated a creative study that illustrates the hybrid nanofluids' heat transmission properties while accounting for various physical scenarios.

The amount of entropy that is often created during irreversible processes, such as diffusion, chemical reactions, and heat flowing through thermal resistance, is known as entropy generation. Das et al. cite das 2015 entropy numerically examine the shaky laminar mag-netohydrodynamics (MHD) boundary layer stream and warm exchange of nanofluids over an quickening convectively warmed extended sheet within the nearness of a transverse attractive field and warm source/sink. The Runge-Kutta-Fehlberg scheme is used in the firing approach to solve the unstable governing equations. Three types of water-based nanofluids are investigated: copper, aluminum oxide, and titanium dioxide.

In the context of existing research, there is a compelling need for a more profound investigation into the behavior of non-Newtonian Williamson nanofluids. While previous studies have delved into specific aspects of fluid dynamics, there exists a notable gap in the literature when it comes to a comprehensive framework that integrates various factors.

This research aims to fill these gaps by synthesizing diverse elements, ultimately creating a unified comprehension of fluid dynamics.

This research focuses on studying a new type of fluid called hybrid nanofluid, specifically $GO-Cu/SA$. To understand how it works, we use an advanced numerical technique, the shooting method. By doing this, we gain new insights into fluid dynamics and highlight the importance of using numerical methods in this field. The significance of this research lies in its potential to reveal fresh insights into the behavior of hybrid nanofluids, specifically regarding the effects under investigation.

The significance of this research lies in its potential to reveal fresh insights into the behavior of hybrid nanofluids, specifically regarding the effects under investigation. The non-Newtonian Williamson parameter (λ), the Forchheimer number (Fr), the magnetic field parameter (M), the velocity slip (Λ), the porous medium parameter (K), the time relaxation parameter (Ω), the Prandtl number (Pr), the Eckert number (Ec), the suction/injection parameter (S), the thermophoresis parameter (Nt), the Brownian motion parameter (Nb), the chemical reaction parameter (Kc), and the Schmidt number parameter (Sc are just a few of the parameters that are affected by these effects. The temperature ($\theta(\chi)$), velocity ($f'(\chi)$), and nanoparticle concentration profile ($\phi(\chi)$) are all influenced by these parameters. In essence, by addressing these research gaps and embarking on a multifaceted exploration, this study not only reshapes our understanding of fluid behavior but also paves the way for innovative applications in engineering and science.

1.2 Thesis Structure

Chapter 1 includes the survey of the relevant literature.

Chapter 2 serves as an introduction to the thesis and provides essential definitions and terminologies that are crucial for understanding the concepts discussed in subsequent chapters. This chapter aims to establish a foundational understanding of the key terms and concepts that will be used throughout the thesis.

We offer a thorough numerical investigation of the Williamson HNF $GO-Cu/SA$ flow over a stretched sheet in **Chapter 3**.

Along side other impacts such as the Cattaneo-Christov warm flux w ithin the vitality condition of the proposed demonstrate, the effects of the attractive field and Forchheimer stream on the force condition are considered within the Chapter 4 demonstrate pre-sented in Chapter 3. Furthermore, as we incorporate the hybrid nanofluid's concentration equation, taking diffusion effects and chemical reactions in to account, in the suggested model.

Chapter 5 presents the concluding remarks and highlights the significant findings obtained from the research conducted in this thesis.

The **Bibliography** section includes a comprehensive list of all the references and sources used in the thesis.

Chapter 2

Preliminaries

In this chapter, we will elucidate fundamental definitions, essential laws, terminologies, and key concepts necessary for the analysis of nonlinear partial differential equations. These foundational elements are crucial for comprehending the subsequent chapters of this thesis and will provide a solid framework for the development of a comprehensive understanding.

2.1 Foundational Concepts

2.1.1 Fluid

"A substance in the liquid or gas phase is referred to as a fluid. Distinction between a solid and a fluid is made on the basis of the substances ability to resist an applied shear (or tangential) stress that to change its shape. A solid can resist an applied shear stress by deforming, whereas a fluid deforms continuously under the influence of shear stress no matter how small. In solid stress is proportional to strain, but in fluids, stress is proportional to strain rate." [29]

2.1.2 Fluid Dynamics

"Fluid dynamics is the study of the motion of liquids, gases and plasma from one place to another." [30]

2.1.3 Fluid Mechanics

"Fluid mechanics is that branch of science which deals with the behavior of the fluid

(liquids or gases) at rest as well as in motion." [31]

2.1.4 Viscosity

" Viscosity is defined as the property of a fluid which offers resistance to the movement of one layers of fluid over another adjacent layer of the fluid. When two layers of a fluid, a distance 'dy' apart, move one over the other at different velocities, say u and $u + du$ as shown in the viscosity together with relative velocity causes a shear stress acting between the fluid layers."

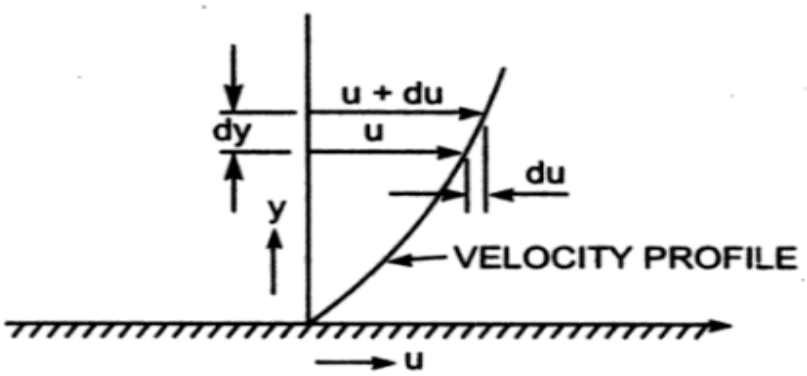

FIGURE 2.1: Velocity variation near a solid surface.

"The top layer causes a shear stress on the adjacent lower layer while the lower layer causes a shear stress on the adjacent top layer. This shear stress is proportional to the rate of change of velocity with respect to y. it is denoted by symbol τ called Tau. Mathematically,

$$\begin{aligned} \tau &\propto \frac{du}{dy} \\ \Rightarrow \quad \tau &= \mu \frac{du}{dy} \\ \Rightarrow \quad \mu &= \frac{\tau}{\frac{\partial u}{\partial y}} \end{aligned} \tag{2.1}$$

where μ is viscosity coefficient, τ is shear stress and $\frac{\partial u}{\partial y}$ represents the velocity gradient or rate of shear strain." [31]

2.1.5 Kinematic Viscosity

"Kinematic viscosity is defined as the ratio between the dynamic viscosity and density of fluid. It is denoted by the Greek symbol ν, thus mathematically,

$$\nu = \frac{\text{Viscosity}}{\text{Density}} = \frac{\mu}{\rho}$$

where the unit of kinematic viscosity is m^2/sec." [31]

2.1.6 Nanofluid

"Nanofluids are engineered by suspending nanoparticles with average size below 100 nm in traditional heat transfer fluids such as water, oil and ethylene glycol. A very small amount of guest nanoparticles, when dispersed uniformly and suspended stably in host fluids, can provide dramatic improvements in the thermal properties of host fluids." [32]

2.1.7 Hybrid Nanofluid

"Hybrid nanofluid is a very new type of nanofluids that contains two or more various nanoparticles. The use of hybrid nanofluids is aimed at simultaneously using the physical and chemical properoties of two or more different types of nanoparticles, for improving the base fluid properties." [33]

2.1.8 Magnetohydrodynamics

"Magnetohydrodynamics (MHD) is concerned with the flow of electrically conducting fluids in the presence of magnetic fields, either externally applied or generated within the fluid by inductive action." [34]

2.2 Classification of Fluid

There are following types of fluid:

2.2.1 Real Fl uid

"A fluid, which possesses viscosity, is known as a real fluid. All the fluids, in actual practice, are real fluids." [31]

2.2.2 Ideal Fluid

"A fluid which is incompressible and is having no viscosity, is known as an ideal fluid. Ideal fluid is only an imaginary fluid as all the fluids, which exist, have some viscosity." [31]

2.2.3 Ideal Plastic Fluid

"A fluid, in which shear stress is more than the yield value and shear stress is proportional to the rate of shear strain (or velocity gradient), is known as ideal plastic fluid." [31]

2.2.4 Newtonian Fluid

"A real fluid, in which shear stress is directly, proportional to the rate of shear strain (or

velocity gradient), is known as a Newtonian fluid." [31]

2.2.5 Non-Newtonian Fluid

"A real fluid, in which the shear stress is not proportional to the rate of shear strain (or velocity gradient), is known as a Non-Newtonian fluid." [31]

2.3 Kinds of Heat Transfer

2.3.1 Conduction

"The mechanism of heat transfer due to a temperature gradient in a stationary medium is called conduction. The medium may solid or a fluid. A very popular example of conduction heat transfer is that when one end of metallic spoon is dipped into a cup of hot tea, the other end becomes gradually hot. In solids, the conduction of heat is attributed to two effects:

(i) The flow o f free electrons and

(ii) The lattice vibrational waves caused by the vibrational motions of the molecules at relatively fixed p ositions called a lattice." [35]

2.3.2 Convectio

"The mode by which heat is transferred between a solid surface and the adjacent fluid in motion when there is a temperature difference between the two is known a s convection heat transfer. The temperature of the fluid stream refers either to its bulk or free stream temperature." [35]

2.3.3 Forced Convection

"In forced convection, the fluid is forced to flow over a solid surface by external means such as fan, pump or atmospheric wind." [35]

2.3.4 Free Convection

"When the fluid motion is caused by the buoyancy forces that are induced by density differences due to the variation in temperature or species concentration (in case of multicomponent systems) and in the fluid, and the convection is called natural (or free) convection." [35]

2.3.5 Thermal Radiatio

"Thermal radiation is defined as radiant (electromagnetic) energy emitted by a medium

and is solely to the temperature of the medium. Sometimes radiant energy is taken to be transported by electromagnetic wave while at other times it is supposed to be transported by particle like photons. " [36]

2.4 Conservation Laws

2.4.1 Law of Conservation of Mass

"The principle of conservation of mass can be stated as the time rate of change of mass in a fixed volume is equal to the net rate of ow of mass across the surface. The mathematical statement of the principle results in the following equation, known as the continuity (of mass) equation

$$\frac{\partial \rho}{\partial t} + \delta.\left(\rho V\right), \tag{2.2}$$

where ρ is the density (kg/m^3) of the medium, V the velocity vector (ms^{-1}), and δ is the nabla or del operator. The continuity equation in (2.2) is in conservation (or divergence) form since it can be derived directly from an integral statement of mass conservation. By introducing the material derivative or Eulerian derivative operator $\frac{D}{Dt}$

$$\frac{D}{Dt} = \frac{\partial}{\partial t} + V.\delta, \tag{2.3}$$

the continuity equation (2.2) can be expressed in the alternate, non-conservation form

$$\frac{\partial \rho}{\partial t} + V.\delta\rho + \rho\delta.V = \frac{D\rho}{Dt} + \rho\delta.V \tag{2.4}$$

For steady-state conditions the continuity equation becomes

$$\delta.\left(\rho V\right) = 0 \tag{2.5}$$

When the density changes following a fluid particle are negligible, the continuum is termed incompressible and we have $\frac{D\rho}{Dt}$.
The continuity equation (2.4) the becomes

$$\delta.V = 0, \tag{2.6}$$

which is often referred to as the incompressibility condition or incompressibility constraint" [36].

2.4.2 Momentum Equation

"The principle of conservation of linear momentum (or Newton's Second Law of motion) states that the time rate of change of linear momentum of a given set of particles is equal to the vector sum of all the external forces acting on the particles of the set, provided Newton's Third Law of action and reaction governs the internal forces. Newton's Second Law can be written as

$$\frac{\partial}{\partial t}(\rho V) + \delta.(\rho V \otimes V) = \delta.\sigma + \rho f, \tag{2.7}$$

where $\otimes$ is the tensor (or dyadic) product of two vectors, σ is the Cauchy stress tensor (N/m^2) and f is the body force vector, measured per unit mass and normally taken to be the gravity vector." [36].

2.4.3 Law of Conservation of Energy

"The law of conservation of energy (or the First Law of Thermodynamics) states that the time rate of change of the total energy is equal to the sum of the rate of work done by applied forces and the change of heat content per unit time.

In the general case, the First Law of Thermodynamics can be expressed in conservation form as

$$\frac{\partial \rho e^t}{\partial t} + \delta.\rho v e^t = -\delta.q + \delta.(\sigma.v) + Q + \rho f.v, \tag{2.8}$$

where $e^t = e + 1/2v.v$ is the total energy (J/m^3), e is the internal energy, q is he heat flux vector (W/m^2) and Q is the internal heat generation (W/m^3)" [36].

2.5 Types of Flow

In this section, different types of fluid flows have been described which are experienced in different scenarios while investigating the motion of a fluid.

2.5.1 Compressible Flow

"Compressible flow is that type of flow in which the density of the fluid changes from point to point or in other words the density (ρ) is not constant for the fluid. Mathematically,

$$\rho \neq k,$$

where k is constant." [30]

2.5.2 Incompressible Flow

"Incompressible flow is that type of flow in which the density is constant for the fluid flow. Liquids are generally incompressible while gases are compressible, Mathematically,

$$\rho = k,$$

where k is constant." [30]

2.5.3 Rotational Flow

"Rotational flow is that type of flow in which the fluid particles while flowing along stream-lines, also rotate about their own axis." [30]

2.5.4 Irrotational Flow

"Irrotational flow is that type of flow in which the fluid particles while flowing along stream-lines, do not rotate about their own axis." [30]

2.5.5 Laminar Flow

"Laminar flow is defined as that type of flow in which the fluid particles move along well-defined paths or stream lines and all the stream-lines are straight and parallel." [30]

2.5.6 Turbulent Flow

"Turbulent flow is that type of flow in which the fluid particles move in a zig-zag way." [30]

2.5.7 Steady Flow

"Steady flow is defined as that type of flow in which the fluid characteristics like velocity, pressure, density, etc., at a point do not change with time. Thus for steady flow, Mathematically, we have

$$\frac{\partial Q}{\partial t} = 0,$$

where Q is any fluid property." [30]

2.5.8 Unsteady Flow

"Unsteady flow is defined as that type of flow in which the fluid characteristics like velocity, pressure, density, etc., at a point do change with time. Thus for Unsteady flow, Mathematically, we have,

$$\frac{\partial Q}{\partial t} \neq 0,$$

where Q is any fluid property." [30]

2.5.9 Viscous Flow

"Flows in which the frictional effects are significant are called viscous flows." [37]

2.5.10 Internal Flow

"Flows completely bounded by a solid surfaces are called internal or duct flows." [37]

2.5.11 External Flow

"Flows over bodies immersed in an unbounded fluid are said to be an external flows." [37]

2.6 Dimensionless Numbers

2.6.1 Reynolds Number (Re)

"It is the most significant dimensionless number which is used to identify the different flow behaviors like laminar or turbulent flow. Mathematically, it is expressed as

$$Re = \frac{LU}{\nu}$$

where U denotes the free stream velocity, L is the characteristic length and ν stands for kinematic viscosity." [38]

2.6.2 Nusselt Number (Nu)

"It is the relationship between the convective to the conductive heat transfer through the boundary of the surface. Mathematically, it is defined as

$$Nu = \frac{hL}{k}$$

where h stands for convective heat transfer, L stands for characteristic length and k stands for thermal conductivity." [38]

2.6.3 Prandtl Number (Pr)

"The ratio of kinematic diffusivity to heat the diffusivity is said to be Prandtl number. It is denoted by Pr. Mathematically, it can be written as

$$Pr = \frac{\nu}{\alpha} = \frac{\mu c_p}{\rho k}$$

where μ and α denote the momentum diffusivity or kinetic diffusivity and thermal diffusivity respectively." [38]

2.6.4 Schmidt Number

"It is the ratio between kinematic viscosity ν_f and molecular diffusion D_B. It is denoted by Sc and mathematically we can write it as:

$$Sc = \frac{\nu_f}{D_B},$$

where ν_f is the kinematic viscosity and D_B is the mass diffusivity." [38]

2.6.5 Skin Friction Coefficient (Cf_x)

"The skin friction coefficient is typically defined as

$$Cf = \frac{\tau_w}{\rho U_w^2}$$

where τ_w is the local wall shear stress, ρ is the fluid density and U_w is the free stream velocity (usually taken outside the boundary layer or at the inlet)." [38]

2.6.6 Sherwood Number (Sh_x)

"It is a non-dimensional quantity which describes the ratio of the mass transport by convection to the transfer of mass by diffusion. Mathematically,

$$Sh = \frac{xq_m}{D_B},$$

here q_m is characteristics length, D_B is the mass diffusivity and x is the mass transfer coefficient." [38]

2.6.7 Thermophoresis Parameter

"In a temperature gradient, small particles are pushed towards the lower temperature because of the asymmetry of molecular impacts." [38]

2.6.8 Eckert Number

"It is a dimensionless number used in continuum mechanics. It describes the relation between flows and the boundary layer enthalpy difference and it is used for characterized heat dissipation. Mathematically,

$$Ec = \frac{U_w^2}{(c_p)_f \delta T}." [38]$$

2.6.9 Biot Number

"This number expresses the ratio of the heat flow transferred by convection on a body surface to the heat flow transferred by conduction in a body. Mathematically,

$$B_i = \alpha(2\pi f \lambda c Q)^{-1/2},$$

where α is the heat transfer coefficient, f is the frequency, c is the specific heat capacity, Q is the density and λ is thermal conductivity." [39]

2.7 Shooting Method

The shooting method, a numerical scheme for computing the solution of a boundary value problem, is illustrated in this section. To see how the shooting strategy works, consider the taking after boundary esteem issue:

$$\left.\begin{aligned} M''(x) &= M(x)M'(x) + 2M^2(x) \\ M(0) &= 0, \qquad M(H) = G. \end{aligned}\right\} \tag{2.9}$$

Introduce the following notations to reduce the order of the above boundary value problem.

$$\left.\begin{aligned} M &= Z_1 \\ M' &= Z_1' = Z_2, \\ M'' &= Z_2'. \end{aligned}\right\} \tag{2.10}$$

As a result, (2.9) is transformed into the following system of first order ODEs.

$$Z_1' = Z_2, \qquad Z_1(0) = 0, \tag{2.11}$$

$$Z_2' = Z_1 Z_2 + 2Z_1^2, \qquad Z_2(0) = S. \tag{2.12}$$

where s is the missing initial condition which will be guessed. The above IVP will be numerically solved by the RK-4 method. The missing condition S is to be chosen such

that:

$$Z_1(H, S) = G. \tag{2.13}$$

For convenience, now onward $Z_1(H, S)$ will be denoted by $Z_1(S)$.

Let us further denote $Z_1(S) - G$ by $\phi(S)$, so that

$$\phi(S) = 0. \tag{2.14}$$

The over condition can be illuminated by utilizing any fitting root-finding procedure, e.g., Newton's strategy which has the taking after iterative equation:

$$S_{n+1} = S_n - \frac{\phi(S_n)}{\left(\frac{\partial \phi(S)}{\partial S}\right)_{S=S_n}},$$

or

$$S_{n+1} = S_n - \frac{Z_1(S_n) - G}{\left(\frac{\partial Z_1(S)}{\partial S}\right)_{S=S_n}}. \tag{2.15}$$

To find $\frac{\partial Z_1(S)}{\partial S}$, we introduce the following new notations:

$$\frac{\partial Z_1}{\partial S} = Z_3, \quad \frac{\partial Z_2}{\partial S} = Z_4. \tag{2.16}$$

Newton's iterative scheme can be obtained with these notations, yielding the form:

$$S_{n+1} = S_n - \frac{Z_1(S_n) - G}{Z_3(S_n)}. \tag{2.17}$$

Now differentiating the ODEs (2.11) and (2.12) w.r.t s, we get another system of ODEs, as follows:

$$Z_3' = Z_4, \qquad Z_3(0) = 0, \tag{2.18}$$

$$Z_4' = Z_3 Z_2 + Z_1 Z_4 + 4 Z_1 Z_3, \qquad Z_4(0) = 1. \tag{2.19}$$

Finally, we have the following IVP:

$$\begin{aligned} Z_1' &= Z_2, & Z_1(0) &= 0, \\ Z_2' &= Z_1 Z_2 + 2Z_1^2, & Z_2(0) &= t, \\ Z_3' &= Z_4, & Z_3(0) &= 0, \\ Z_4' &= Z_3 Z_2 + Z_1 Z_4 + 4Z_1 Z_3, & Z_4(0) &= 1. \end{aligned}$$

We will use any appropriate numerical method (e.g., RK-4 method) to solve the above IVP. The stopping criteria is set as,

$$| Z_1(S) - G | < \epsilon,$$

where $\epsilon > 0$ is an sufficiently small positive number.

Chapter 3

Dynamics of Radiative Williamson Hybrid Nanofluid with Entropy Generation

3.1 Introduction

Entropy generation in the flow of a Williamson hybrid nanofluid over an expanding sheet is the main topic of this chapter [8]. Using the shooting strategy, numerical solutions to the energy and momentum equations have been obtained. The base fluid, sodium alginate (SA), is mixed with graphene oxide (GO) and copper (Cu) to create the hybrid nanofluid. Numerous control variables have been thoroughly studied, including temperature, shear stress, velocity, frictional element, and Nusselt number. The effect of dispersing nano-solid particles, namely copper and graphene oxide, in sodium alginate on the overall performance of the nanofluid has been examined. The findings of the study indicate that the incorporation of these particles, in conjunction with the assessment of several elements such as radiation, viscous dissipation, and thermal conduction, considerably improves the efficiency of airplane wings that are exposed to heat transmission and general entropy within the parameters established by Tiwari and Das. Based on a comparative investigation, the hybrid nanofluid performs better at transferring heat than regular nanofluids.

This result emphasizes the hybrid nanofluid's superior performance and possible uses in heat transfer scenarios, especially when it comes to applications involving airplane wings.

3.2 Physical Model

Assume an infinitely penetrable two-dimensional flow plate across which a laminar, unstable boundary layer flow of inviscid, optically thick hybrid nanofluid is present. For hybrid nanofluids, the non-Newtonian Williamson mathematical model is assumed. The y-axis is normal to the x-axis, which has a porous surface running down it, when using Cartesian coordinates. This work uses sodium alginate (SA) as the base fluid and hybrid nanoparticles made of copper (Cu) and graphene oxide (GO). ϕ_1 and ϕ_2 represent distinct volume fractions for Cu and SA, respectively. The hybrid nanofluid's nanoparticle volume concentration is described as $\phi_{hnf} = \phi_1 + \phi_2$. The tensor of stress in the Williamson type is specified as follows:

$$S^* = -pI + \tau_{ij}, \tag{3.1}$$

where

$$\tau_{ij} = \left[\mu_\infty + \frac{\mu_0 - \mu_\infty}{1 - \zeta\tilde{\gamma}}\right] A_\beta, \tag{3.2}$$

The added stress-tensor, limited viscosity when shear rate is zero, limited viscosity when shear rate is infinite, and the 1st Rivlin–Erickson tensor are represented, respectively, by the variables τ_{ij}, μ_0, μ_∞, $\zeta > 0$, and A_β. Additionally,

$$\tilde{\gamma} = \sqrt{\frac{1}{2}\pi}, \tag{3.3}$$

$$\pi = trace\left(A_\beta^2\right). \tag{3.4}$$

In this case, we assumed that $\tilde{\gamma} < 1$ and $\mu_\infty = 0$. As a result, formula (3.2) can be written as follows:

$$\tau_{ij} = \left[\frac{\mu_0}{1 - \zeta\tilde{\gamma}}\right] A_\beta, \tag{3.5}$$

which can further be described as follows by using the binomial-expansion:

$$\tau_{ij} = \left[\mu_0(1+\zeta\tilde{\gamma})\right]A_\beta. \tag{3.6}$$

The stretching speed and porous surface temperature are:

$$Uw(x,t) = \frac{bx}{1-\epsilon t}, \quad T_w(x,t) = T_\infty + \frac{b^* x}{1-\epsilon t}. \tag{3.7}$$

The original stretching rate and temperature variation are denoted by b and b^*, respectively. The surface and surrounding temperatures are denoted by the numbers T_w and T_∞, respectively. Additionally, the hybrid nanofluid is initially expressed at an interaction volume fraction ϕ_1, fixed at 0.09 during testing, by adding copper (Cu) solid nanoparticles to a SA-based liquid. The mixture was supplemented with graphene oxide (GO) nanomolecules to produce a hybrid nanofluid with a concentrated size of ϕ_2.

Mass Conservation Equation:

$$\frac{\partial G_1}{\partial x} + \frac{\partial G_2}{\partial y} = 0. \tag{3.8}$$

Momentum Equation:

$$\frac{\partial G_1}{\partial t} + G_1\frac{\partial G_1}{\partial x} + G_2\frac{\partial G_1}{\partial y} = \frac{\mu_{hnf}}{\rho_{hnf}}\frac{\partial^2 G_1}{\partial y^2} + \frac{\mu_{hnf}}{\rho_{hnf}}\sqrt{2}\zeta\left[\frac{\partial G_1}{\partial y}\frac{\partial^2 G_1}{\partial y^2}\right] - \frac{\mu_{hnf}}{\rho_{hnf}k}G_1. \tag{3.9}$$

Energy Equation:

$$\frac{\partial T}{\partial t} + G_1\frac{\partial T}{\partial x} + G_2\frac{\partial T}{\partial y} = \frac{\kappa_{hnf}}{(\rho C_p)_{hnf}}\frac{\partial^2 T}{\partial y^2} - \frac{1}{(\rho C_P)_{hnf}}\frac{\partial q_r}{\partial y} + \frac{\mu_{hnf}}{(\rho C_p)_{hnf}}\left(\frac{\partial G_1}{\partial y}\right)^2. \tag{3.10}$$

Boundary Conditions :

$$\left.\begin{aligned} &G_1(x,0) = U_w + N_w\left(1+\zeta\frac{\partial G_1}{\partial y}\right)\frac{\partial G_1}{\partial y},\ G_2(x,0) = V_w, \\ &-k_f\frac{\partial T}{\partial y} = h_f(T_w - T), \quad as \quad \mathrm{y} = 0, \\ &G_1 \to 0, \quad T \to T_\infty, \quad \text{as} \quad y \to \infty. \end{aligned}\right\} \tag{3.11}$$

Here G_1 and G_2 are horizontal and vertical velocities respectively. Vector form of fluid velocity is well-defined as

$$\vec{G} = \Big\{G_1(x,y,t), G_2(x,y,t), 0\Big\}.$$

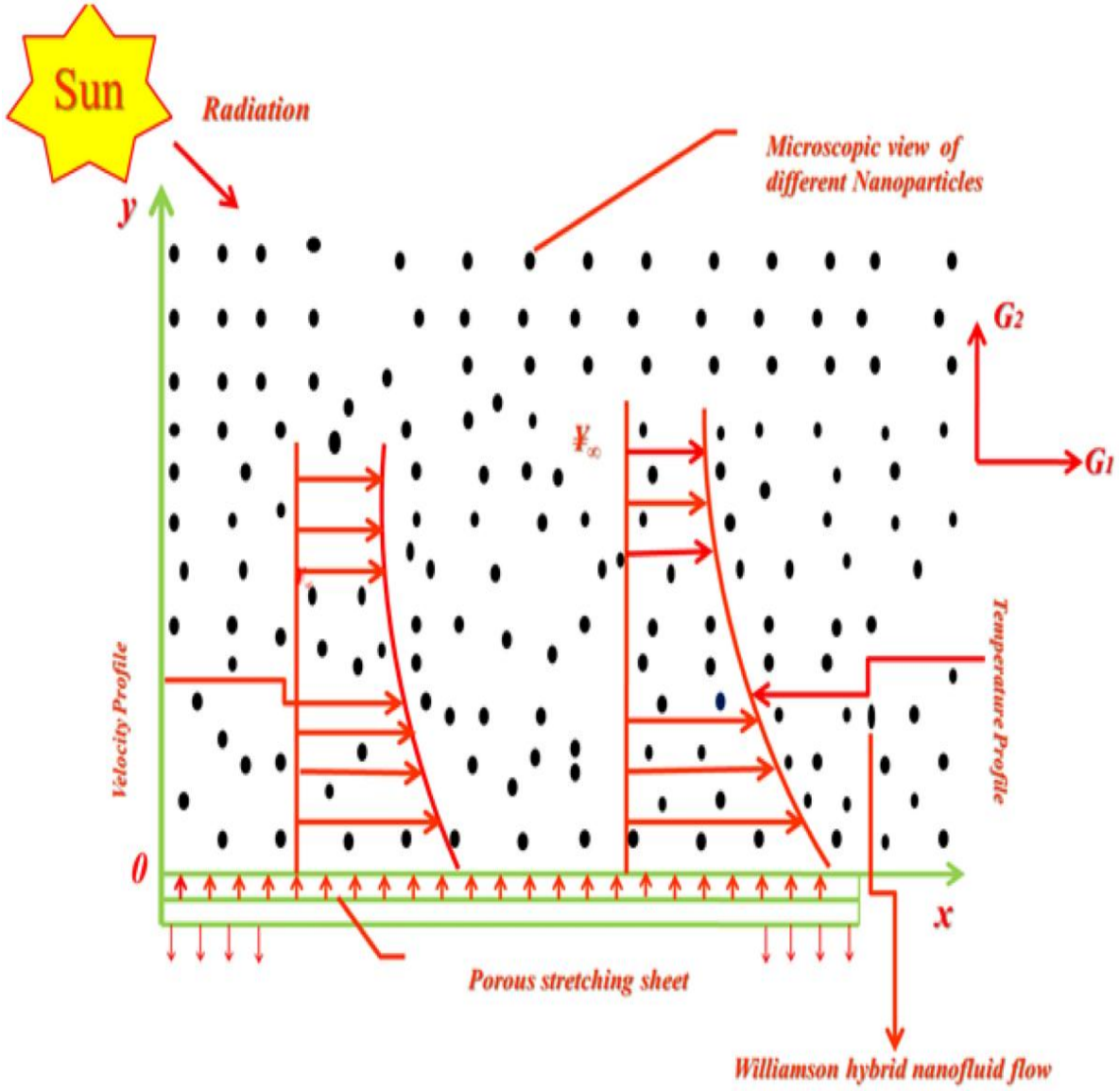

FIGURE 3.1: Flow Pattern Illustration.

3.3 Similarity Transformation and Non- Dimensionalization of Mathematical Model

The non-dimensionalization procedure for the mathematical model controlling the hybrid nanofluid's behavior is described in this section. In order to simplify the original equations, the process necessitates adding dimensionless variables and parameters. We

are able to better understand the physical phenomena and simplify the analysis by employing the dimensionless quantities. The mathematical model will be transformed into a system of ODEs using the following similarity transformation:

$$\psi(x,y)=\sqrt{\frac{\nu_f b}{1-\epsilon t}}xf(\chi),\qquad \chi(x,y)=\sqrt{\frac{b}{\nu_f(1-\epsilon t)}}y,\qquad \theta(\chi)=\frac{T-T_\infty}{T_w-T_\infty}. \tag{3.12}$$

The following derivative are required to satisfy the mass conservation equation (3.8).

$$G_1=\frac{\partial\psi}{\partial y}=\frac{\partial}{\partial y}\left(\frac{\sqrt{\nu_f b}}{\sqrt{1-\epsilon t}}xf(\chi)\right)=\frac{\sqrt{\nu_f b}}{\sqrt{1-\epsilon t}}\frac{\sqrt{b}}{\sqrt{(1-\epsilon t)\nu_f}}xf'(\chi)=\frac{b}{1-\epsilon t}xf'(\chi).$$

$$G_2=-\frac{\partial\psi}{\partial x}=-\frac{\partial}{\partial x}\left(\frac{\sqrt{\nu_f b}}{\sqrt{1-\epsilon t}}xf(\chi)\right)=-\sqrt{\frac{\nu_f b}{1-\epsilon t}}f(\chi).$$

$$\frac{\partial G_1}{\partial x}=\frac{\partial}{\partial x}\left(\frac{b}{1-\epsilon t}xf'(\chi)\right)=\frac{b}{1-\epsilon t}f'(\chi).$$

$$\frac{\partial G_2}{\partial y}=\frac{\partial}{\partial y}\left(-\sqrt{\frac{\nu_f b}{1-\epsilon t}}f(\chi)\right)=-\sqrt{\frac{\nu_f b}{1-\epsilon t}}f'(\chi)\frac{\partial\chi}{\partial y}=-\frac{b}{1-\epsilon t}f'(\chi).$$

Finally, by using the above derivatives in (3.8), we obtain

$$\frac{\partial G_1}{\partial x}+\frac{\partial G_2}{\partial y}=\frac{b}{1-\epsilon t}f'(\chi)-\frac{b}{1-\epsilon t}f'(\chi)=0. \tag{3.13}$$

Hence equation (3.8) is identically satisfied.

TABLE 3.1: Hybrid nanofluid's thermophysical characteristics

Properties	**Hybrid Nanofluid**
Viscosity (μ)	$\mu_{hnf}=\mu_f(1-\phi_1)^{-2.5}(1-\phi_2)^{-2.5}$
Density (ρ)	$\rho_{hnf}=(1-\phi_2)\big((1-\phi_1)\rho_f+\phi_1\rho_{p_1}\big)+\phi_2\rho_{p_2}$
Heat Capacity (ρC_p)	$(\rho C_p)_{hnf}=(1-\phi_2)\Big[(1-\phi_1)(\rho C_p)_f+\phi_1(\rho C_p)_{p_1}\Big]+\phi_2(\rho C_p)_{p_2}$
Thermal conductivity (K)	$\frac{K_{hnf}}{K_{nf}}=\frac{K_{p_2}+(m-1)K_{nf}-(m-1)\phi_2(K_{nf}-K_{p_2})}{K_{p_2}+(m-1)K_{nf}+\phi_2(k_{nf}-K_{p_2})}$, $\frac{K_{nf}}{K_f}=\frac{K_{p_1}+(m-1)K_f-(m-1)\phi_1(K_f-K_{p_1})}{K_{p_1}+(m-1)K_f+\phi_1(K_f-K_{p_1})}$

TABLE 3.2: Thermo-physical characteristics

Thermophysical	**Copper**	**Sodium alginate**	**Grapphene oxide**
ρ(kg/m^3)	8933	989	1800
C$_p$(J/kgK)	385.0	4175	717
k(W/m)	401.00	0.6376	5000

Some expressions involving the above thermo-physical properties, denoted by P_i ($i = a, b, c, d$), have been defined below. These notations will simplify the dimensionless model to be achieved in the upcoming sections.

$$\left.\begin{aligned} P_a &= (1-\phi_1)^{2.5}(1-\phi_2)^{2.5}, \\ P_b &= (1-\phi_2)\left((1-\phi_1)+\phi_1\frac{\rho_{p1}}{\rho_f}\right)+\phi_2\frac{\rho_{p2}}{\rho_f}, \\ P_c &= (1-\phi_2)\left((1-\phi_1)+\phi_1\frac{(\rho_{Cp})_{p1}}{(\rho_{Cp})_f}\right)+\phi_2\frac{(\rho_{Cp})_{p2}}{(\rho_{Cp})_f}, \\ P_d &= \frac{(\kappa_{p2}+2\kappa_{nf}-2\phi_2(\kappa_{nf}-\kappa_{p2}))\,(\kappa_{p1}+2\kappa_f-2\phi_1(\kappa_f-\kappa_{p1}))}{(\kappa_{p2}+2\kappa_{nf}+\phi_2(\kappa_{nf}-\kappa_{p2}))\,(\kappa_{p1}+2\kappa_f+\phi_1(\kappa_f-\kappa_{p1}))}. \end{aligned}\right\} \tag{3.14}$$

3.3.1 Non-Dimensionalization of Momentum Equation

The momentum equation (3.9) requires the derivatives of the following:

$$\frac{\partial\chi}{\partial t}=\frac{\partial}{\partial t}\left(\sqrt{\frac{b}{\nu_f(1-\epsilon t)}}y\right)=\frac{\sqrt{b}}{\sqrt{\nu_f}}y\frac{\partial}{\partial t}\left(\frac{1}{\sqrt{1-\epsilon t}}\right)=\frac{\sqrt{b}y\epsilon}{2\sqrt{\nu_f}(1-\epsilon t)^{\frac{3}{2}}}.$$

$$\frac{\partial\chi}{\partial y}=\frac{\partial}{\partial y}\left(\sqrt{\frac{b}{\nu_f(1-\epsilon t)}}y\right)=\sqrt{\frac{b}{\nu_f(1-\epsilon t)}}.$$

$$\begin{aligned}\frac{\partial G_1}{\partial t}&=\frac{\partial}{\partial t}\left(\frac{b}{1-\epsilon t}xf'(\chi)\right)=bxf'(\chi)\frac{\partial}{\partial t}\left(\frac{1}{1-\epsilon t}\right)+\frac{bx}{1-\epsilon t}f''(\chi)\frac{\partial\chi}{\partial t}\\&=\frac{\epsilon b}{(1-\epsilon t)^2}xf'(\chi)+\frac{\epsilon b^{\frac{3}{2}}}{2\sqrt{\nu_f}(1-\epsilon t)^{\frac{5}{2}}}xyf''(\chi).\end{aligned} \tag{3.15}$$

$$\frac{\partial G_1}{\partial y}=\frac{\partial}{\partial y}\left(\frac{b}{1-\epsilon t}xf'(\chi)\right)=\frac{b}{1-\epsilon t}xf''(\chi)\frac{\partial\chi}{\partial y}$$

$$= \frac{b^{\frac{3}{2}}}{\sqrt{\nu_f}(1-\epsilon t)^{\frac{3}{2}}} x f''(\chi). \tag{3.16}$$

$$\frac{\partial^2 G_1}{\partial y^2} = \frac{\partial}{\partial y}\left(\frac{b^{\frac{3}{2}}}{\sqrt{\nu_f}(1-\epsilon t)^{\frac{3}{2}}} x f''(\chi)\right) = \frac{b^{\frac{3}{2}}}{\nu_f(1-\epsilon t)^{\frac{3}{2}}} x f'''(\chi)\frac{\partial \chi}{\partial y}$$

$$= \frac{b^2}{\nu_f(1-\epsilon t)^2} x f'''(\chi). \tag{3.17}$$

Now, the dimensionless form of the momentum equation (3.9), becomes:

$$\frac{\epsilon b}{(1-\epsilon t)^2} x f'(\chi) + \frac{\epsilon b^{\frac{3}{2}}}{2\sqrt{\nu_f}(1-\epsilon t)^{\frac{5}{2}}} xy f''(\chi) + \left(\frac{bx}{1-\epsilon t} f'(\chi)\right)\left(\frac{b}{1-\epsilon t} f'(\chi)\right)$$

$$+\left(-\sqrt{\frac{\nu_f b}{1-\epsilon t}} f(\chi)\right)\frac{b^{\frac{3}{2}}}{\sqrt{\nu_f}(1-\epsilon t)^{\frac{3}{2}}} x f''(\chi) = \frac{\mu_{hnf}}{\rho_{hnf}} \frac{b^2}{\nu_f(1-\epsilon t)^2} x f'''(\chi)$$

$$+\frac{\mu_{hnf}}{\rho_{hnf}}\sqrt{2}\zeta \frac{b^{\frac{3}{2}}}{\sqrt{\nu_f}(1-\epsilon t)^{\frac{3}{2}}} x f''(\chi)\left(\frac{b^2}{\nu_f(1-\epsilon t)^2} x f'''(\chi)\right) - \frac{\mu_{hnf}}{\rho_{hnf} k}\frac{b}{1-\epsilon t} x f'(\chi).$$

$$\Rightarrow \quad \frac{b^2 x}{\nu_f(1-\epsilon t)^2}\frac{\mu_{hnf}}{\rho_{hnf}}\left[\frac{\epsilon}{b}\frac{\rho_{hnf}}{\mu_{hnf}}\nu_f f'(\chi) + \frac{\epsilon\sqrt{\nu}_f}{2\sqrt{b}\sqrt{1-\epsilon t}} y \frac{\rho_{hnf}}{\mu_{hnf}} f''(\chi) + \nu_f \frac{\rho_{hnf}}{\mu_{hnf}}(f'(\chi))^2\right.$$

$$\left. -\nu_f \frac{\rho_{hnf}}{\mu_{hnf}} f(\chi) f''(\chi)\right] = \frac{\mu_{hnf}}{\rho_{hnf}} \frac{b^2 x}{\nu_f(1-\epsilon t)^2}\left[f'''(\chi)\right.$$

$$\left. +\sqrt{2}\zeta \frac{b^{\frac{3}{2}}}{\sqrt{\nu}_f(1-\epsilon t)^{\frac{3}{2}}} x f''(\chi) f'''(\chi) - \nu_f \frac{1-\epsilon t}{bk} f'(\chi)\right].$$

$$\Rightarrow \quad \frac{\epsilon}{b}\frac{\rho_{hnf}}{\mu_{hnf}}\nu_f f'(\chi) + \frac{\epsilon\sqrt{\nu_f}}{2\sqrt{b(1-\epsilon t)}} y \frac{\rho_{hnf}}{\mu_{hnf}} f''(\chi) + \nu_f \frac{\rho_{hnf}}{\mu_{hnf}}(f'(\chi))^2 - \nu_f \frac{\rho_{hnf}}{\mu_{hnf}} f(\chi) f''(\chi)$$

$$= f'''(\chi) + \sqrt{2}\zeta \frac{b^{\frac{3}{2}}}{\sqrt{\nu_f}(1-\epsilon t)^{\frac{3}{2}}} x f''(\chi) f'''(\chi) - \nu_f \frac{1-\epsilon t}{bk} f'(\chi).$$

$$\Rightarrow \quad \nu_f \frac{\rho_{hnf}}{\mu_{hnf}}\left[\frac{\epsilon}{b} f'(\chi) + \frac{\epsilon}{2\sqrt{b\nu_f(1-\epsilon t)}} y f''(\chi) + (f'(\chi))^2 - f(\chi) f''(\chi)\right]$$

$$= f'''(\chi) + \frac{\sqrt{2} b^{\frac{3}{2}} \zeta x}{\sqrt{\nu}_f(1-\epsilon t)^{\frac{3}{2}}} f''(\chi) f'''(\chi) - K f'(\chi).$$

$$\Rightarrow \quad f'''(\chi)\big(1+\lambda f''(\chi)\big) = -P_a P_b\left[f(\chi) f''(\chi) - (f'(\chi))^2 - A\left(f'(\chi) + \frac{\chi}{2} f''(\chi)\right)\right]$$

$$+K f'(\chi). \tag{3.18}$$

3.3.2 Non-Dimensionalization of Energy Equation

This section covers the non-dimensionalization of our hybrid nanofluid model's energy equation, (3.10).

$$\theta(\chi) = \frac{T - T_\infty}{T_w - T_\infty}.$$

$$\Rightarrow \quad T = (T_w - T_\infty)\theta(\chi) + T_\infty$$

$$= \left(T_\infty + \frac{b^* x}{1 - \epsilon t} - T_\infty\right)\theta(\chi) + T_\infty$$

$$= \left(\frac{b^* x}{1 - \epsilon t}\right)\theta(\chi) + T_\infty.$$

$$\Rightarrow \quad \frac{\partial T}{\partial t} = \frac{\partial}{\partial t}\left(\frac{b^* x}{1 - \epsilon t}\theta(\chi) + T_\infty\right)$$

$$= \frac{b^* x}{1 - \epsilon t}\theta'(\chi)\frac{\partial \chi}{\partial t} + \theta(\chi)\frac{\partial}{\partial t}\left(\frac{b^* x}{1 - \epsilon t}\right)$$

$$= b^* x\left[\frac{\sqrt{b}\epsilon}{2\sqrt{\nu_f}(1-\epsilon)^{\frac{5}{2}}} y\theta'(\chi) + \frac{\epsilon}{(1-\epsilon t)^2}\theta(\chi)\right],$$

$$\Rightarrow \quad \frac{\partial T}{\partial x} = \frac{\partial}{\partial x}\left(\frac{b^* x}{1 - \epsilon t}\right)\theta(\chi) = \left(\frac{b^*}{1 - \epsilon t}\right)\theta(\chi),$$

$$\frac{\partial T}{\partial y} = \frac{b^* x}{1 - \epsilon t}\theta'(\chi)\frac{\partial \chi}{\partial y} = \frac{b^{\frac{1}{2}} b^* x}{\sqrt{\nu_f}(1 - \epsilon t)^{\frac{3}{2}}}\theta'(\chi).$$

$$\Rightarrow \quad \frac{\partial^2 T}{\partial y^2} = \frac{b^{\frac{1}{2}} b^* x}{\sqrt{\nu_f}(1 - \epsilon t)^{\frac{3}{2}}}\theta''(\chi)\frac{\partial \chi}{\partial y} = \frac{b b^* x}{\nu_f (1 - \epsilon t)^2}\theta''(\chi).$$

The radiation heat flux q_r can be expressed as:

$$q_r = -\frac{4}{3}\frac{\sigma *}{k*}\frac{\partial T^4}{\partial y}. \tag{3.19}$$

The Stefan-Boltzman constant is denoted by σ^*, and the absorption coefficient is represented by k^*. The Taylor series expansion can be taken in account to express T^4 about T_∞ as follows:

$$T^4 = T_\infty^4 + 4T_\infty^3(T - T_\infty) + 6T_\infty^2(T - T_\infty)^2 + ...$$

By neglecting the higher terms, we get

$$T^4 \ = T_\infty^4 + 4T_\infty^3(T - T_\infty) \Rightarrow \quad T^4 \ = 4T_\infty^3 T - 3T_\infty^4 \Rightarrow \quad \frac{\partial T^4}{\partial y} = \ 4T_\infty^3 \frac{\partial T}{\partial y}.$$

Equation (3.19) becomes:

$$q_r \quad = -\frac{4}{3}\frac{\sigma *}{k*}(4T_\infty^3)\frac{\partial T}{\partial y}.$$

$$\Rightarrow \qquad \frac{\partial q_r}{\partial y} = -\frac{16}{3}\frac{\sigma *}{k*}T_\infty^3 \frac{\partial^2 T}{\partial y^2}$$

$$= -\frac{16\sigma^*}{3k^*}\frac{bb^* x T_\infty^3}{\nu_f(1-\epsilon t)^2}\theta''(\chi). \tag{3.20}$$

The energy equation's dimensionless form that results is as follows:

$$b^* x\frac{\epsilon}{(1-\epsilon t)^2}\theta(\chi) + \frac{1}{2}b^*\epsilon\frac{\sqrt{b}}{\sqrt{\nu_f}(1-\epsilon t)^{\frac{5}{2}}}xy\theta'(\chi) + \frac{b^* x b}{(1-\epsilon t)^2}f'(\chi)\theta(\chi)$$

$$-\frac{\sqrt{\nu_f b}}{\sqrt{1-\epsilon t}}\frac{b^*\sqrt{b}}{\sqrt{\nu_f(1-\epsilon t)}}\frac{x}{1-\epsilon t}f(\chi)\theta'(\chi) = \frac{\kappa_{hnf}}{(\rho C_p)_{hnf}}\frac{b^* b x}{\nu_f(1-\epsilon t)^2}\theta''(\chi)$$

$$+\frac{1}{(\rho C_p)_{hnf}}\frac{b^* b x}{\nu_f(1-\epsilon t)^2}\left(\frac{16\sigma^*}{3k^*}T_\infty^3\theta''(\chi)\right) + \frac{\mu_{hnf}}{(\rho C_p)_{hnf}}\frac{b^3 x^2}{(1-\epsilon t)^3\nu_f}(f''(\chi))^2.$$

$$\Rightarrow \qquad b^* x\frac{b}{(1-\epsilon t)^2}\left[\frac{\epsilon}{b}\theta(\chi) + \frac{\epsilon\sqrt{b}}{2b\sqrt{\nu_f(1-\epsilon t)}}y\theta'(\chi) + f'(\chi)\theta(\chi)\right] - \frac{bb^* x}{(1-\epsilon t)^2}f(\chi)\theta'(\chi)$$

$$= \frac{\kappa_{hnf}}{(\rho C_p)_{hnf}}\frac{b^* b x}{\nu_f(1-\epsilon t)^2}\left[\theta''(\chi) + \frac{1}{\kappa_{hnf}}\left(\frac{16\sigma^*}{3k^*}T_\infty^3\theta''(\chi)\right)\right.$$

$$\left.+\frac{\mu_{hnf}}{\kappa_{hnf}}\frac{b^2 x}{b^*(1-\epsilon t)}(f''(\chi))^2\right].$$

$$\Rightarrow \qquad b^* x\frac{b}{(1-\epsilon t)^2}\left[\frac{\epsilon}{b}\left(\theta(\chi) + \frac{\chi}{2}\theta'(\chi)\right) + f'(\chi)\theta(\chi) - f(\chi)\theta'(\chi)\right]$$

$$= \frac{\kappa_{hnf}}{(\rho C_p)_{hnf}}\frac{\kappa_f(\rho C_p)_f}{\kappa_f(\rho C_p)_f}\frac{b^* b x}{\nu_f(1-\epsilon t)^2}\left[\theta''(\chi) + \frac{1}{\kappa_{hnf}}\frac{16\sigma^*}{3k^*}T_\infty^3\theta''(\chi)\right.$$

$$\left.+\frac{\mu_{hnf}}{\kappa_{hnf}}\frac{\nu_f\kappa_f(\rho C_p)_f}{\nu_f\kappa_f(\rho C_p)_f}\frac{b^2 x}{b^*(1-\epsilon t)}(f''(\chi))^2\right].$$

$$\Rightarrow \qquad \frac{\epsilon}{b}\left(\theta(\chi) + \frac{\chi}{2}\theta'(\chi)\right) + f'(\chi)\theta(\chi) - f(\chi)\theta'(\chi)$$

$$= \frac{P_d}{P_c P_r}\left[\left(1 + \frac{P_r N_r}{P_d}\right)\theta''(\chi) + \frac{P_r}{P_a P_d}\frac{1-\epsilon t}{b^* x(C_p)_f}(Uw)^2(f''(\chi))^2\right]. \qquad \text{(Table 3.1)}$$

$$\Rightarrow \quad \frac{P_cP_r}{P_d}\left[A\left(\theta(\chi)+\frac{\chi}{2}\theta'(\chi)\right)+f'(\chi)\theta(\chi)-f(\chi)\theta'(\chi)\right]=\left(1+\frac{P_rN_r}{P_d}\right)\theta''(\chi)$$
$$+\frac{P_r}{P_aP_d}\frac{(Uw)^2}{(T_w-T_\infty)(C_P)_f}(f''(\chi))^2.$$

$$\Rightarrow \quad \frac{P_cP_r}{P_d}\left[A\left(\theta(\chi)+\frac{\chi}{2}\theta'(\chi)\right)+f'(\chi)\theta(\chi)-f\theta'(\chi)\right]=\left(1+\frac{P_rN_r}{P_d}\right)\theta''(\chi)$$
$$+\frac{E_cP_r}{P_aP_d}(f''(\chi))^2.$$

$$\Rightarrow \quad \left(1+\frac{P_rN_r}{P_d}\right)\theta''(\chi)+\frac{E_cP_r}{P_aP_d}(f''(\chi))^2-\frac{P_cP_r}{P_d}\left[A\left(\theta(\chi)+\frac{\chi}{2}\theta'(\chi)\right)+f'(\chi)\theta(\chi)\right.$$
$$\left.-f(\chi)\theta'(\chi)\right]=0.$$

$$\Rightarrow \quad \left(1+\frac{P_rN_r}{P_d}\right)\theta''(\chi)+\frac{P_cP_r}{P_d}\left[\frac{E_c}{P_aP_c}(f''(\chi))^2-A\left(\theta(\chi)+\frac{\chi}{2}\theta'(\chi)\right)-f'(\chi)\theta(\chi)\right.$$
$$\left.+f(\chi)\theta'(\chi)\right]=0.$$

$$\Rightarrow \quad \left(1+\frac{P_rN_r}{P_d}\right)\theta''(\chi)=-\frac{P_cP_r}{P_d}\left[\frac{E_c}{P_aP_c}(f''(\chi))^2-A\left(\theta(\chi)+\frac{\chi}{2}\theta'(\chi)\right)-f'(\chi)\theta(\chi)\right.$$
$$\left.+f(\chi)\theta'(\chi)\right]=0.$$

$$\Rightarrow \quad \theta''(\chi)=-\frac{P_cP_r}{P_d\left(1+\frac{P_rN_r}{P_d}\right)}\left[\frac{E_c}{P_aP_c}(f''(\chi))^2-A\left(\theta(\chi)+\frac{\chi}{2}\theta'(\chi)\right)-f'(\chi)\theta(\chi)\right.$$
$$\left.+f(\chi)\theta'(\chi)\right]=0.$$

$$\Rightarrow \quad \theta''(\chi)=-\frac{P_cP_r}{P_d+P_rN_r}\left[\frac{E_c}{P_aP_c}(f''(\chi))^2-A\left(\theta(\chi)+\frac{\chi}{2}\theta'(\chi)\right)-f'(\chi)\theta(\chi)\right.$$
$$\left.+f(\chi)\theta'(\chi)\right] \tag{3.21}$$

3.3.3 Non-Dimensionalization of Boundary Conditions

The following process converts the appropriate BCs into a non-dimensional form.

- $G_2(x,0)=V_w, \qquad at \quad y=0.$

$$\Rightarrow \quad V_w = -\sqrt{\frac{b\nu_f}{1-\epsilon t}} f(0),$$

$$\Rightarrow \quad f(0) = -V_w \sqrt{\frac{1-\epsilon t}{b\nu_f}},$$

$$\Rightarrow \quad f(0) = S.$$

- $G_1(x,0) = U_w + N_w\left(1 + \frac{\zeta}{\sqrt{2}}\frac{\partial G_1}{\partial y}\right)\frac{\partial G_1}{\partial y}, \qquad at \quad y = 0.$

$$\Rightarrow \qquad \frac{bx}{1-\epsilon t} f'(0) = \frac{bx}{1-\epsilon t} + N_w\left(1 + \frac{\zeta}{\sqrt{2}}\frac{b^{\frac{3}{2}}}{\sqrt{\nu}_f(1-\epsilon t)^{\frac{3}{2}}} x f''(0)\right)\frac{b^{\frac{3}{2}}}{\sqrt{\nu}_f(1-\epsilon t)^{\frac{3}{2}}} x f''(0).$$

$$\Rightarrow \quad \frac{bx}{1-\epsilon t} f'(0)$$

$$= \frac{bx}{1-\epsilon t} + \Lambda\sqrt{\frac{\nu_f(1-\epsilon t)}{b}}\left(1 + \frac{\zeta}{\sqrt{2}}\frac{b^{\frac{3}{2}}}{\sqrt{\nu}_f(1-\epsilon t)^{\frac{3}{2}}} x f''(0)\right)\frac{b^{\frac{3}{2}}}{\sqrt{\nu}_f(1-\epsilon t)^{\frac{3}{2}}} x f''(0).$$

$$\Rightarrow \qquad \frac{bx}{1-\epsilon t} f'(0) = \frac{bx}{1-\epsilon t} + \Lambda\frac{bx}{1-\epsilon t}\left(1 + \frac{\zeta}{\sqrt{2}}\frac{b^{\frac{3}{2}}}{\sqrt{\nu}_f(1-\epsilon t)^{\frac{3}{2}}} x f''(0)\right) f''(0).$$

$$\Rightarrow \qquad \frac{bx}{1-\epsilon t} f'(0) = \frac{bx}{1-\epsilon t}\left(1 + \Lambda\left(1 + \frac{\zeta}{\sqrt{2}}\frac{b^{\frac{3}{2}}}{\sqrt{\nu}_f(1-\epsilon t)^{\frac{3}{2}}} x f''(0)\right)\right) f''(0).$$

$$\Rightarrow \qquad f'(0) = 1 + \Lambda\left(f''(0) + \frac{\zeta}{\sqrt{2}}\frac{\sqrt{2}}{\sqrt{\nu}_f(1-\epsilon t)^{\frac{1}{2}}}\frac{\sqrt{b}}{1-\epsilon t} bx (f''(0))^2\right).$$

$$\Rightarrow \qquad f'(0) = 1 + \Lambda\left(f''(0) + \frac{\zeta}{2}\frac{\sqrt{2b}}{\sqrt{\nu}_f(1-\epsilon t)^{\frac{1}{2}}} U_w (f''(0))^2\right).$$

$$\Rightarrow \qquad f'(0) = 1 + \Lambda\left(f''(0) + \frac{\lambda}{2}(f''(0))^2\right).$$

$$\Rightarrow \qquad f'(0) = 1 + \Lambda\left(f''(0) + \frac{\lambda}{2}(f''(0))^2\right).$$

- $\frac{\partial T}{\partial y} = -\frac{h_f}{k_0}(T_w - T), \qquad at \quad y = 0.$

$$\Rightarrow \qquad \sqrt{\frac{b}{\nu_f(1-\epsilon t)}}\frac{b^* x}{1-\epsilon t}\theta'(0) = -\frac{h_f}{k_f}\left(\frac{b^* x}{1-\epsilon t} + T_\infty - \theta(0)\frac{b^* x}{1-\epsilon t} - T_\infty\right).$$

$$\Rightarrow \qquad \sqrt{\frac{b}{\nu_f(1-\epsilon t)}}\frac{b^* x}{1-\epsilon t}\theta'(0) = -\frac{h_f}{k_f}\left(\frac{b^* x}{1-\epsilon t} - \theta(0)\frac{b^* x}{1-\epsilon t}\right).$$

$$\Rightarrow \qquad \sqrt{\frac{b}{\nu_f(1-\epsilon t)}}\frac{b^*x}{1-\epsilon t}\theta'(0) = -\frac{h_f}{k_f}\frac{b^*x}{1-\epsilon t}(1-\theta(0)).$$

$$\Rightarrow \qquad \theta'(0)(T_w - T_\infty) = -\frac{h_f}{k_f}\sqrt{\frac{\nu_f(1-\epsilon t)}{b}}(T_w - T_\infty)(1-\theta(0)).$$

$$\Rightarrow \qquad \theta'(0) = -Bi(1-\theta(0)).$$

- $G_1 \longrightarrow 0, \qquad as \quad y \longrightarrow \infty.$

$\Rightarrow \quad f'(\chi) \longrightarrow 0, \qquad as \quad \chi \longrightarrow \infty.$

- $T \to T_\infty, \qquad as \quad y \longrightarrow \infty.$

$\Rightarrow \quad \theta(\chi) \to 0, \qquad as \quad \chi \longrightarrow \infty.$

Finally,

$$\left.\begin{aligned} &f(0) = S, \quad f'(0) = 1 + \Lambda\left(f''(0) + \frac{\lambda}{2}(f''(0))^2\right), \\ &\theta'(0) = -Bi(1-\theta(0)), \\ &f' \to 0, \quad \theta' \to 0, \qquad as \quad \chi \to \infty. \end{aligned}\right\} \tag{3.22}$$

The dimensionless parameters used in equation (3.28), are:

$$A = \frac{\epsilon}{b},\ \alpha_f = \frac{K_f}{(\rho C_P)_f},\ P_r = \frac{\nu_f}{\alpha_f}, E_c = \frac{(Uw)^2}{(C_P)_f(T_w - T_\infty)},\ N_r = \frac{16\sigma^*}{3K^*}\frac{T_\infty^3}{\nu_f(\rho C_P)_f}.$$

3.3.4 Non-Dimensionalization of Physical Quantities

This section focuses on the dimensionless physical quantities; the skin friction and the Nusselt number.

Skin Friction Cofficient:

$$C_f = \frac{\tau_w}{\rho_f(Uw)^2},$$

where

$$\tau_w = \mu_{hnf}\left(\frac{\partial G_1}{\partial y} + \frac{\zeta}{2}\left(\frac{\partial G_1}{\partial y}\right)^2\right)\Bigg|_{y=0}.$$

As a result, we get

$$C_f = \frac{\mu_f}{\rho_f Pa(Uw)^2}\left(\frac{\partial}{\partial y}\frac{b}{1-\epsilon t}xf'(\chi) + \frac{\zeta}{\sqrt{2}}\left(\frac{\partial}{\partial y}\frac{b}{1-\epsilon t}x(f'(\chi))^2\right)\right)\Bigg|_{\chi=0}$$

$$= \frac{\nu_f}{Pa(Uw)^2}\left(\frac{b^{\frac{3}{2}}}{\sqrt{\nu}_f(1-\epsilon t)^{\frac{3}{2}}}xf''(\chi) + \frac{\zeta}{\sqrt{2}}\frac{b^3}{\nu_f(1-\epsilon t)^3}x^2(f''(\chi))^2\right)\Bigg|_{\chi=0}$$

$$= \frac{1}{Pa}\left(\frac{\nu_f}{(Uw)^2}\frac{b^{\frac{3}{2}}}{\sqrt{\nu}_f(1-\epsilon t)^{\frac{3}{2}}}xf''(0) + \frac{\nu_f}{(Uw)^2}\frac{\zeta}{\sqrt{2}}\frac{b^3}{\nu_f(1-\epsilon t)^3}x^2(f''(0))^2\right)$$

$$= \frac{1}{Pa}\left(\frac{\nu_f}{(Uw)^2}\frac{b^{\frac{3}{2}}\sqrt{x}}{\sqrt{x}\sqrt{\nu}_f(1-\epsilon t)^{\frac{3}{2}}}xf''(0) + \frac{\nu_f}{(Uw)^2}\frac{\zeta}{\sqrt{2}}\frac{(Uw)^3}{x}(f''(0))^2\right)$$

$$= \frac{1}{Pa}\left(\frac{\sqrt{\nu}_f}{(Uw)^2}\frac{b^{\frac{3}{2}}x^{\frac{3}{2}}}{\sqrt{x}(1-\epsilon t)^{\frac{3}{2}}}f''(0) + \frac{\nu_f}{(Uw)^2}\frac{\zeta}{\sqrt{2}}\frac{(Uw)^3}{x}(f''(0))^2\right)$$

$$= \frac{1}{Pa}\left(\frac{\sqrt{\nu_f}(Uw)^{\frac{3}{2}}}{\sqrt{x}(Uw)^2}f''(0) + \frac{\zeta}{\sqrt{2}}\frac{\sqrt{2}}{\sqrt{2}}\frac{Uw}{x}(f''(0))^2\right)$$

$$= \frac{1}{Pa}\left(\frac{\sqrt{\nu_f}}{\sqrt{Uw}}\frac{1}{\sqrt{x}}f''(0) + \frac{\zeta}{2}\frac{\sqrt{2b}}{\sqrt{\nu_f(1-\epsilon t)}}\frac{\sqrt{\nu_f(1-\epsilon t)}}{\sqrt{b}}\frac{\sqrt{x}}{\sqrt{x}}\frac{Uw}{x}(f''(0))^2\right)$$

$$= \frac{1}{Pa}\left(\frac{\sqrt{\nu_f}}{\sqrt{Uw}}\frac{1}{\sqrt{x}}f''(0) + \frac{\zeta}{2}\frac{\sqrt{2b}}{\sqrt{\nu_f(1-\epsilon t)}}\frac{\sqrt{x}\sqrt{\nu_f}}{\sqrt{Uwx}}Uw(f''(0))^2\right)$$

$$= \frac{1}{Pa}\left(\frac{1}{\sqrt{Re_x}}f''(0) + \frac{\lambda\sqrt{\nu_f}}{2\sqrt{x}\sqrt{Uw}}(f''(0))^2\right)$$

$$= \frac{1}{Pa}\left(\frac{1}{\sqrt{Re_x}}f''(0) + \frac{\lambda}{2\sqrt{Re_x}}(f''(0))^2\right)$$

$$\Rightarrow \quad Re_x^{\frac{1}{2}}C_f = \frac{1}{Pa}f''(0)(1+\frac{\lambda}{2}f''(0)). \tag{3.23}$$

Here $Re_x = \frac{U_w x}{\nu_f}$ denotes the local Reynolds number.

Nusselt Number:

$$Nu_x = \frac{xq_w}{\kappa_f(T_w - T_\infty)}, \quad \text{‘} \tag{3.24}$$

where

$$q_w = -\kappa_{hnf}\left(1 + \frac{16\sigma^* T_\infty^3}{3k^*\nu_f(\rho Cp)_f}\frac{\partial T}{\partial y}\right)\Bigg|_{y=0}. \tag{3.25}$$

Hence,

$$Nu_x = -\frac{x\kappa_{hnf}}{\kappa_f(T_w - T_\infty)}\left(1+\frac{16\sigma^* T_\infty^3}{3k^*\nu_f(\rho Cp)_f}\frac{\partial T}{\partial y}\right)\Big|_{y=0}$$

$$= -\frac{x\kappa_{hnf}}{\kappa_f(\frac{b^* x}{1-\epsilon t})}(1+N_r)\left(\frac{b^*\sqrt{b}x}{\sqrt{\nu_f}(1-\epsilon t)^{\frac{3}{2}}}\right)\theta'(0)$$

$$= -\frac{x\sqrt{x}\kappa_{hnf}}{\sqrt{x}\kappa_f}(1+Nr)\frac{\sqrt{b}}{\sqrt{\nu_f(1-\epsilon t)}}\theta'(0)$$

$$= -\frac{\sqrt{x}\kappa_{hnf}}{\kappa_f}(1+Nr)\frac{\sqrt{bx}}{\sqrt{\nu_f(1-\epsilon t)}}\theta'(0)$$

$$= -\frac{\sqrt{xUw}\kappa_{hnf}}{\sqrt{\nu_f}\kappa_f}(1+Nr)\theta'(0)$$

$$= -\frac{\sqrt{Re_x}\kappa_{hnf}(1+Nr)}{\kappa_f}\theta'(0).$$

$$\Rightarrow \quad Re_x^{-\frac{1}{2}} Nu_x = -\frac{\kappa_{hnf}(1+Nr)}{\kappa_f}\theta'(0). \tag{3.26}$$

Here $Re_x = \frac{U_w x}{\nu_f}$ is the Reynolds number.

Sherwood Number:

$$Sh_x = -\frac{xq_m}{D_B(C_w - C_\infty)},$$

where

$$q_m = -D_B\left(\frac{\partial C}{\partial y}\right)_{y=0}.$$

Therefore,

$$Sh_x = -\frac{xD_B(C_w - C_\infty)\sqrt{\frac{b}{\nu_f(1-\epsilon t)}}\phi'(0)}{D_B(C_w - C_\infty)}$$

$$= -\sqrt{\frac{b}{\nu_f(1-\epsilon t)}}x\phi'(0)$$

$$\Rightarrow \qquad Re_x^{-\frac{1}{2}} Sh_x = -\phi'(0).$$

Entropy Generation:

The entropy generation rate N_G is defined as:

$$N_G = \frac{(T_\infty)^2 b^2 E_G}{\kappa_f (T_w - T_\infty)^2}, \tag{3.27}$$

where

$$E_G = \frac{\kappa_{hnf}}{T_\infty^2}\left(\frac{\partial T}{\partial y}\right)^2 + \frac{16\sigma^* T_\infty^3}{3k^*\nu_f(\rho Cp)_f}\left(\frac{\partial T}{\partial y}\right)^2 + \frac{\mu_{hnf}}{T_\infty}\left(\frac{\partial G_1}{\partial y}\right)^2 + \frac{\mu_{hnf}}{KT_\infty}(G_1)^2. \tag{3.28}$$

Hence

$$N_G = \frac{T_\infty^2 b^2}{k_f \frac{(b^*x)^2}{(1-\epsilon t)^2}}\left(\frac{\kappa_{hnf}}{(T_\infty)^2}\left[\left(\frac{\partial T}{\partial y}\right)^2 + Nr\left(\frac{\partial T}{\partial y}\right)^2\right] + \frac{\mu_{hnf}}{T_\infty}\left(\left(\frac{\partial G_1}{\partial y}\right)^2 + \frac{1}{K}(G_1)^2\right)\right)$$

$$= \frac{(1-\epsilon t)^2 b^2}{(b^*x)^2}\left(\frac{\kappa_{hnf}}{k_f}\left[\left(\frac{\partial T}{\partial y}\right)^2 + Nr\left(\frac{\partial T}{\partial y}\right)^2\right] + \frac{\mu_{hnf}T_\infty}{k_f}\left(\left(\frac{\partial G_1}{\partial y}\right)^2 + \frac{1}{K}(G_1)^2\right)\right)$$

$$= P_d(1+Nr)\left(\frac{\sqrt{b}b^*x}{\sqrt{\nu_f}(1-\epsilon t)^{\frac{3}{2}}}\theta'(\chi)\right)^2 \frac{(1-\epsilon t)^2 b^2}{(b^*x)^2}$$

$$+\frac{\mu_f T_\infty}{k_f Pa}\left(\left(\frac{b^{\frac{3}{2}}}{\sqrt{\nu_f}(1-\epsilon t)^{\frac{3}{2}}}xf''(\chi)\right)^2 + \frac{1}{k}\left(\frac{bx}{1-\epsilon t}f'(\chi)\right)^2\right)\frac{(1-\epsilon t)^2 b^2}{(b^*x)^2}$$

$$= P_d(1+Nr)\frac{b^3}{\nu_f(1-\epsilon t)}(\theta'(\chi))^2 + \frac{\mu_f T_\infty}{k_f Pa}\left(\frac{b^3}{\nu_f(1-\epsilon t)^3}x^2(f''(\chi))^2 + \frac{1}{k}\left(\frac{b^2x^2}{(1-\epsilon t)^2}(f'(\chi))^2\right)\frac{(1-\epsilon t)^2 b^2}{(b^*x)^2}\right.$$

$$= \frac{P_d(1+Nr)b^3 x}{\nu_f(1-\epsilon t)x}(\theta'(\chi))^2 + \frac{\mu_f T_\infty}{k_f Pa}\left((f''(\chi))^2 + \frac{\nu_f(1-\epsilon t)}{bk}(f'(\chi))^2\right)\frac{(1-\epsilon t)^2 b^2}{(b^*x)^2}\frac{b^3}{\nu_f(1-\epsilon t)^3}x^2$$

$$= \frac{P_d(1+Nr)b^2 Uw}{\nu_f x}(\theta'(\chi))^2 + \frac{\mu_f T_\infty}{k_f Pa}\left((f''(\chi))^2 + K(f'(\chi))^2\right)\frac{b^5}{(b^*)^2\nu_f(1-\epsilon t)}$$

$$= \frac{P_d(1+Nr)b^2 Uw}{\nu_f x}(\theta'(\chi))^2 + \frac{\mu_f T_\infty}{k_f Pa}\frac{b^5x^3(1-\epsilon t)^2}{(b^*)^2x^3(1-\epsilon t)^2\nu_f(1-\epsilon t)}\left((f''(\chi))^2\right.$$

$$+K(f'(\chi))^2\Bigg).$$

$$= \frac{P_d(1+Nr)b^2Uw}{\nu_f x}(\theta'(\chi))^2 + \frac{\mu_f T_\infty}{k_f Pa}\frac{b^2}{x\nu_f}\frac{b^3x^3}{(1-\epsilon t)^3}\frac{(1-\epsilon t)^2}{(b^*)^2x^2}\Bigg((f'')^2 + K(f'(\chi))^2\Bigg)$$

$$= \frac{P_d(1+Nr)b^2Uw}{\nu_f x}(\theta'(\chi))^2 + \frac{\mu_f T_\infty}{k_f Pa}\frac{b^2(Uw)^3}{x\nu_f(T_w-T_\infty)^2}\Bigg((f''(\chi))^2 + K(f')^2\Bigg)$$

$$= \Bigg(P_d(1+Nr)(\theta'(\chi))^2 + \frac{1}{P_a}\frac{T_\infty}{T_w-T_\infty}\frac{\mu_f(Uw)^2}{\kappa_f(T_w-T_\infty)}(f''(\chi))^2\Bigg)\frac{Uwb^2}{\nu_f x}$$

$$N_G = Re\Bigg(P_d(1+Nr)(\theta'(\chi))^2 + \frac{1}{P_a}\frac{Br}{\Omega}(f''(\chi))^2\Bigg). \tag{3.29}$$

Here $Re = \frac{U_w x}{\nu_f}, Br = \frac{\mu_f U_w^2}{\kappa f(T_w - T_\infty)}, and \Omega = \frac{T_\infty}{(T_w - T_\infty)}$ denote the Reynolds number, Brinkmann number, and dimensionless temperature gradient, respectively.

3.4 Solution Framework

The numerical solutions are found by the shooting method. It applies Newton's method to refine the missing conditions and uses the fourth-order Runge-Kutta methodology to compute the solution of the initial value problem. The dimensionless momentum equation (3.18), which needs to be solved, can first be approached using the following notations:

$$f = F_1, \qquad f' = F_1' = F_2, \qquad f'' = F_1'' = F_2' = F_3.$$

Next, the momentum equation is converted into the system of first ODEs that follows:

$$F_1' = F_2, \qquad F_1(0) = S.$$

$$F_2' = F_3, \qquad F_2(0) = 1 + \Lambda\Bigg[F_2(0) + \frac{\lambda}{2}(F_2(0))^2\Bigg].$$

$$F_3' = -\frac{1}{1+\lambda F_3}\Bigg[P_a P_b\Bigg(F_1F_3 - (F_2)^2 - A\Bigg(\frac{\chi}{2}F_3 + F_2\Bigg)\Bigg) - KF_2\Bigg], \qquad F_3(0) = p. \tag{3.30}$$

The Runge-Kutta method of order four will be used to numerically solve the aforementioned IVP.If $\chi = \chi_\infty$, then the domain of the problem is bounded, i.e., [0, χ_∞], where χ_∞ is a positive real number, and the variation in the solution is negligible. It is necessary

to select the missing condition p so that:

$$F_2(\chi_\infty, p) = 0.$$

Newton's method will be used to update the missing p, using the following iterative scheme:

$$p_{n+1} = p_n - \frac{F_2(\chi_\infty, p_n)}{\left(\frac{\partial}{\partial p} F_2(\chi_\infty, p)\right)_{p=p_n}}. \tag{3.31}$$

We further introduce the following notations:

$$\frac{\partial F_1}{\partial p} = F_4, \qquad \frac{\partial F_2}{\partial p} = F_5, \qquad \frac{\partial F_3}{\partial p} = F_6.$$

Hence the iterative scheme (3.30) will get the form:

$$p_{n+1} = p_n - \frac{F_2(\chi_\infty, p_n)}{F_5(\chi_\infty, p_n)}.$$

To make another system of Odes, presently differentiate the ultimate framework of the primary arrange Odes with respect to p. This is often how it appears to be:

$$F_4' = F_5, \qquad F_4(0) = 0.$$

$$F_5' = F_6, \qquad F_5(0) = \Lambda(1+\lambda F_5(0)).$$

$$F_6' = -\frac{1}{(1+\lambda F_3)^2}\left[(1+\lambda F_3)\left(P_a P_b\left(F_4F_3 + F_1F_6 - 2F_2F_5 - A\left(\frac{\chi}{2}F_6 + F_5\right)\right) - KF_5\right)\right.$$
$$\left.-(\lambda F_6)\left(P_a P_b\left(F_1F_3 - F_2^2 - A\left(\frac{\chi}{2}F_3 + F_2\right)\right) + KF_2\right)\right], \qquad F_6(0) = 1.$$

The stoping criteria for Newton's technique is set as:

$$|F_2(\chi_\infty, p)| < \epsilon,$$

where a positive number, $\epsilon > 0$, can be arbitrarily small. Henceforth, ϵ is interpreted as 10^{-10}. Assuming f is a known function, we will use the shooting technique to approximate

the ordinary differential equation (3.21). For this, we employ the following ideas:

$$\theta = T_1, \qquad \theta' = T_1' = T_2.$$

The energy equation is then transformed into the following system of first-order ODEs:

$$T_1' = T_2, \qquad T_1(0) = q.$$

$$T_2' = - \quad \frac{PrP_c}{P_d + PrNr}\left[\frac{E_c}{P_aP_c}(F_3)^2 - A\left(T_1 + \frac{\chi}{2}T_2\right) + F_2T_1 - F_1T_2\right],$$

$$T_2(0) = -B_i(1 - T_1(0)).$$

We will numerically solve the above initial value problem (IVP) using the Runge-Kutta method of order 4. The missing condition q must be chosen in order for:

$$T_1(\chi_\infty, q) = 0.$$

Newton's method can be used to solve the above equation using the iterative formula below.

$$q_{n+1} = q_n - \frac{T_1(\chi_\infty, q_n)}{\left(\frac{\partial}{\partial q}T_1(\chi_\infty, q)\right)_{q=q_n}}. \tag{3.32}$$

We also present the subsequent notations:

$$\frac{\partial T_1}{\partial d} = T_3, \qquad \frac{\partial T_2}{\partial d} = T_4.$$

The iterative scheme (3.31) proposed by Newton looks like this:

$$q_{n+1} = q_n - \frac{T_1(\chi_\infty, q_n)}{T_3(\chi_\infty, q_n)}.$$

The final system of two first-order ODEs can now be differentiated with respect to d to obtain the following additional system of ODEs:

$$T_3' = T_4, \qquad T_3(0) = 1.$$

$$T_4' = -\frac{P_cP_r}{P_d + P_rN_r}\left[G_1T_4 - G_2T_3 - A\left(T_3 + \frac{\chi}{2}T_4\right)\right], \qquad T_4(0) = -B_i.$$

The stopping criterion for Newton's method is set as:

$$|T_1(\chi_\infty, q)| < \epsilon,$$

where a positive number, $\epsilon > 0$, can be arbitrarily small. Henceforth, ϵ is interpreted as 10^{-10}.

3.5 Result Interpretation

The purpose of this section is to assess the physical properties of energy and velocity profiles in relation to changes in a number of important physical parameters, including the porous medium parameter (K), thermal radiation parameter (Nr), Eckert number (Ec), Biot number (Bi), suction parameter (S), Williamson parameter (λ), and velocity slip (Λ). The assessment is carried out using graphical depictions of temperature and velocity profiles. In addition, the effects of these parameters on physical characteristics like skin friction and Nusselt number are estimated and analyzed by varying the values of dimensionless parameters.

The graphical representations of velocity and temperature profiles provide visual insights into the behavior of the system as the physical parameters vary. By observing the trends in these profiles, a better understanding of the system's physical characteristics can be obtained. The graphical representations allow for the analysis of how changes in K, Nr, λ, Ec, Re, Bi, Λ, and S affect the velocity and energy profiles.

3.5.1 Analysis of Computational Results

Tables 3.3 and 3.4 display the skin friction coefficient and local Nusselt number values for the $GO - Cu/SA$ hybrid nanofluid, accounting for different inputs of N_r, λ, Ec, Bi, Λ, and S. The results show that higher absolute values of local skin friction coefficients, which indicate a decrease in fluid velocity, are produced by increases in λ and Λ. The absolute values of the local skin friction coefficient rise in response to increases in K and S, which suggests a drop in fluid velocity.

Additionally, Table 3.4's results show that the Nusselt number rises with increasing Nr and Bi values, indicating improved heat transfer. Furthermore, it is observed that there is a reciprocal decrease between the Nusselt number and the Eckert number (Ec).

An abrupt rise in the thermal profile and entropy rate in relation to the induced temperature in the flow domain using the radiation process, denoted by the factor of thermal radiation N_r, are depicted in Figures 3.2 and 3.3, respectively. Additionally, radiation has a negligible impact on entropy generation, which could be attributed to a significant impact on flow limitations (refer to Figure 3.3).

The Cu–SA nanofluid is more promis-ing than the GO–Cu/SA hybrid one in this aspect. The variations in heat and entropy generation associated with the Eckert numbers (Ec) for GO–Cu/SA and Cu–SA fluids are depicted in Figures 3.4 and 3.5, respectively.

As we can see in Figures 3.4 and 3.5 that when both the nanofluid and the hybrid nanofluid encounter an increasing behavior in the Eckert number (Ec), they exhibit a rise in temperature and entropy generation. Pysically, the fluid's energy conversion can be used to understand how the Eckert number affects the temperature distribution.

The temperature of the nanofluids as a function of Biot number is shown in Figure 3.6. The temperature profile's relationship with Biot Number Bi is depicted in the graph. The fluid's ratio of internal conduction to surface convection displayed by the Biot number. When the sheet convection parameter rises, the convection coefficient at the fluid's surface is dominated by heat transfer by conduction. The rise in Bi indicates that the stretching surface is heated by the hot fluid inside the boundary layer, raising the thermal system's temperature.

The effect of Reynolds number Re on entropy formation is seen in Figure 3.7. It is evident that as Re values increase, entropy creation increases as well. The ratio of viscous to inertial forces is known as the Reynolds number. Therefore, a higher Reynolds number indicates that inertial forces predominate and that entropy is generated more strongly. The suction parameter (S) velocity profile is displayed in Figure 3.8. The velocity profile's relationship with the suction parameter is depicted in the graph. The velocity profile decreases with increasing S.

Figures 3.9, 3.10, and 3.11, respectively, show the effects of λ on the temperature profile, velocity profile, and entropy generation. The temperature and velocity profiles decrease as λ increases, as shown in Figures 3.9 and 3.10. In terms of mechanics, a higher value of λ leads to a more robust buoyancy force, which ultimately produces a higher quantity of moving energy. This energy creates the confrontation through the flow. Figure 3.11 illustrates how the entropy production grows with λ. The effects of velocity slip on the temperature profile, velocity profile, and entropy production were shown in Figures 3.12, 3.13, and 3.14, respectively.

Figure 3.12 shows a decrease in the nanofluid velocity at the barrier as velocity slip increases. The stretching force of the surface is partially transferred to the fluid by an increase in lubrication and slipperiness at the surface, which slows down the flow and makes the velocity decrease obvious. As Λ increases, the thickness of the momentum barrier layer decreases. The temperature distribution in the boundary layer as a function of Λ is shown in Figure 3.13. It has been shown that the temperature of the nanofluid decreases with increasing velocity slip. Figure 3.14 displays a rising trend in the entropy generation. The value of Λ rises, and so does the entropy generation N_G.

For the positive variation in the porosity parameter K, the velocity profile e x hibits a falling trend (see Figure 3.15). The impacts of the nanoparticle volume fraction parameter ϕ are depicted in Figures 3.16, 3.17, and 3.18, respectively. An analysis considering several values of the volume fraction parameter ϕ_1 is carried out with ϕ_2 set at 0.09 in Figures 3.16, 3.17, and 3.19. It is found that the temperature rises and the velocity of the nanofluid decreases with an increase in parameter ϕ.

These values are in agreement with the observed physical behavior, which indicates that a denser nanoparticle volume fraction causes the momentum boundary layer to narrow and the heat transfer rate to decrease. The temperature inside the boundary layer and the overall thermal conductiv-ity of nanofluids rise with the volume of nanoparticles, and solid particles have a higher thermal conductivity than the base fluid.

Moreover, the collision of nanoparticles releases heat energy and raises the temperature of the system. It is clear that the temperature of the hybrid nanofluid rises faster than that of the other nanofluids.

The volume fraction parameter increases, the entropy increases as well, as Figure 3.18 illus-trates.

TABLE 3.3: The results of the skin friction coefficients $C_f\sqrt{Re_x}$ for values of λ, K, Λ and S parameters when $Pr = 6.5$, $Ec = 0.1$, $Nr = 0.2$ and $Bi = 0.2$.

λ	S	K	ϕ_1	ϕ_2	Λ	$C_f\sqrt{Re_x}$ (HNF)	$C_f\sqrt{Re_x}$ (NF)
0.1	0.1	0.1	0.09	0.09	0.3	-1.3322	-1.1354
0.2						-1.3178	-1.1225
0.3						-1.3018	-1.1080
	0.2					-1.3178	-1.1787
	0.3					-1.4253	-1.2233
		0.3				-1.4050	-1.1850
		0.4				-1.4387	-1.2082
			0.03			-1.0869	-0.9157
			0.06			-1.2066	-1.0233
				0.06		-1.2611	-1.2611
				0.03		-1.1957	-1.1957
					0.2	-1.4842	-1.2755
					0.3	-1.3322	-1.1354

TABLE 3.4: The results of the local Nusselt number $\frac{Nu_x}{\sqrt{Re_x}}$ for values of Nr, Ec and Bi parameters when $\lambda = 0.1$,$K = 0.1$, $\Lambda = 0.3$ and $S = 0.1$.

Nr	Ec	Bi	$\frac{Nu_x}{\sqrt{Re_x}}$ (HNF)	$\frac{Nu_x}{\sqrt{Re_x}}$ (NF)
0.2	0.1	0.2	0.3401	0.0.2668
0.1			0.3159	0.2480
0.3			0.3640	0.2853
0.5			0.4107	0.3215
	0.3		0.3062	0.2438
	0.5		0.2723	0.2208
	0.7		0.2338	0.1944
		0.1	0.1803	0.1407
		0.3	0.4827	0.3804

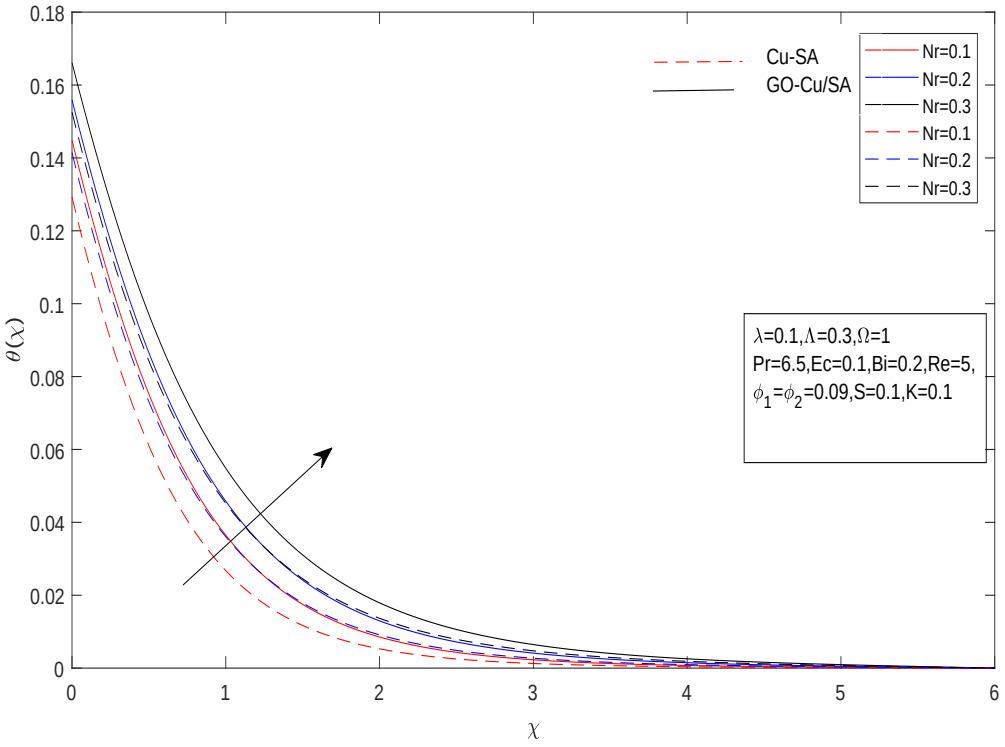

FIGURE 3.2: Impact of Nr on $\theta(\chi)$

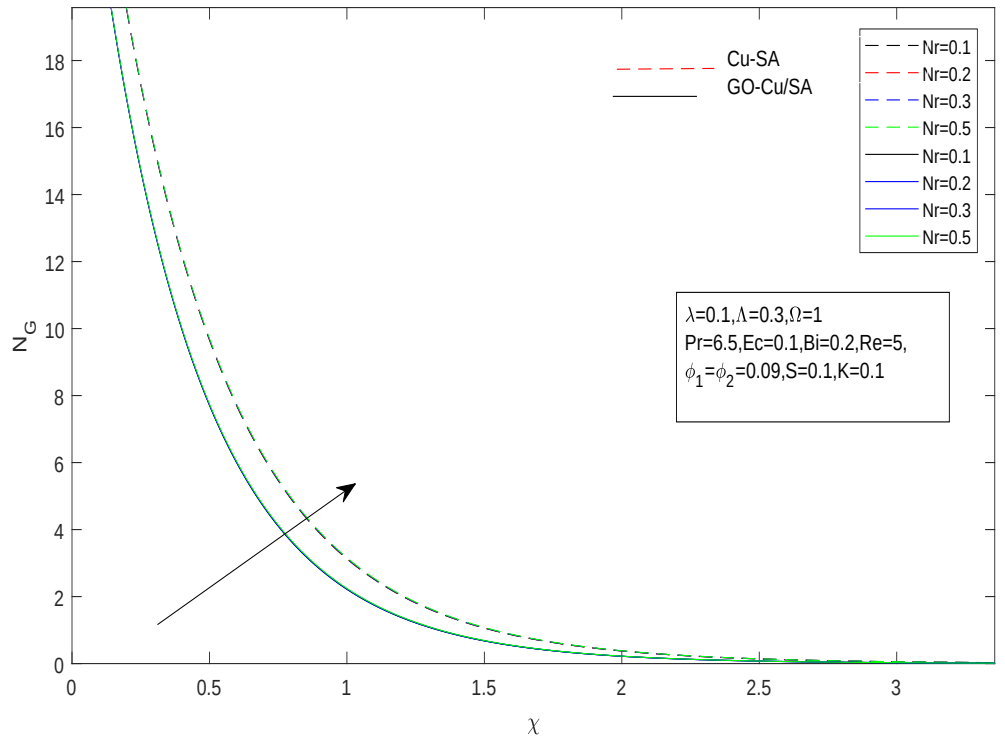

FIGURE 3.3: Impact of Nr on N_G

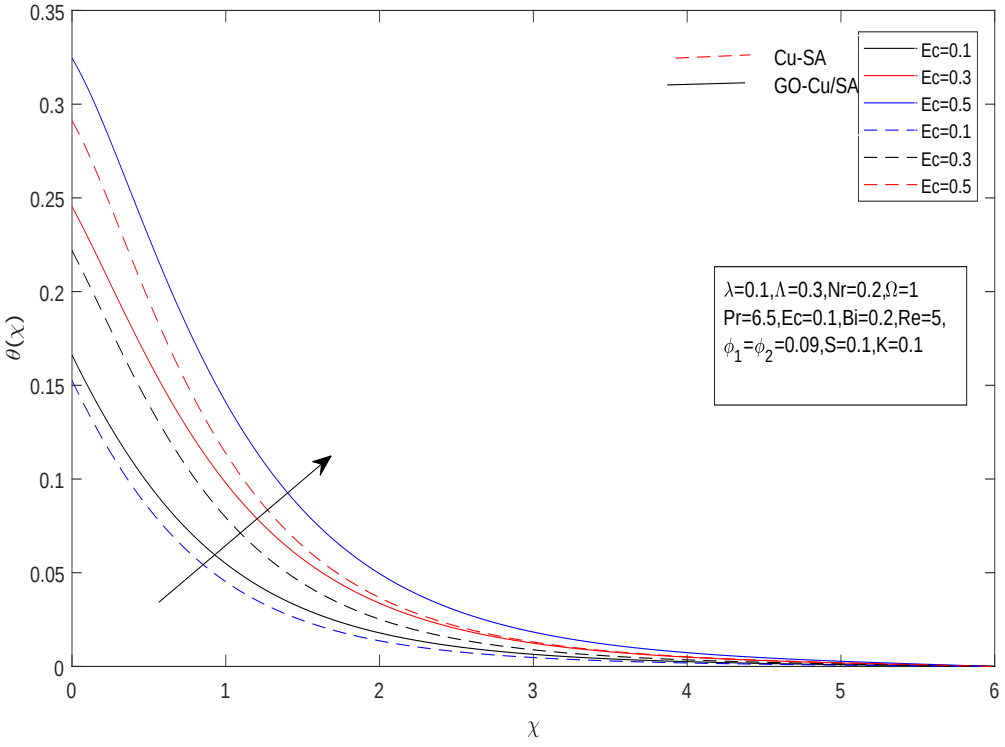

FIGURE 3.4: Impact of Ec on $\theta(\chi)$

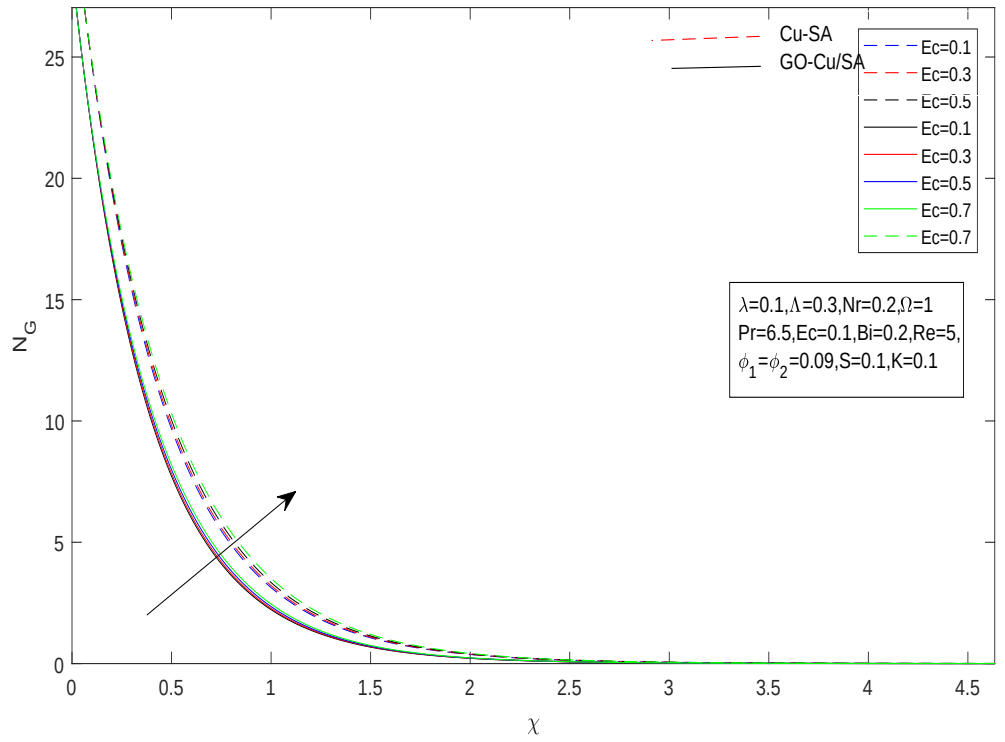

FIGURE 3.5: Impact of Ec on N_G

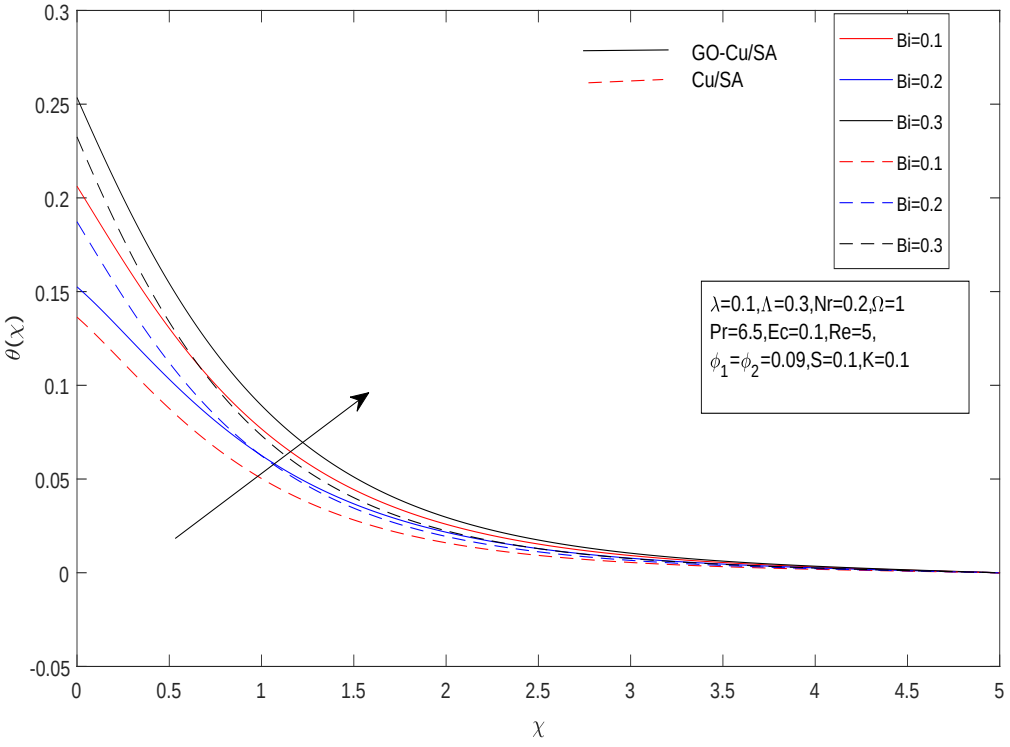

FIGURE 3.6: Impact of Bi on $\theta(\chi)$

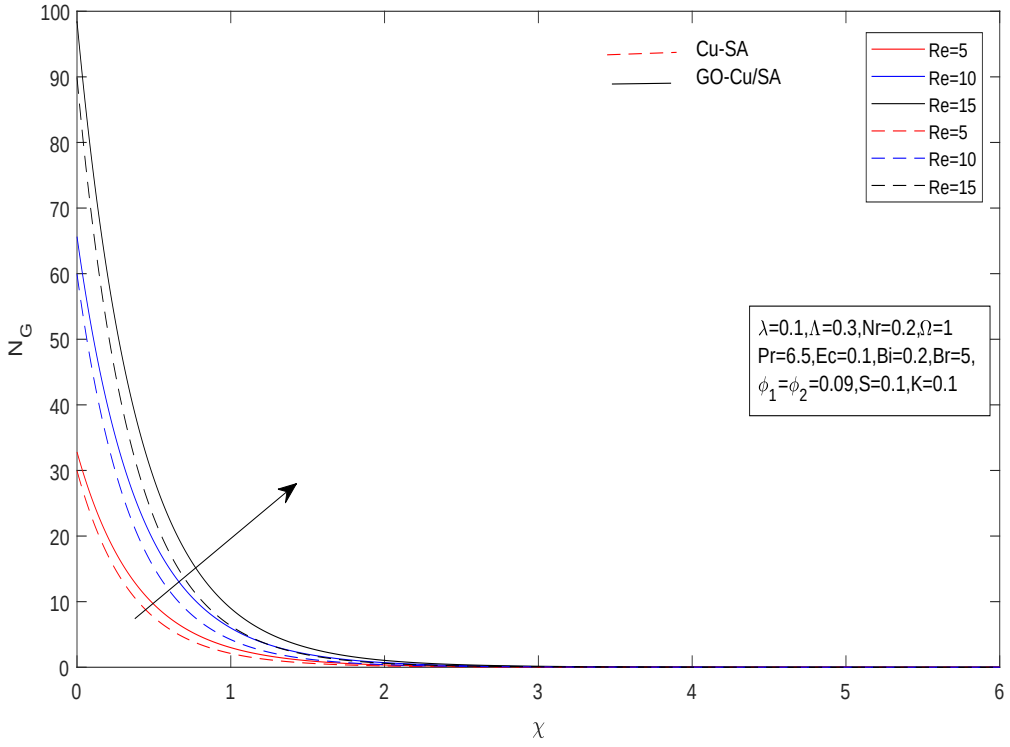

FIGURE 3.7: Impact of Re on N_G

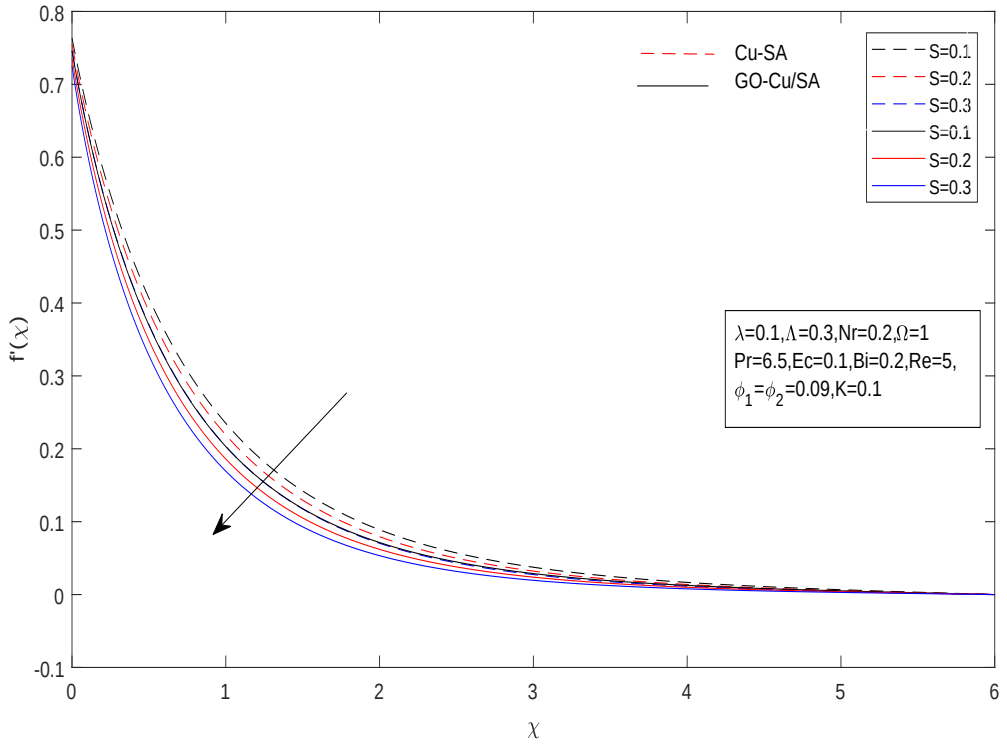

FIGURE 3.8: Impact of S on $f'(\chi)$

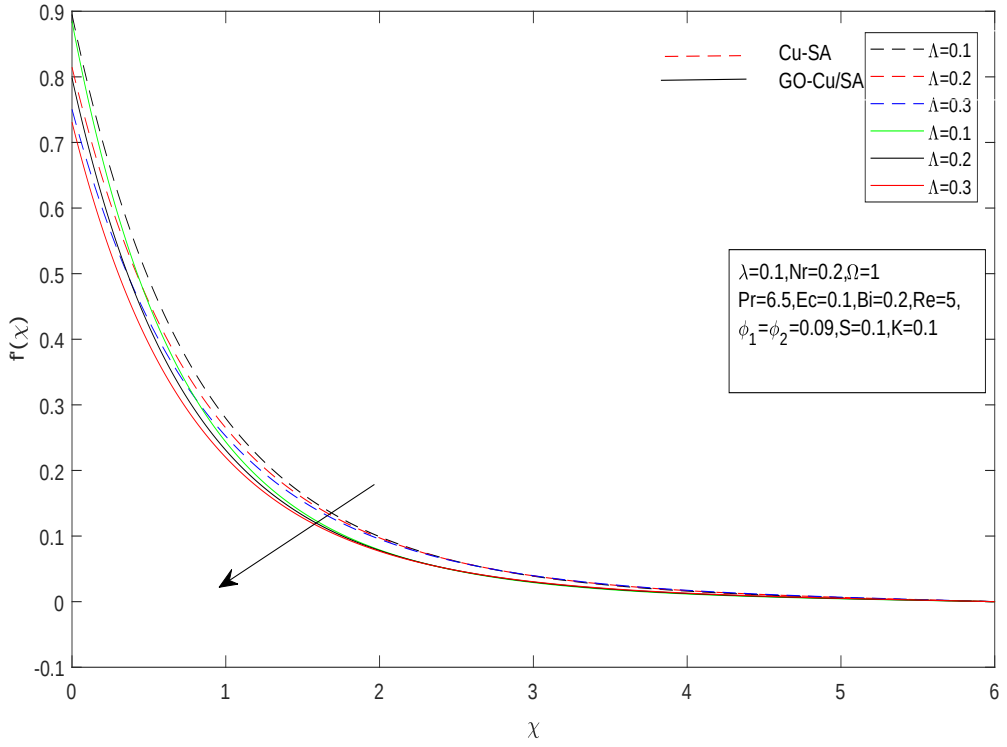

FIGURE 3.9: Impact of λ on $f'(\chi)$

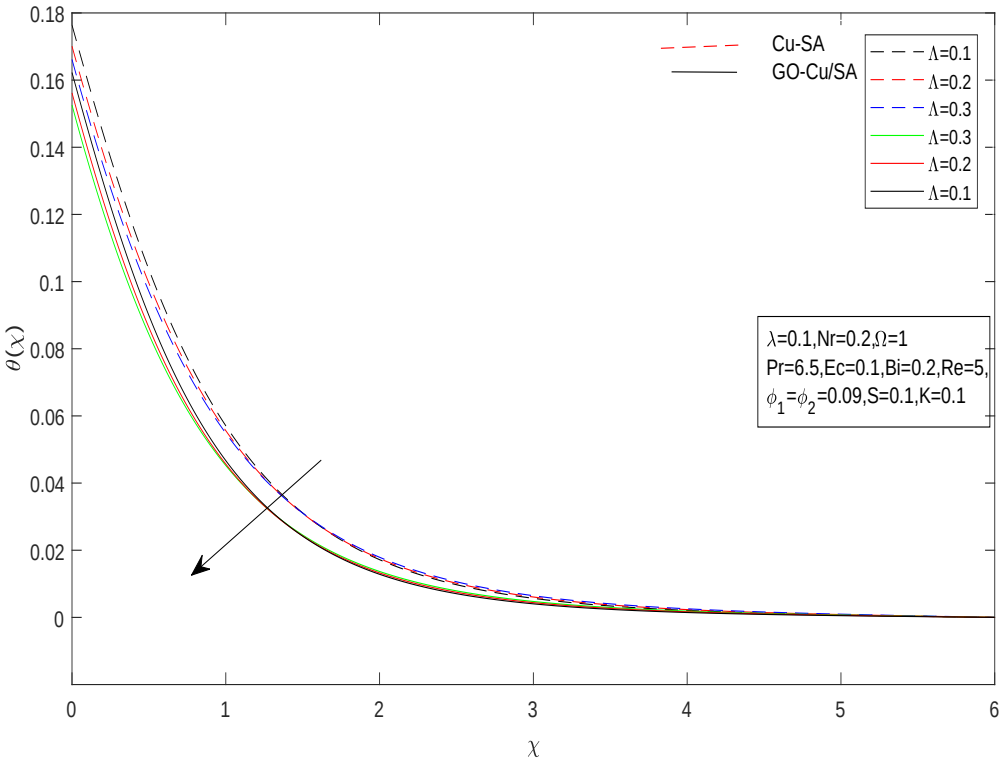

FIGURE 3.10: Impact of λ on $\theta(\chi)$

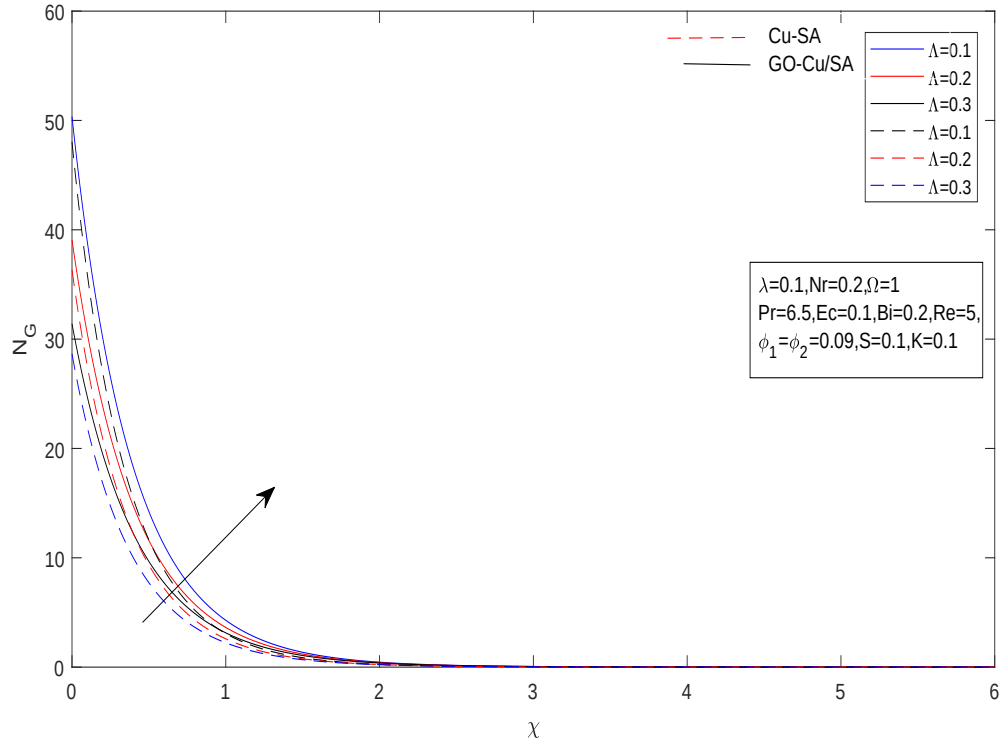

FIGURE 3.11: Impact of λ on N_G

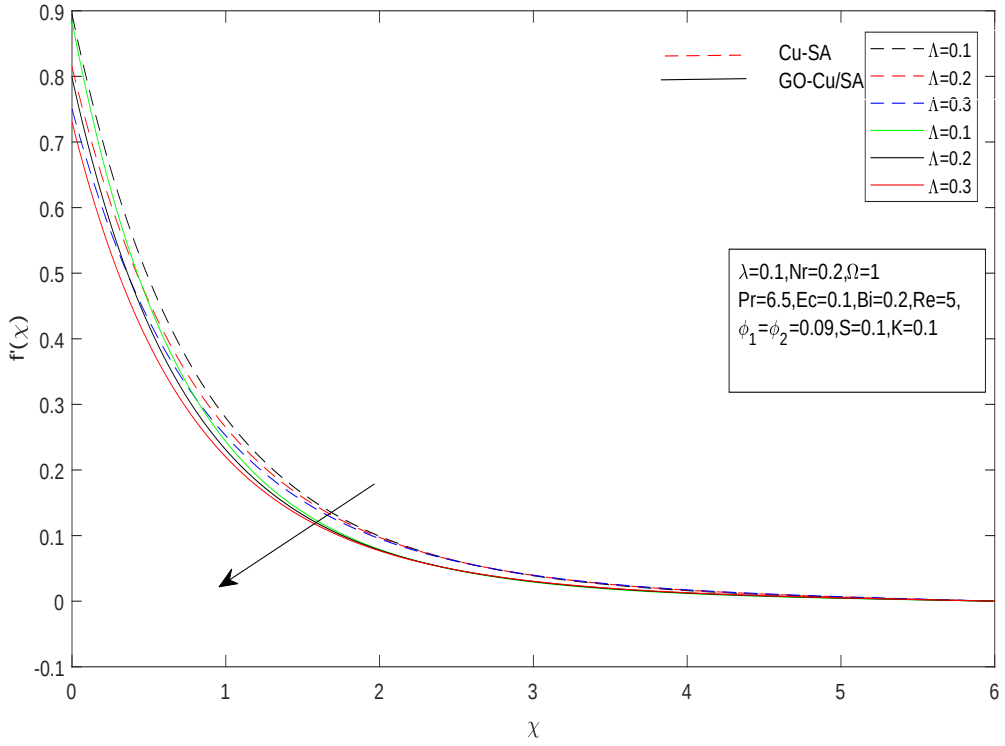

FIGURE 3.12: Impact of Λ on $f'(\chi)$

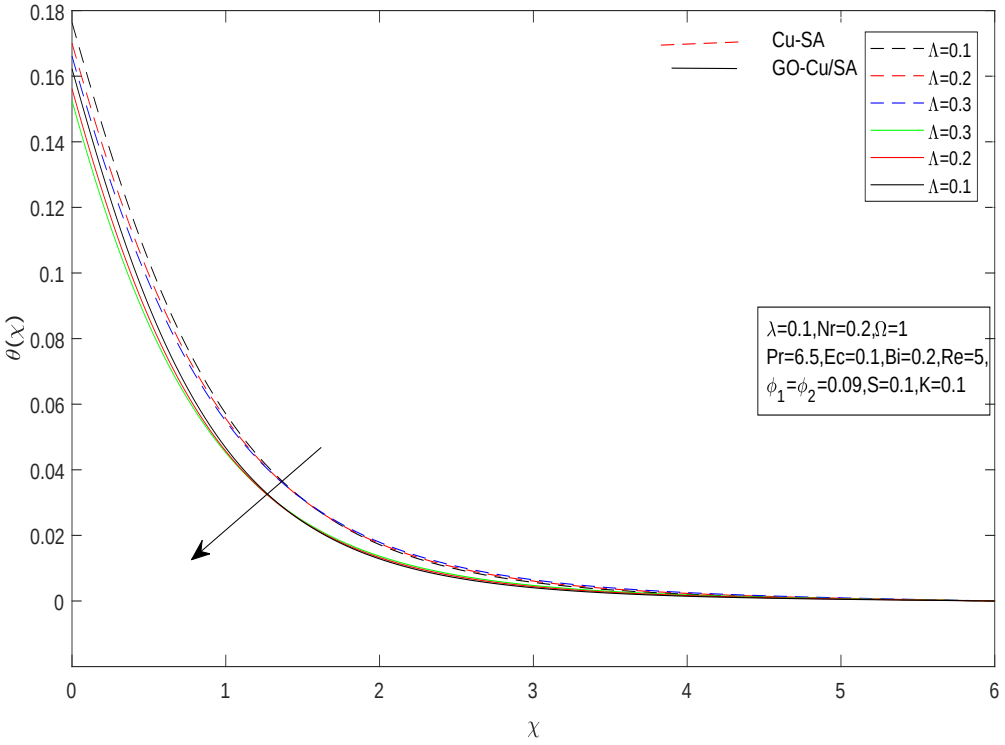

FIGURE 3.13: Impact of Λ on $\theta(\chi)$

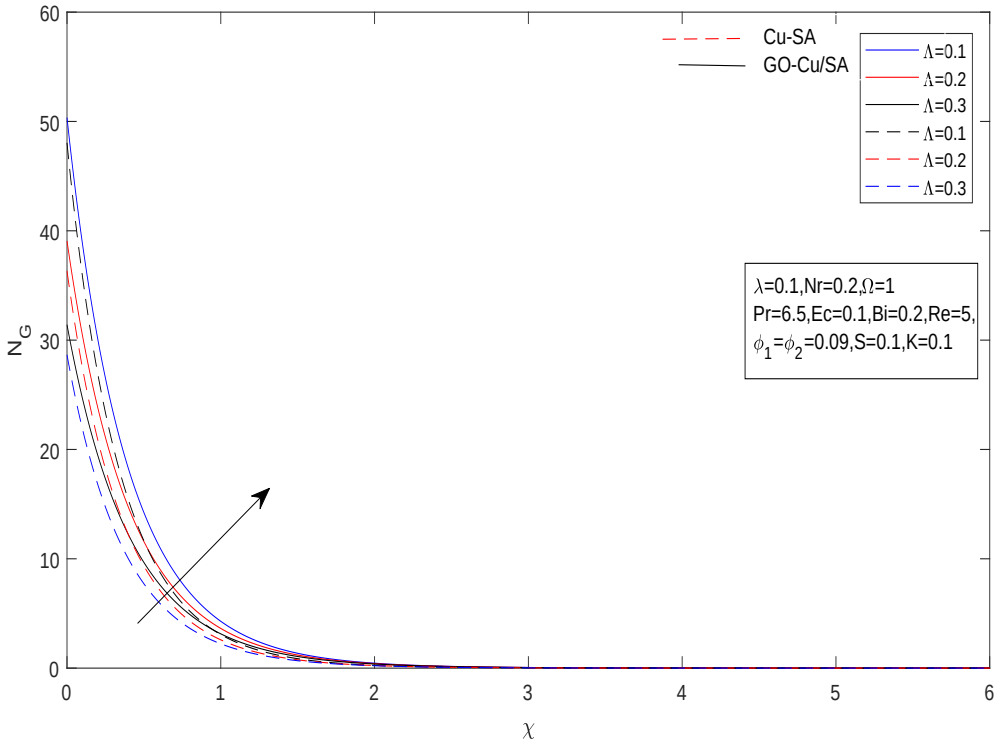

FIGURE 3.14: Impact of Λ on N_G

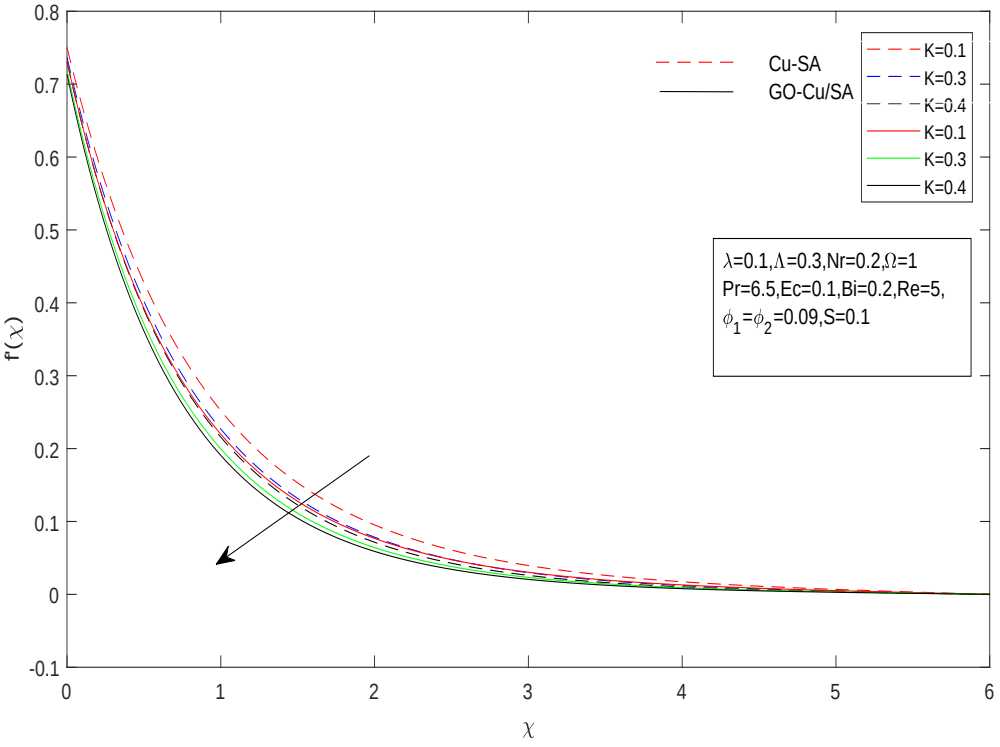

FIGURE 3.15: Impact of K on $f'(\chi)$

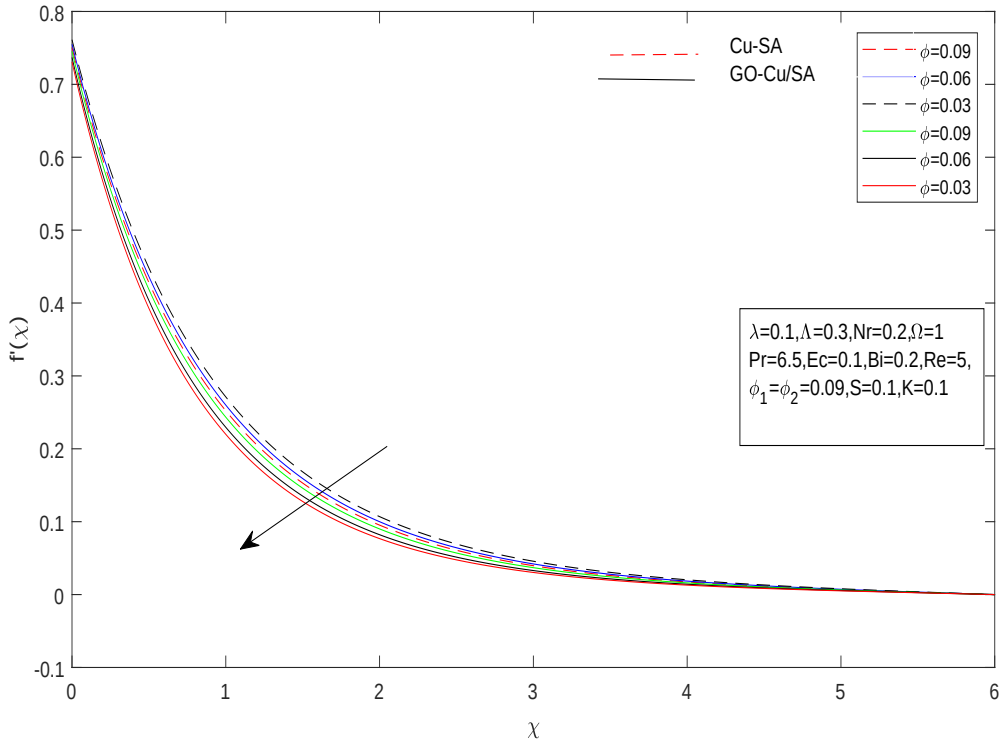

FIGURE 3.16: Impact of ϕ on $f'(\chi)$

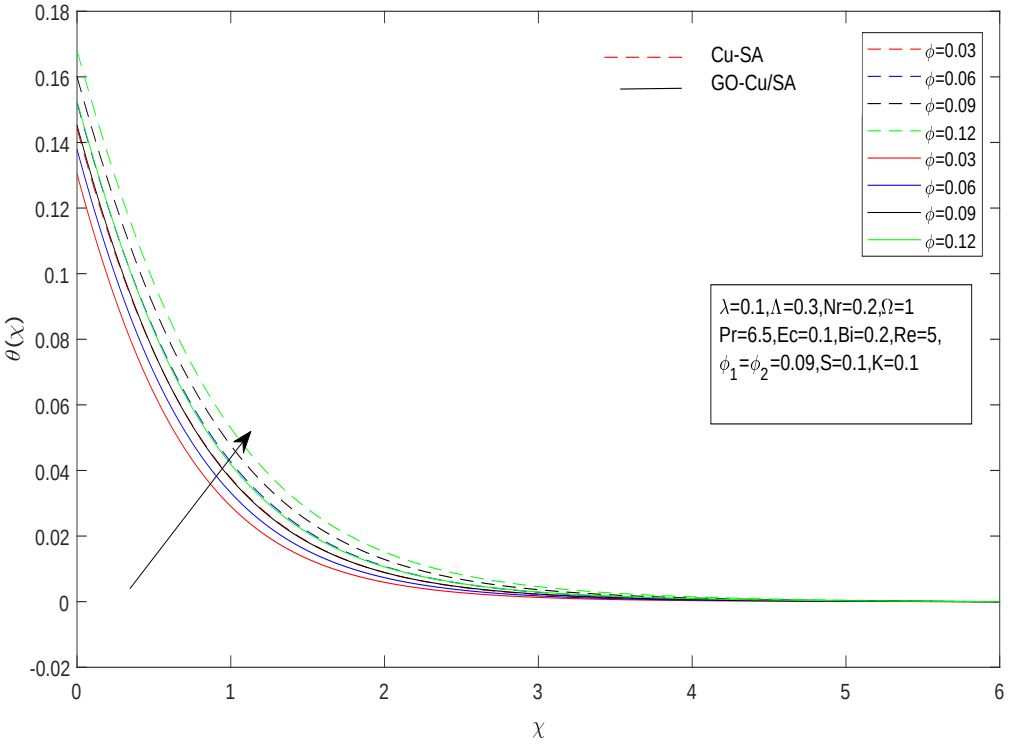

FIGURE 3.17: Impact of ϕ on $\theta(\chi)$

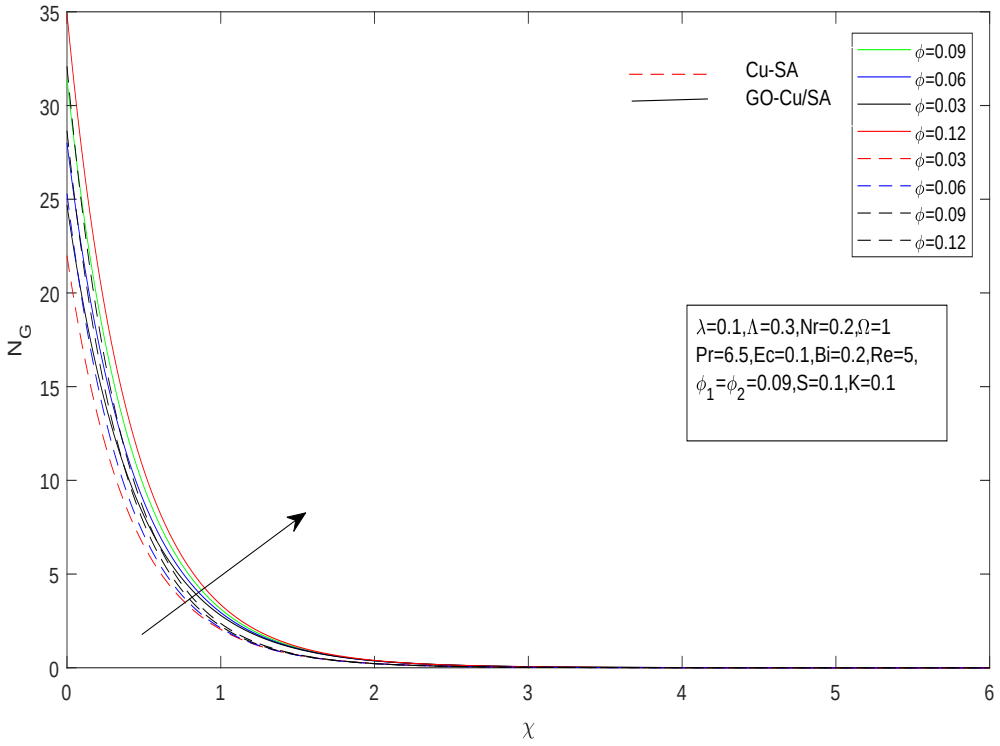

FIGURE 3.18: Impact of ϕ on N_G

Chapter 4

A Hybrid Williamson Nanofluid Flow: An Investigation Involving Cattaneo-Christov Model, Magnetic Field, Diffusion, Forchheimer Flow, and Chemical Reaction

4.1 Introduction

The model covered in Chapter 3 has been extended to include a magnetic field, the momentum equation uses a Forchheimer flow, while the energy equation uses a Cattaneo-Christov heat flux. In our study, we simultaneously take into account the concentration equation that incorporates the chemical reaction. The combination of these numerous adjustments provides a framework for analyzing how these parameters affect fluid flow across a stretching sheet. Our objective is to elucidate the intricate relationships among these variables and meticulously examine how their combined impact impacts the overall behavior of the fluid flow through the application of numerical simulations and a comprehensive analysis. This all-encompassing method makes it easier to understand the

intricate dynamics controlling the system that is being studied. The governing nonlinear partial differential equations are changed into a collection of dimensionless ordinary differential equations (Odes) through similarity transformations. These Odes can be numerically illuminated employing a strategy called the shooting approach.

4.2 Mathematical Modeling

This work aims to evaluate the two-dimensional steady boundary layer flow characteristics of a Williamson hybrid nano-fluid across a stretched sheet. In Cartesian coordinates, the y-axis is normal to the porous surface that runs along the x-axis. It is significant to remember that the wall is treated as incompressible in this study. to investigate mass diffusion and heat transfer by incorporating the interface between the applied magnetic field, dynamic viscosity, and a porous material in the investigation. The flow phenomenon is assumed to take place under certain crucial conditions, including Brownian diffusion, chemical reaction, thermophysical diffusion, Cattaneo-Christov heat flux, a magnetic field, and Forchheimer flow. Additionally, the system assumes a surface velocity and temperature. These assumptions lay the foundation for investigating the complex interactions and effects governing the flow over the stretching sheet. The stretching speed and porous surface temperature are:

$$U_w(x,t) = \frac{bx}{1-\epsilon t}, \quad T_w(x,t) = T_\infty + \frac{b^* x}{1-\epsilon t}. \tag{4.1}$$

The original stretching rate and temperature variation are denoted by b and b^* in this case, while the surface and surrounding temperatures are represented by T_w and T_∞, respectively. Copper (Cu) and graphene oxide (GO) with volume fractions of ϕ_1 and ϕ_2, respectively, are suspended in sodium alginate (SA) to form a hybrid nanofluid.

A uniform magnetic field of strength

$$B(t) = \frac{B_0}{\sqrt{1-\epsilon t}}, \tag{4.2}$$

is applied in the transverse direction to the flow and the induced magnetic field is considered negligible. The temperature and concentration near the surface are T_w and C_w

while the constant ambient temperature and concentration of the hybrid nanofluid are T_∞ and C_∞, respectively.

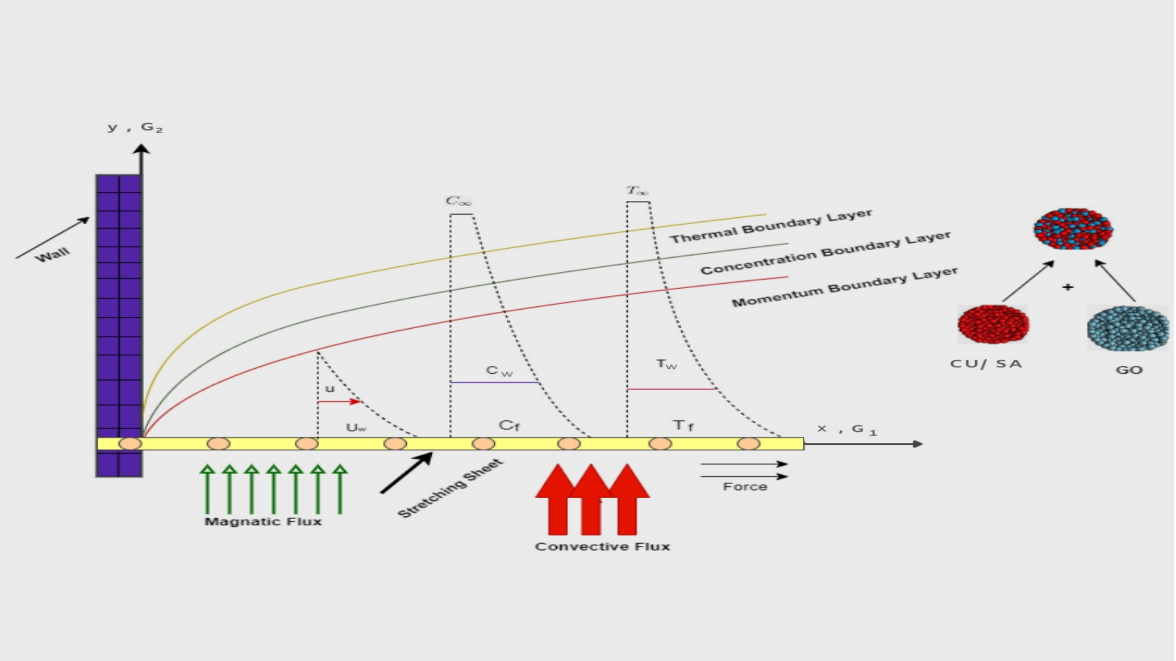

FIGURE 4.1: Flow Pattern Illustration.

The following equations express the continuity, momentum, energy, and concentration equations governing the problem mentioned above under standard boundary layer approximations.

Mass conservation:

$$\frac{\partial G_1}{\partial x} + \frac{\partial G_2}{\partial y} = 0. \tag{4.3}$$

Momentum Equation:

$$\frac{\partial G_1}{\partial t} + G_1\frac{\partial G_1}{\partial x} + G_2\frac{\partial G_1}{\partial y} = \frac{\mu_{hnf}}{\rho_{hnf}}\frac{\partial^2 G_1}{\partial y^2} + \frac{\mu_{hnf}}{\rho_{hnf}}\sqrt{2}\zeta\left[\frac{\partial G_1}{\partial y}\frac{\partial^2 G_1}{\partial y^2}\right] - \frac{\mu_{hnf}}{\rho_{hnf}k}G_1$$

$$-\frac{(B(t))^2\sigma_{hnf}}{\rho_{hnf}}G_1 - \frac{C_F}{\sqrt{K^*}}(G_1)^2. \tag{4.4}$$

Energy Equation:

$$G_1\frac{\partial T}{\partial x} + G_2\frac{\partial T}{\partial y} = \frac{\kappa_{hnf}}{(\rho C_p)_{hnf}}\frac{\partial^2 T}{\partial y^2} - \frac{1}{(\rho C_P)_{hnf}}\frac{\partial q_r}{\partial y} + \frac{\mu_{hnf}}{(\rho C_p)_{hnf}}(\frac{\partial G_1}{\partial y})^2$$

$$-\lambda\Bigg(G_1\frac{\partial G_1}{\partial x}\frac{\partial T}{\partial x} + G_2\frac{\partial G_2}{\partial y}\frac{\partial T}{\partial y} + G_1\frac{\partial G_2}{\partial x}\frac{\partial T}{\partial y} + G_2\frac{\partial G_1}{\partial y}\frac{\partial T}{\partial x}$$

$$+G_1^2\frac{\partial^2 T}{\partial x^2} + G_2^2\frac{\partial^2 T}{\partial y^2} + 2G_1G_2\frac{\partial^2 T}{\partial x\partial y}\Bigg). \tag{4.5}$$

Concentration Equation:

$$\frac{\partial C}{\partial t}+G_1\frac{\partial C}{\partial x}+G_2\frac{\partial C}{\partial y}=D_B\frac{\partial^2 C}{\partial y^2}+\frac{D_T}{T_\infty}\frac{\partial^2 T}{\partial y^2}-K_1(C-C_\infty). \tag{4.6}$$

Boundary Conditions:

The boundary conditions corresponding to the current fluid problem are as follows:

$$\left.\begin{array}{l} G_1(x,0)=U_w+N_w\left(1+\zeta\dfrac{\partial G_1}{\partial y}\right)\dfrac{\partial G_1}{\partial y},\ G_2(x,0)=V_w, \\ -k_f\dfrac{\partial T}{\partial y}=h_f(T_w-T),\quad as\quad \mathrm{y}=0,\quad C(x,0)=C_w\quad \text{at}\quad y=0, \\ G_1\to 0,\quad T\to T_\infty,\quad \text{as}\quad y\to\infty.\qquad C\to C_\infty\quad \text{as}\quad y\to\infty. \end{array}\right\} \tag{4.7}$$

Here G_1 and G_2 are the horizontal and vertical velocities respectively. Fluid velocity in vector form is defined as

$$\vec{G}=\Big\{G_1(x,y,t),G_2(x,y,t),0\Big\}.$$

The radiation heat flux q_r can be expressed as:

$$q_r=-\frac{4}{3}\frac{\sigma^*}{k^*}\frac{\partial T^4}{\partial y}. \tag{4.8}$$

The Stefan-Boltzman constant is denoted by σ^*, and the absorption coefficient is represented by k^*. The Taylor series expansion can be taken in account to express T^4 about T_∞ as follows:

$$T^4=T_\infty^4+4T_\infty^3(T-T_\infty)+6T_\infty^2(T-T_\infty)^2+.....$$

By neglecting the higher terms, we get

$$T^4\ =T_\infty^4+4T_\infty^3(T-T_\infty)\Rightarrow\quad T^4\ =4T_\infty^3T-3T_\infty^4\Rightarrow\quad \frac{\partial T^4}{\partial y}=\ 4T_\infty^3\frac{\partial T}{\partial y}.$$

Equation (4.8) becomes:

$$q_r\quad =-\frac{4}{3}\frac{\sigma*}{k*}(4T_\infty^3)\frac{\partial T}{\partial y}.$$

$$\Rightarrow\quad \frac{\partial q_r}{\partial y}=-\frac{16}{3}\frac{\sigma*}{k*}T_\infty^3\frac{\partial^2 T}{\partial y^2}=-\frac{16\sigma^*}{3k^*}\frac{bb^*xT_\infty^3}{\nu_f(1-\epsilon t)^2}\theta''(\chi). \tag{4.9}$$

4.2.1 Formulation and Thermo-Physical Characteristics

To provide a clear comparison, the valuable thermo-physical characteristics of both the HNF and the NF are presented in Table 4.1.

TABLE 4.1: Physical Properties

Feature	Sodium Alginate (SA)	Copper (Cu)	Graphene Oxide (GO)
ρ (kg/m^3)	989	8933	1800
C_p (J/kg·K)	4175	385	717
k (W/m·K)	0.6376	401	5000
σ (S/m)	2.6×10^{-4}	5.96×10^{7}	1.1×10^{-5}

TABLE 4.2: Thermophysical characteristics of nanoparticles and water-based fluid.

Nanofluid	**Hybrid Nanofluid**
Viscosity (μ)	$\mu_{hnf} = \mu_f(1-\phi_1)^{-2.5}(1-\phi_2)^{-2.5}$
Density (ρ)	$\rho_{hnf} = (1-\phi_2)\big((1-\phi_1)\rho_f + \phi_1\rho_{p_1}\big) + \phi_2\rho_{p_2}$
Heat Capacity (ρC_p)	$\frac{(\rho C_p)_{hnf}}{(\rho C_p)_f} = (1-\phi_2)\big((1-\phi_1)(\rho C_p)_f + \phi_1\frac{(\rho C_p)_{p_1}}{(\rho C_p)_f}\big) + \phi_2\frac{(\rho C_p)_{p_2}}{(\rho C_p)_f}$
Thermal conductivity (K)	$\frac{K_{hnf}}{K_{bf}} = \frac{K_{p_2}+(n-1)K_{bf}-(n-1)\phi_2(K_{bf}-K_{p_2})}{p_2+(n-1)K_{bf}+\phi_2(k_{bf}-K_{p_2})}$, $\frac{K_{bf}}{K_f} = \frac{K_{p_1}+(n-1)K_f-(n-1)\phi_1(K_f-K_{p_1})}{K_{p_1}+(n-1)K_f+\phi_1(K_f-K_{p_1})}$
Electrical Conductivity (σ)	$\frac{\sigma_{hnf}}{\sigma_f} = 1 + \frac{\frac{3(\phi_1\sigma_{p1}+\phi_2\sigma_{p2})}{\sigma_f} - (\phi_1+\phi_2)}{(\frac{\phi_1\sigma_{p1}+\phi_2\sigma_{p2}}{(\phi_1+\phi_2)\sigma_f}+2) - \frac{\phi_1\sigma_{p1}+\phi_2\sigma_{p2}}{(\phi_1+\phi_2)\sigma_f} - (\phi_1+\phi_2))}$

The following notations have been added for convenience:

$$
\begin{aligned}
P_a &= (1-\phi_1)^{2.5}(1-\phi_2)^{2.5},\\
P_b &= (1-\phi_2)\left((1-\phi_1) + \phi_1\frac{\rho_{p1}}{\rho_f}\right) + \phi_2\frac{\rho_{p2}}{\rho_f},\\
P_c &= (1-\phi_2)\left((1-\phi_1) + \phi_1\frac{(\rho_{Cp})_{p1}}{(\rho_{Cp})_f}\right) + \phi_2\frac{(\rho_{Cp})_{p2}}{(\rho_{Cp})_f},\\
P_d &= \frac{(\kappa_{p2}+2\kappa_{nf}-2\phi_2(\kappa_{nf}-\kappa_{p2}))\,(\kappa_{p1}+2\kappa_f-2\phi_1(\kappa_f-\kappa_{p1}))}{(\kappa_{p2}+2\kappa_{nf}+\phi_2(\kappa_{nf}-\kappa_{p2}))\,(\kappa_{p1}+2\kappa_f+\phi_1(\kappa_f-\kappa_{p1}))}.\\
P_e &= 1 + \frac{\frac{3(\phi_1\sigma_{p1}+\phi_2\sigma_{p2})}{\sigma_f} - (\phi_1+\phi_2)}{(\frac{\phi_1\sigma_{p1}+\phi_2\sigma_{p2}}{(\phi_1+\phi_2)\sigma_f}+2) - \frac{\phi_1\sigma_{p1}+\phi_2\sigma_{p2}}{(\phi_1+\phi_2)\sigma_f} - (\phi_1+\phi_2))}.
\end{aligned}
\tag{4.10}
$$

Table 4.3: Different Dimensionless parameters used in governing ODEs

Symbols	**Name**	**Appearance**
M	Magnetic parameter	$M = \frac{\sigma_f}{b\rho_f} B_0^2$
Fr	Forchheimer parameter	$Fr = \frac{C_F x}{\sqrt{K^*}}$
A	Unsteadiness parameter	$A = \frac{\epsilon}{b}$
λ	Williamson parameter	$\lambda = \zeta U w \sqrt{\frac{2b}{\nu_f(1-\epsilon t)}}$
P_r	Prandtl number	$P_r = \frac{\nu_f}{\alpha_f}$
Φ	Volume friction	$-$
N_r	Thermal radiation parameter	$N_r = \frac{16}{3} \frac{\sigma^*(T_\infty^3)}{K^* \nu_f (\rho C_P)_f}$
S	Suction/injection parameter	$S = -V_w \sqrt{\frac{1-\epsilon t}{\nu_f b}}$
K	Porous medium parameter	$K = \frac{\nu_f(1-\epsilon t)}{bk}$
Λ	Velocity slip	$\Lambda = \sqrt{\frac{b}{\nu_f(1-\epsilon t)}} N_w$
B_i	Biot number	$B_i = \frac{h_f}{K_o} \sqrt{\frac{\nu_f(1-\epsilon t)}{b}}$
E_c	Eckert number	$E_c = \frac{(Uw)^2}{(C_P)_f (T_w - T_\infty)}$
B_r	Brinkman number	$B_r = \frac{\nu_f (Uw)^2}{K_f (T_w - T_\infty)}$
K_c	Chemical reaction	$K_c = K_1(\frac{1-\epsilon t}{b})$
N_t	Thermodiffusion	$N_t = \frac{\tau D_T (T_w - T_\infty)}{\nu_f T_\infty}$
N_b	Brownian motion	$N_b = \frac{\tau D_B (C_w - C_\infty)}{\nu_f}$
S_c	Schmidt number	$S_c = \frac{\nu_f}{D_B}$

4.3 Similarity Transformation and Non- Dimensionalization of Mathematical Model

In this section, we outline the non-dimensionalization process for the mathematical model that governs the behavior of our hybrid nanofluid. This procedure involves introducing the dimensionless variables and parameters to transform the original equations into a

more streamlined form. Utilizing dimensionless quantities allows for a more profound understanding of the physical phenomena and renders the analysis more manageable.

The mathematical model will be converted into a system of ordinary differential equations (ODEs) using a similarity transformation. This conversion is essential for making the equations more understandable and enabling a deeper analysis of the underlying dynamics.

$$\left.\begin{aligned} \psi(x,y) &= \sqrt{\frac{\nu_f b}{1-\epsilon t}}\, x f(\chi), \quad \chi(x,y) = \sqrt{\frac{b}{\nu_f(1-\epsilon t)}}\, y, \\ \theta(\chi) &= \frac{T-T_\infty}{T_w-T_\infty}, \quad \phi(\chi) = \frac{C-C_\infty}{C_w-C_\infty}. \end{aligned}\right\} \tag{4.11}$$

where ψ denotes the stream function and χ is the similarity variable. Equation (4.3) is already identically satisfied in Chapter 3.

4.3.1 Non-Dimensionalization of Momentum Equation

From the previous chapter, we will consider the following expressions For the momentum equation (4.4):

$$G_1 = \frac{b}{1-\epsilon t} x f'(\chi). \tag{4.12}$$

$$G_2 = -\sqrt{\frac{\nu_f b}{1-\epsilon t}} f(\chi). \tag{4.13}$$

$$\frac{\partial G_1}{\partial x} = \frac{b}{1-\epsilon t} f'(\chi). \tag{4.14}$$

$$\begin{aligned} \frac{\partial G_1}{\partial t} &= b x f'(\chi) \frac{\partial}{\partial t}\left(\frac{1}{1-\epsilon t}\right) + \frac{bx}{1-\epsilon t} f''(\chi) \frac{\partial \chi}{\partial t} \\ &= \frac{\epsilon b}{(1-\epsilon t)^2} x f'(\chi) + \frac{\epsilon b^{\frac{3}{2}}}{2\sqrt{\nu_f}(1-\epsilon t)^{\frac{5}{2}}} x y f''(\chi). \end{aligned} \tag{4.15}$$

$$\frac{\partial G_1}{\partial y} = \frac{b^{\frac{3}{2}}}{\sqrt{\nu_f}(1-\epsilon t)^{\frac{3}{2}}} x f''(\chi). \tag{4.16}$$

$$\frac{\partial^2 G_1}{\partial y^2} = \frac{b^2}{\nu_f(1-\epsilon t)^2} x f'''(\chi). \tag{4.17}$$

$$\frac{\partial G_2}{\partial y} = -\frac{b}{1-\epsilon t} f'(\chi). \tag{4.18}$$

$$\frac{\partial G_2}{\partial x} = 0. \tag{4.19}$$

Now, non-dimensional form of momentum equation (4.4) can be obtained by using equations (4.12)-(4.17) as follows

$$\frac{\epsilon b}{(1-\epsilon t)^2} x f'(\chi) + \frac{\epsilon b^{\frac{3}{2}}}{2\sqrt{\nu_f}(1-\epsilon t)^{\frac{5}{2}}} xy f''(\chi) + \left(\frac{bx}{1-\epsilon t} f'(\chi)\right)\left(\frac{b}{1-\epsilon t} f'(\chi)\right)$$

$$+\left(-\sqrt{\frac{\nu_f b}{1-\epsilon t}} f(\chi)\right) \frac{b^{\frac{3}{2}}}{\sqrt{\nu_f}(1-\epsilon t)^{\frac{3}{2}}} x f''(\chi) = \frac{\mu_{hnf}}{\rho_{hnf}} \frac{b^2}{\nu_f(1-\epsilon t)^2} x f'''(\chi)$$

$$+\frac{\mu_{hnf}}{\rho_{hnf}} \sqrt{2}\zeta \frac{b^{\frac{3}{2}}}{\sqrt{\nu_f}(1-\epsilon t)^{\frac{3}{2}}} x f''(\chi)\left(\frac{b^2}{\nu_f(1-\epsilon t)^2} x f'''(\chi)\right) - \frac{\mu_{hnf}}{\rho_{hnf} k} \frac{b}{1-\epsilon t} x f'(\chi)$$

$$-\frac{(B(t))^2 \sigma_{hnf}}{\rho_{hnf}} \frac{bx}{1-\epsilon t} f'(\chi) - \frac{C_F}{\sqrt{K^*}} \frac{b^2}{(1-\epsilon t)^2} x^2 (f'(\chi))^2.$$

$$\Rightarrow \quad \frac{b^2 x}{\nu_f(1-\epsilon t)^2} \frac{\mu_{hnf}}{\rho_{hnf}} \left[\frac{\epsilon}{b} \frac{\rho_{hnf}}{\mu_{hnf}} \nu_f f'(\chi) + \frac{\epsilon\sqrt{\nu}_f}{2\sqrt{b}\sqrt{1-\epsilon t}} y \frac{\rho_{hnf}}{\mu_{hnf}} f''(\chi)\right.$$

$$\left.+\nu_f \frac{\rho_{hnf}}{\mu_{hnf}} (f'(\chi))^2 - \nu_f \frac{\rho_{hnf}}{\mu_{hnf}} f(\chi) f''(\chi)\right] = \frac{\mu_{hnf}}{\rho_{hnf}} \frac{b^2 x}{\nu_f(1-\epsilon t)^2} \left[f'''(\chi)\right.$$

$$+\sqrt{2}\zeta \frac{b^{\frac{3}{2}}}{\sqrt{\nu}_f(1-\epsilon t)^{\frac{3}{2}}} x f''(\chi) f'''(\chi) - \nu_f \frac{1-\epsilon t}{bk} f'(\chi)$$

$$\left.-\frac{(B(t))^2 \sigma_{hnf}}{\mu_{hnf}} \frac{\sigma_f \nu_f (1-\epsilon t)}{\sigma_f b} f'(\chi) - \frac{C_F}{\sqrt{K^*}} \frac{\nu_f \rho_{hnf}}{\mu_{hnf}} x (f'(\chi))^2\right].$$

$$\Rightarrow \quad \frac{\epsilon}{b} \frac{\rho_{hnf}}{\mu_{hnf}} \nu_f f'(\chi) + \frac{\epsilon\sqrt{\nu_f}}{2\sqrt{b(1-\epsilon t)}} y \frac{\rho_{hnf}}{\mu_{hnf}} f''(\chi) + \nu_f \frac{\rho_{hnf}}{\mu_{hnf}} (f'(\chi))^2$$

$$-\nu_f \frac{\rho_{hnf}}{\mu_{hnf}} f(\chi) f''(\chi) = f'''(\chi) + \sqrt{2}\zeta \frac{b^{\frac{3}{2}}}{\sqrt{\nu_f}(1-\epsilon t)^{\frac{3}{2}}} x f''(\chi) f'''(\chi)$$

$$-\nu_f \frac{1-\epsilon t}{bk} f'(\chi)$$

$$-\frac{(B(0))^2 \sigma_{hnf}}{\mu_{hnf}} \frac{\sigma_f \mu_f}{\sigma_f \rho_f} \frac{1-\epsilon t}{b(1-\epsilon t)} f'(\chi) - F_r \frac{\mu_f}{\rho_f} \frac{\rho_{hnf}}{\mu_{hnf}} (f'(\chi))^2.$$

$$\Rightarrow \quad \nu_f \frac{\rho_{hnf}}{\mu_{hnf}}\left[\frac{\epsilon}{b}f'(\chi)+\frac{\epsilon}{2\sqrt{b\nu_f(1-\epsilon t)}}yf''(\chi)+(f'(\chi))^2-f(\chi)f''(\chi)\right]$$

$$= f'''(\chi)+\frac{\sqrt{2}b^{\frac{3}{2}}\zeta x}{\sqrt{\nu}_f(1-\epsilon t)^{\frac{3}{2}}}f''(\chi)f'''(\chi)-Kf'(\chi)-P_aP_eMf'(\chi)$$

$$-P_aP_bF_r(f'(\chi))^2.$$

$$\Rightarrow \quad f'''(\chi)\big(1+\lambda f''(\chi)\big) = -P_aP_b\Bigg[f(\chi)f''(\chi)-(f'(\chi))^2-A\bigg(f'(\chi)+\frac{\chi}{2}f''(\chi)\bigg)$$

$$-\frac{P_e}{P_b}Mf'(\chi)-F_r(f'(\chi))^2\Bigg]+Kf'(\chi). \tag{4.20}$$

4.3.2 Non-Dimensionalization of Energy Equation

In this section, we discuss the non-dimensionalization process of the energy equation (4.5) for our hybrid nanofluid model. For this equation, the following derivatives are required.

$$\frac{\partial^2 T}{\partial x^2} = 0. \tag{4.21}$$

$$\frac{\partial T}{\partial x} = \left(\frac{b^*}{1-\epsilon t}\right)\theta(\chi). \tag{4.22}$$

$$\frac{\partial T}{\partial y} = \frac{b^{\frac{1}{2}}b^*x}{\sqrt{\nu_f}(1-\epsilon t)^{\frac{3}{2}}}\theta'(\chi). \tag{4.23}$$

$$\frac{\partial^2 T}{\partial y^2} = \frac{bb^*x}{\nu_f(1-\epsilon t)^2}\theta''(\chi). \tag{4.24}$$

$$\frac{\partial^2 T}{\partial x \partial y} = \frac{\partial}{\partial x}\left(\frac{b^{\frac{1}{2}}b^*x}{\sqrt{\nu_f}(1-\epsilon t)^{\frac{3}{2}}}\theta'(\chi)\right).$$

$$= \sqrt{\frac{b}{\nu_f(1-\epsilon t)}}\frac{b^*}{1-\epsilon t}\theta'(\chi). \tag{4.25}$$

Substituting (4.12) - (4.14), (4.16), (4.18)-(4.19) (4.21) - (4.25) and (4.9), the dimensionless governing equation for energy (4.5), can be expressed as:

$$b^*x\frac{\epsilon}{(1-\epsilon t)^2}\theta(\chi)+\frac{1}{2}b^*\epsilon\frac{\sqrt{b}}{\sqrt{\nu_f}(1-\epsilon t)^{\frac{5}{2}}}xy\theta'(\chi)+\frac{b^*bx}{(1-\epsilon t)^2}f'(\chi)\theta(\chi)$$

$$-\frac{\sqrt{\nu_f b}}{\sqrt{1-\epsilon t}}\frac{b^*\sqrt{b}}{\sqrt{\nu_f(1-\epsilon t)}}\frac{x}{1-\epsilon t}f(\chi)\theta'(\chi) = \frac{\kappa_{hnf}}{(\rho C_p)_{hnf}}\frac{b^*bx}{\nu_f(1-\epsilon t)^2}\theta''(\chi)$$

$$+\frac{1}{(\rho C_p)_{hnf}}\frac{b^*bx}{\nu_f(1-\epsilon t)^2}\left(\frac{16\sigma^*}{3k^*}T_\infty^3\theta''(\chi)\right)+\frac{\mu_{hnf}}{(\rho C_p)_{hnf}}\frac{b^3x^2}{(1-\epsilon t)^3\nu_f}(f''(\chi))^2$$

$$-\lambda\Bigg[\frac{b^2b^*x}{(1-\epsilon t)^3}(f'(\chi))^2\theta(\chi)+\frac{b^*b^2x}{\nu_f(1-\epsilon t)^3}f(\chi)f'(\chi)\theta'(\chi)+0$$

$$-\frac{b^*b^2x}{\nu_f(1-\epsilon t)^3}f(\chi)f''(\chi)\theta(\chi)-2\frac{b^*b^2x}{\nu_f(1-\epsilon t)^3}f(\chi)f'(\chi)\theta'(\chi)$$

$$+\frac{b^*b^2x}{\nu_f(1-\epsilon t)^3}(f(\chi))^2\theta''(\chi)\Bigg].$$

$$\Rightarrow\quad b^*x\frac{b}{(1-\epsilon t)^2}\left[\frac{\epsilon}{b}\theta(\chi)+\frac{\epsilon\sqrt{b}}{2b\sqrt{\nu_f(1-\epsilon t)}}y\theta'(\chi)+f'(\chi)\theta(\chi)\right]$$

$$-\frac{bb^*x}{(1-\epsilon t)^2}f(\chi)\theta'(\chi)=\frac{\kappa_{hnf}}{(\rho C_p)_{hnf}}\frac{b^*bx}{\nu_f(1-\epsilon t)^2}\left[\theta''(\chi)+\frac{1}{\kappa_{hnf}}\left(\frac{16\sigma^*}{3k^*}T_\infty^3\theta''(\chi)\right)\right.$$

$$\left.+\frac{\mu_{hnf}}{\kappa_{hnf}}\frac{b^2x}{b^*(1-\epsilon t)}(f''(\chi))^2\right]-\lambda\frac{b^*b^2x}{\nu_f(1-\epsilon t)^3}\Bigg[(f'(\chi))^2\theta(\chi)+f(\chi)f'(\chi)\theta'(\chi)$$

$$-f(\chi)f''(\chi)\theta(\chi)-2f(\chi)f'(\chi)\theta'(\chi)+(f(\chi))^2\theta''(\chi)\Bigg].$$

$$\Rightarrow\quad b^*x\frac{b}{(1-\epsilon t)^2}\left[\frac{\epsilon}{b}\left(\theta(\chi)+\frac{\chi}{2}\theta'(\chi)\right)+f'(\chi)\theta(\chi)-f(\chi)\theta'(\chi)\right]$$

$$=\frac{\kappa_{hnf}}{(\rho C_p)_{hnf}}\frac{b^*bx}{\nu_f(1-\epsilon t)^2}\left[\theta''(\chi)+\frac{1}{\kappa_{hnf}}\frac{16\sigma^*}{3k^*}T_\infty^3\theta''(\chi)\right.$$

$$+\frac{\mu_{hnf}}{\kappa_{hnf}}\frac{\nu_f\kappa_f(\rho C_p)_f}{\nu_f\kappa_f(\rho C_p)_f}\frac{b^2x}{b^*(1-\epsilon t)}(f''(\chi))^2-\lambda\frac{(\rho C_p)_{hnf}}{\kappa_{hnf}}\frac{b}{(1-\epsilon t)}\Bigg((f'(\chi))^2\theta(\chi)$$

$$\left.+f(\chi)f'(\chi)\theta'(\chi)-f(\chi)f''(\chi)\theta(\chi)-2f(\chi)f'(\chi)\theta'(\chi)+(f(\chi))^2\theta''(\chi)\Bigg)\right].$$

$$\Rightarrow\quad \frac{P_cP_r}{P_d}\left[A\left(\theta(\chi)+\frac{\chi}{2}\theta'(\chi)\right)+f'(\chi)\theta(\chi)-f(\chi)\theta'(\chi)\right]=\left(1+\frac{P_rN_r}{P_d}\right)\theta''(\chi)$$

$$+\frac{P_r}{P_aP_d}\frac{(Uw)^2}{(T_w-T_\infty)(C_P)_f}(f''(\chi))^2-\beta\frac{P_rP_c}{P_d}\Bigg[(f'(\chi))^2\theta(\chi)+f(\chi)f'(\chi)\theta'(\chi)$$

$$-f(\chi)f''(\chi)\theta(\chi)-2f(\chi)f'(\chi)\theta'(\chi)+(f(\chi))^2\theta''(\chi)\Bigg].$$

$$\Rightarrow\quad \left(1+\frac{P_rN_r}{P_d}\right)\theta''+\frac{E_cP_r}{P_aP_d}(f'')^2-\beta\frac{P_rP_c}{P_d}\Bigg[(f')^2\theta+ff'\theta'-ff''\theta-2ff'\theta'$$

$$+f^2\theta''\Bigg]-\frac{P_cP_r}{P_d}\left[A(\theta+\frac{\chi}{2}\theta')+f'\theta(\chi)-f\theta'\right]=0.$$

$$\Rightarrow \quad \left(1+\frac{P_rN_r}{P_d}\right)\theta''+\frac{P_cP_r}{P_d}\left[\frac{E_c}{P_aP_c}(f'')^2-\beta\left[(f')^2\theta-ff'\theta'-ff''\theta+f^2\theta''\right]\right.$$
$$\left.-A(\theta+\frac{\chi}{2}\theta')+f'\theta(\chi)-f\theta'\right]=0.$$

$$\Rightarrow \quad \left(1+\frac{P_rN_r}{P_d}-\beta\frac{P_rP_c}{P_d}f^2\right)\theta''+\frac{P_cP_r}{P_d}\left[\frac{E_c}{P_aP_c}(f'')^2-\beta\left[(f')^2\theta-ff'\theta'-ff''\theta\right]\right.$$
$$\left.-A(\theta+\frac{\chi}{2}\theta')+f'\theta(\chi)-f\theta'\right]=0. \tag{4.26}$$

4.3.3 Non-Dimensionalization of Concentration Equation

Here, we focus on the non-dimensionalization process specifically applied to the concentration equation (4.6) in our hybrid nanofluid model. For this purpose, the following derivatives are also required:

$$\frac{\partial C}{\partial t}=(C_w-C_\infty)\frac{\sqrt{b}\epsilon y}{2\sqrt{\nu_f}(1-\epsilon t)^{\frac{3}{2}}}\phi'(\chi).$$

$$\frac{\partial C}{\partial x}=0.$$

$$\frac{\partial^2 C}{\partial y^2}=(C_w-C_\infty)\frac{b}{\nu_f(1-\epsilon t)}\phi''(\chi).$$

$$\frac{\partial C}{\partial y}=(C_w-C_\infty)\sqrt{\frac{b}{\nu_f(1-\epsilon t)}}\phi'(\chi).$$

Equations may now be used to construct the concentration equation (4.6) in its dimensionless version (4.12)-(4.13) and (4.24) as shown below:

$$(C_w-C_\infty)\frac{\sqrt{b}\epsilon y}{2\sqrt{\nu_f}(1-\epsilon t)^{\frac{3}{2}}}\phi'(\chi)+0-\frac{b}{1-\epsilon t}(C_w-C_\infty)f\phi'$$

$$=D_B\frac{b}{\nu_f(1-\epsilon t)}(C_w-C_\infty)\phi''(\chi)+\frac{D_T}{T_\infty}\frac{b}{\nu_f(1-\epsilon t)}(T_w-T_\infty)\theta''(\chi)$$
$$-K_1(C_w-C_\infty)\phi(\chi).$$

$$\Rightarrow \quad \frac{b}{1-\epsilon t}(C_w-C_\infty)\left[\frac{\sqrt{b}\epsilon y}{2b\sqrt{\nu_f(1-\epsilon t)}}\phi'(\chi)-f\phi'(\chi)\right]$$

$$= D_B \frac{b}{\nu_f(1-\epsilon t)}(C_w - C_\infty)\Bigg[\phi''(\chi) + \frac{D_T}{T_\infty}\frac{(T_w - T_\infty)}{D_B(C_w - C_\infty)}\theta''(\chi) - K_1\frac{\nu_f(1-\epsilon t)}{D_B b}\phi(\chi)\Bigg].$$

$$\Rightarrow \quad A\frac{\chi}{2}\phi'(\chi) - f\phi'(\chi) = \frac{1}{S_c}\Bigg[\phi''(\chi) + \frac{N_t}{N_b}\theta''(\chi) - K_c S_c \phi(\chi)\Bigg].$$

$$\Rightarrow \quad S_c\Bigg(A\frac{\chi}{2}\phi'(\chi) - f\phi'(\chi)\Bigg) = \phi''(\chi) + \frac{N_t}{N_b}\theta''(\chi) - K_c S_c \phi(\chi).$$

$$\Rightarrow \quad \phi''(\chi) + \frac{N_t}{N_b}\theta''(\chi) - K_c S_c \phi(\chi) - S_c\Bigg(A\frac{\chi}{2}\phi'(\chi) - f\phi'(\chi)\Bigg) = 0.$$

$$\Rightarrow \quad \phi''(\chi) = -\frac{N_t}{N_b}\theta''(\chi) + K_c S_c \phi(\chi) + S_c\Bigg(A\frac{\chi}{2}\phi'(\chi) - f\phi'(\chi)\Bigg). \tag{4.27}$$

$$\Rightarrow \quad \phi''(\chi) = -\frac{N_t}{N_b}\theta''(\chi) + K_c S_c \phi(\chi) + S_c\Bigg[\Bigg(A\frac{\chi}{2} - f\Bigg)\phi'(\chi)\Bigg]. \tag{4.28}$$

4.3.4 Dimensionless Form of Boundary Conditions

The following process converts the appropriate BCs into the non-dimensional form:

- $G_2(x,0) = V_w, \qquad at \quad y = 0.$

$$\Rightarrow \quad V_w = -\sqrt{\frac{b\nu_f}{1-\epsilon t}}f(0),$$

$$\Rightarrow \quad f(0) = -V_w\sqrt{\frac{1-\epsilon t}{b\nu_f}},$$

$$\Rightarrow \quad f(0) = S.$$

- $G_1(x,0) = U_w + N_w\Bigg(1 + \frac{\zeta}{\sqrt{2}}\frac{\partial G_1}{\partial y}\Bigg)\frac{\partial G_1}{\partial y}, \qquad at \quad y = 0.$

$$\Rightarrow \quad \frac{bx}{1-\epsilon t}f'(0) = \frac{bx}{1-\epsilon t} + N_w\Bigg(1 + \frac{\zeta}{\sqrt{2}}\frac{b^{\frac{3}{2}}}{\sqrt{\nu}_f(1-\epsilon t)^{\frac{3}{2}}}xf''(0)\Bigg)\frac{b^{\frac{3}{2}}}{\sqrt{\nu}_f(1-\epsilon t)^{\frac{3}{2}}}xf''(0).$$

$$\Rightarrow \quad \frac{bx}{1-\epsilon t}f'(0)$$

$$= \frac{bx}{1-\epsilon t} + \Lambda\sqrt{\frac{\nu_f(1-\epsilon t)}{b}}\Bigg(1 + \frac{\zeta}{\sqrt{2}}\frac{b^{\frac{3}{2}}}{\sqrt{\nu}_f(1-\epsilon t)^{\frac{3}{2}}}xf''(0)\Bigg)\frac{b^{\frac{3}{2}}}{\sqrt{\nu}_f(1-\epsilon t)^{\frac{3}{2}}}xf''(0).$$

$$\Rightarrow \qquad \frac{bx}{1-\epsilon t}f'(0) = \frac{bx}{1-\epsilon t} + \Lambda\frac{bx}{1-\epsilon t}\left(1 + \frac{\zeta}{\sqrt{2}}\frac{b^{\frac{3}{2}}}{\sqrt{\nu}_f(1-\epsilon t)^{\frac{3}{2}}}xf''(0)\right)f''(0).$$

$$\Rightarrow \qquad \frac{bx}{1-\epsilon t}f'(0) = \frac{bx}{1-\epsilon t}\left(1 + \Lambda\left(1 + \frac{\zeta}{\sqrt{2}}\frac{b^{\frac{3}{2}}}{\sqrt{\nu}_f(1-\epsilon t)^{\frac{3}{2}}}xf''(0)\right)\right)f''(0).$$

$$\Rightarrow \qquad f'(0) = 1 + \Lambda\left(f''(0) + \frac{\zeta}{\sqrt{2}}\frac{\sqrt{2}}{\sqrt{2}}\frac{\sqrt{b}}{\sqrt{\nu}_f(1-\epsilon t)^{\frac{1}{2}}}\frac{bx}{1-\epsilon t}(f''(0))^2\right).$$

$$\Rightarrow \qquad f'(0) = 1 + \Lambda\left(f''(0) + \frac{\zeta}{2}\frac{\sqrt{2b}}{\sqrt{\nu}_f(1-\epsilon t)^{\frac{1}{2}}}U_w(f''(0))^2\right).$$

$$\Rightarrow \qquad f'(0) = 1 + \Lambda\left(f''(0) + \frac{\lambda}{2}(f''(0))^2\right).$$

- $$\frac{\partial T}{\partial y} = -\frac{h_f}{k_0}(T_w - T), \qquad at \quad y = 0.$$

$$\Rightarrow \qquad \sqrt{\frac{b}{\nu_f(1-\epsilon t)}}\frac{b^*x}{1-\epsilon t}\theta'(0) = -\frac{h_f}{k_f}\left(\frac{b^*x}{1-\epsilon t} + T_\infty - \theta(0)\frac{b^*x}{1-\epsilon t} - T_\infty\right).$$

$$\Rightarrow \qquad \sqrt{\frac{b}{\nu_f(1-\epsilon t)}}\frac{b^*x}{1-\epsilon t}\theta'(0) = -\frac{h_f}{k_f}\left(\frac{b^*x}{1-\epsilon t} - \theta(0)\frac{b^*x}{1-\epsilon t}\right).$$

$$\Rightarrow \qquad \sqrt{\frac{b}{\nu_f(1-\epsilon t)}}\frac{b^*x}{1-\epsilon t}\theta'(0) = -\frac{h_f}{k_f}\frac{b^*x}{1-\epsilon t}(1 - \theta(0)).$$

$$\Rightarrow \qquad \theta'(0)(T_w - T_\infty) = -\frac{h_f}{k_f}\sqrt{\frac{\nu_f(1-\epsilon t)}{b}}(T_w - T_\infty)(1 - \theta(0)).$$

$$\Rightarrow \qquad \theta'(0) = -Bi(1 - \theta(0)).$$

- $$D_B\frac{\partial C}{\partial y} + \frac{D_T}{T_\infty}\frac{\partial T}{\partial y} = 0, \qquad at \quad \text{`}y = 0.$$

$$\Rightarrow \quad D_B(C_w - C_\infty)\sqrt{\frac{b}{\nu_f(1-\epsilon t)}}\phi'(0) = -\frac{D_T}{T_\infty}\frac{b^{\frac{3}{2}}x}{\sqrt{\nu_f}(1-\epsilon t)^{\frac{3}{2}}}\theta'(0).$$

$$\Rightarrow \quad \phi'(0) = -\frac{D_T}{T_\infty}\frac{T_w - T_\infty}{D_B(C_w - C_\infty)}\theta'(0).$$

$$\Rightarrow \quad \phi'(0) = -\frac{N_t}{N_b}\theta'(0).$$

$$\Rightarrow \quad \phi'(0) = \frac{N_t}{N_b}Bi(1 - \theta(0)).$$

- $G_1 \longrightarrow 0,$ $\qquad as \quad y \longrightarrow \infty.$

$\Rightarrow \quad f'(\chi) \longrightarrow 0, \qquad as \chi \longrightarrow \infty.$

- $T \to T_\infty, \qquad as \quad y \longrightarrow \infty.$

$\Rightarrow \quad \theta(\chi) \to 0, \qquad as \quad \chi \longrightarrow \infty.$

- $C \to C_\infty, \qquad as \quad y \longrightarrow \infty.$

$\Rightarrow \quad \phi(\chi) \to 0, \qquad as \quad \chi \longrightarrow \infty.$

Finally,

$$\left.\begin{aligned} & f(0) = S, \quad f'(0) = 1 + \Lambda\left(f''(0) + \frac{\lambda}{2}(f''(0))^2\right) \\ & \theta'(0) = -Bi(1-\theta(0)), \quad \phi(0) = \frac{N_t}{N_b} Bi(1-\theta(0)), \\ & f' \to 0, \quad \theta' \to 0, \quad \phi' \to 0, \quad as \quad \chi \to \infty. \end{aligned}\right\} \tag{4.29}$$

The quantities of physical interest; skin friction $Re_x^{\frac{1}{2}} C_{f_x}$, Nusselt number $Re_x^{-\frac{1}{2}} Nu_x$ and Sherwood number $Re_x^{-\frac{1}{2}} Sh_x$ are comparable in the dimensionless form, as covered in Chapter 3.

4.4 Solution Framework

The numerical answers are computed using the shooting method by the application of the fourth-order Runge-Kutta approach. Figure 4.4 elaborates and shows the shooting method's computational process. The first step in solving the ODE (4.20) has been to take into consideration the following notations:

$$f = F_1, \quad f' = F_1' = F_2, \quad f'' = F_1'' = F_2' = F_3.$$

The momentum equation is transformed into the system of first ODEs as shown below:

$F_1' = F_2, \qquad F_1(0) = S.$

$$F_2' = F_3, \qquad F_2(0) = 1 + \Lambda\left(F_3(0) + \frac{\lambda}{2}(F_3(0))^2\right).$$

$$F_3' = -\frac{1}{1+\lambda F_3}\left[P_a P_b\left(F_1 F_3 - (F_2)^2 - A\left(\frac{\chi}{2}F_3 + F_2\right) - \frac{P_e}{P_b}MF_2 - Fr(F_2)^2\right) - KF_2\right],$$

$$F_3(0) = p.$$

The above IVP will be numerically solved using the Runge-Kutta method of order four. The problem domain is considered confined when $\chi = \chi_\infty$, that is, $[0,\ \chi_\infty]$, where χ_∞ is a positive real integer and the variation in the solution is small.

It is necessary to select the missing condition p such that.

$$F_2(\chi_\infty, p) = 0.$$

Newton's method will be used to update the missing p, using the following iterative scheme.

$$p_{n+1} = p_n - \frac{F_2(\chi_\infty, p_n)}{\left(\frac{\partial}{\partial p}F_2(\chi_\infty, p)\right)_{p=p_n}}. \tag{4.30}$$

We further introduce the following notations:

$$\frac{\partial F_1}{\partial p} = F_4, \quad \frac{\partial F_2}{\partial p} = F_5, \quad \frac{\partial F_3}{\partial p} = F_6.$$

Hence the iterative scheme (4.21) will get the form:

$$p_{n+1} = p_n - \frac{F_2(\chi_\infty, p_n)}{F_5(\chi_\infty, p)}. \tag{4.31}$$

Presently, in arrange to build another framework of Odes, differentiate the ultimate system of the first order ODEs with respect to p. It appears like typically the case:

$$F_4' = F_5, \qquad F_4(0) = 0.$$

$$F_5' = F_6, \qquad F_5(0) = \Lambda(1+\lambda F_6(0)).$$

$$F_6' = -\frac{1}{(1+\lambda F_3)^2}((1+\lambda F_3)(P_aP_b(F_4F_3+F_1F_6-2F_2F_5-A(\frac{\chi}{2}F_6+F_5))-KF_5)$$

$$-(\lambda F_6)(P_aP_b(F_1F_3-F_2^2-A(\frac{\chi}{2}F_3+F_2)+KF_2)), \qquad F_6(0)=1.$$

The stoping criteria for Newton's techniqye is set as:

$$|F_2(\chi_\infty, p)| < \epsilon,$$

where $\epsilon > 0$ is an arbitrarily small positive number.

The ordinary differential equations (4.26) and (4.28) are coupled in θ and ϕ. For numerical solution of these coupled ODEs, we will use the shooting technique, assuming f, f' and f'' as the known functions. The following notations have been taken:

$$\theta = T_1,\ \theta' = T_1' = T_2,\ \phi = T_3,\ \phi' = T_3' = T_4$$

Next, we convert the equations (4.26) and (4.28) into the system of first-order coupled ODEs that follows:

$$T_1' = T_2, \qquad T_1(0) = d.$$

$$T_2' = -\frac{P_cP_r}{P_d\left(1+\frac{P_rN_r}{P_d}-\beta\frac{P_rP_c}{P_d}(F_1)^2\right)}\left[\frac{E_c}{P_aP_c}(F_3)^2-\beta((F_2)^2T_1-F_1F_2T_2-F_1F_3T_1)\right.$$

$$\left.-A\left(T_1+\frac{\chi}{2}T_2\right)+F_2T_1-F_1T_2\right], \qquad T_2(0) = -B_i(1-T_1(0)).$$

$$T_3' = T_4, \qquad T_3(0) = s.$$

$$T_4' = K_cS_cT_3+S_c\left(A\frac{\chi}{2}-F_1\right)T_4+\frac{N_t}{N_b}\frac{P_cP_r}{P_d\left(1+\frac{P_rN_r}{P_d}-\beta\frac{P_rP_c}{P_d}(F_1)^2\right)}\left(\frac{E_c}{P_aP_c}(F_3)^2\right.$$

$$\left.-\beta((F_2)^2T_1-F_1F_2T_2-F_1F_3T_1)-A\left(T_1+\frac{\chi}{2}T_2\right)+F_2T_1-F_1T_2\right),$$

$$T_4(0) = \frac{N_t}{N_b}B_i(1-T_1(0)).$$

In order to use the fourth-order Runge-Kutta method for the numerical solution of the initial value problem that was previously mentioned, it is necessary to carefully choose

the conditions d and s in the equation system. In the given system of equations, the absent conditions d and s must be selected in a way that guarantees:

$$T_1(\chi_\infty, d) = 0, \quad T_3(\chi_\infty, s) = 0.$$

Newton's method will be used to find d and s. This method has the following iterative scheme.

$$\begin{bmatrix} d \\ s \end{bmatrix}_{(n+1)} = \begin{bmatrix} d \\ s \end{bmatrix}_{(n)} - \begin{bmatrix} \frac{\partial T_1}{\partial d} & \frac{\partial T_1}{\partial s} \\ \frac{\partial T_3}{\partial d} & \frac{\partial T_3}{\partial s} \end{bmatrix}^{-1}_{(n)} \begin{bmatrix} T_1 \\ T_3 \end{bmatrix}_{(n)}.$$

Furthermore, the following notations will be useful for computing the entries of the Jacobian matrix:

$$\begin{aligned} &\frac{\partial T_1}{\partial d} = T_5, \quad \frac{\partial T_2}{\partial d} = T_6, \quad \frac{\partial T_3}{\partial d} = T_7, \quad \frac{\partial T_4}{\partial d} = T_8, \\ &\frac{\partial T_1}{\partial s} = T_9, \quad \frac{\partial T_2}{\partial s} = T_{10}, \quad \frac{\partial T_3}{\partial s} = T_{11}, \quad \frac{\partial T_4}{\partial s} = T_{12}. \end{aligned}$$

Newton's iterative scheme will change the form after utilizing the above mentioned notations as follows:

$$\begin{bmatrix} d \\ s \end{bmatrix}_{(n+1)} = \begin{bmatrix} d \\ s \end{bmatrix}_{(n)} - \begin{bmatrix} T_5 & T_9 \\ T_7 & T_{11} \end{bmatrix}^{-1}_{(n)} \begin{bmatrix} T_1 \\ T_3 \end{bmatrix}_{(n)}. \tag{4.32}$$

$$T_5 = T_6, \qquad T_5(0) = 1.$$

$$T_6' = -\frac{P_c P_r}{P_d\left(1 + \frac{P_r N_r}{P_d} - \beta\frac{P_r P_c}{P_d}(F_1)^2\right)}\Big[-\beta\big((F_2)^2 T_5 - F_1F_2T_6 - F_1F_3T_5\big) - A\left(T_5 + \frac{\chi}{2}T_6\right) + F_2T_5 - F_1T_6\Big], \qquad T_6(0) = -B_i.$$

$$T_7' = T_8, \qquad T_7(0) = 0.$$

$$T_8' = K_cS_cT_7 + S_c\left(A\frac{\chi}{2} - F_1\right)T_8 + \frac{N_t}{N_b}\frac{P_c P_r}{P_d\left(1 + \frac{P_r N_r}{P_d} - \beta\frac{P_r P_c}{P_d}(F_1)^2\right)}\Big[-\beta\big((F_2)^2T_5 - F_1F_2T_6 - F_1F_3T_5\big) - A\left(T_5 + \frac{\chi}{2}T_6\right) + F_2T_5 - F_1T_6\Big], \qquad T_8(0) = \frac{N_t}{N_b}B_i.$$

$$T_9 = T_{10}, \qquad T_9(0) = 0.$$

$$T'_{10} = - \quad \frac{P_c P_r}{P_d\left(1+\frac{P_r N_r}{P_d}-\beta\frac{P_r P_c}{P_d}(F_1)^2\right)}\Bigg[-\beta((F_2)^2 T_9 - F_1F_2T_{10} - F_1F_3T_9)$$

$$-A\left(T_9+\frac{\chi}{2}T_{10}\right)+F_2T_9-F_1T_{10}\Bigg] \qquad T_{10}(0)=0.$$

$$T'_{11} = T_{12}, \qquad T_{11}(0)=1.$$

$$T'_{12} = K_cS_cT_{11}+S_c\left(A\frac{\chi}{2}-F_1\right)T_{12}+\frac{N_t}{N_b}\frac{P_cP_r}{P_d\left(1+\frac{P_rN_r}{P_d}-\beta\frac{P_rP_c}{P_d}(F_1)^2\right)}\Bigg[-\beta((F_2)^2T_9$$

$$-F_1F_2T_10-F_1F_3T_9)-A\left(T_9+\frac{\chi}{2}T_10\right)+F_2T_9-F_1T_10\Bigg], \qquad T_{12}(0)=0.$$

The following is the set of stopping criteria for Newton's method:

$$max\,\{\mid T_1(\xi_\infty,d)\mid,\mid T_3(\xi_\infty,s)\mid\}<\epsilon.$$

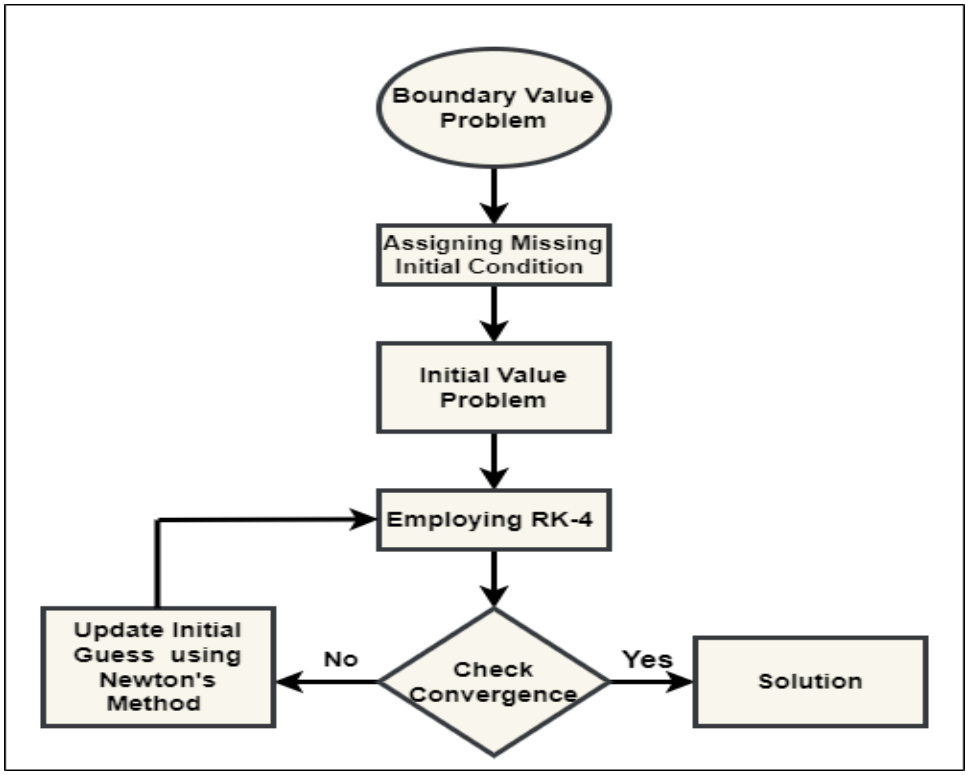

FIGURE 4.2: The shooting method's methodological framework

4.5 Numerical Results and Discussion

The governing partial differential equations (PDEs) characterizing the fluid flow lead to a system of ordinary differential equations (ODEs) with numerous significant parameters.

The implications of these physical factors on the distributions of nanoparticle concentration $\phi(\chi)$, temperature $\theta(\chi)$, and velocity $f'(\chi)$ are thoroughly examined using graphical representations. The study's findings are given in a thorough way, accompanied with an in-depth explanation of the importance and interpretations of each parameter's impact. This analysis provides a thorough understanding of how each parameter contributes to shaping the velocity, temperature and nanoparticle concentration profiles, offering valuable insights into the intricate dynamics of the hybrid nanofluid system under consideration.

4.5.1 Analysis of Computational Results

Here, an investigation is conducted to demonstrate how different physical properties affect the local Sherwood number, the local Nusselt number, and the coefficient of skin friction. Skin friction varies significantly when the Forchheimer parameter and magnetic field coefficient are taken into account. Table 4.4 shows the impact of changing different dimensionless parameters on the skin friction coefficient $C_f(Re_x)^{\frac{1}{2}}$. The skin friction coefficient numerical results which are displayed in Table 4.4 are generated by the shooting technique of the MATLAB software. The table indicates that when the values of the magnetic parameter M, the Forchheimer flow parameter Fr, the Williamson parameter λ, and the velocity slip Λ increase, the skin friction coefficient drops.

TABLE 4.4: The impact of some embedded parameters on local Nusselt when $M = \lambda = \Lambda = Fr = 0.1$ and $A = 0.1$.

Bi	Nr	Ec	β	$Re_x^{-1/2}Nu_x$ HNF	$Re_x^{-1/2}Nu_x$ NF
0.2	0.3	0.1	0.01	0.3553	0.2794
0.4				0.6330	0.5017
0.6				0.8559	0.6827
	0.1			0.3071	0.2419
	0.5			0.4025	0.3159
		0.3		0.3002	0.2415
		0.4		0.2726	0.2225
			0.2	0.3623	0.2844
			0.6	0.3739	0.2928

TABLE 4.5: The numerical results of the skin friction $\left(C_f\sqrt{Re_x}\right)$ when $Pr = 6.5, \Omega = 1$, $K = S = 0.1$.

λ	Λ	A	Fr	M	ϕ_1	ϕ_2	$Re^{1/2}Cf_x$ HNF	$Re^{1/2}Cf_x$ NF
0.1	0.1	0.2	0.1	0.1	0.09	0.09	-1.7340	-1.4943
0.3							-1.6653	-1.4294
0.4							-1.6224	-1.3868
	0						-2.0170	-1.7654
	3						-1.3675	-1.1562
		0.3					-1.3946	-1.5278
		0.4					-1.8093	-1.5607
			0.3				-1.7983	-1.5292
			0.5				-1.8507	-1.5955
				0.2			-1.7840	-1.5292
				0.3			-1.8321	-1.5630
					0.06		-1.5670	-1.3417
					0.03		-1.4074	-0.1945
						0.03	-1.5677	-
						0.06	-1.6473	-

TABLE 4.6: The impact of some embedded parameters on Sherwood number when $M = \lambda = \Lambda = Fr = 0.1,\ A = 0.1,\ Nr = 0.2, Bi = 0.2, Ec = 0.1, \beta = 0.01$.

Sc	Kc	Nt	Nb	$Re_x^{-1/2}Sh_x$ HNF	$Re_x^{-1/2}Sh_x$ NF
3	1	0.5	0.2	0.1333	0.1301
5				0.1076	0.1057
7				0.0925	0.0913
	7			0.0769	0.0767
	9			0.0695	0.0696
		0.7		0.1866	0.1821
		0.9		0.2399	0.2342
			0.3	0.0380	0.0371
			0.7	0.0296	0.0289

Velocity Profile:

The effect of volume fraction ϕ on the velocity profile is seen in Figure 4.3. Figure 4.3 illustrates an increasing trend in the velocity profile with an increase in the value of ϕ. Figure 4.4 illustrates the impact of λ on the velocity profile. It is evident that as λ increases, the velocity profile decreases. Figure 4.5 illustrates the declining tendency of the fluid motion. The velocity profile falls as Λ increases. The influence of the Forchheimer parameter Fr on the velocity profile is seen in Figure 4.6. The results show that the velocity profile exhibits a declining trend as the value of Fr increases. This behavior is due to the direct relationship between the inertia coefficient and the drag coefficient. An increasing Fr value results in an increase in the fluid's resistive force and drag coefficient. The fluid experiences greater flow resistance as a result, which reduces its velocity.

Figure 4.7 illustrates how the magnetic parameter M affects the velocity profile. The transverse magnetic field's strength is determined by the magnetic parameter M, and it gets weaker as fluid velocity increases. The fluid dynamics in this scenario is significantly influenced by the Lorentz force. The Lorentz force, which is produced when an applied transverse magnetic field causes electrically conducting nanofluids to react as a resistive force, is to blame for this. It is shown in Figure 4.8 how A influences the velocity profile. The velocity profile rises as A does, as seen in Figure 4.8.

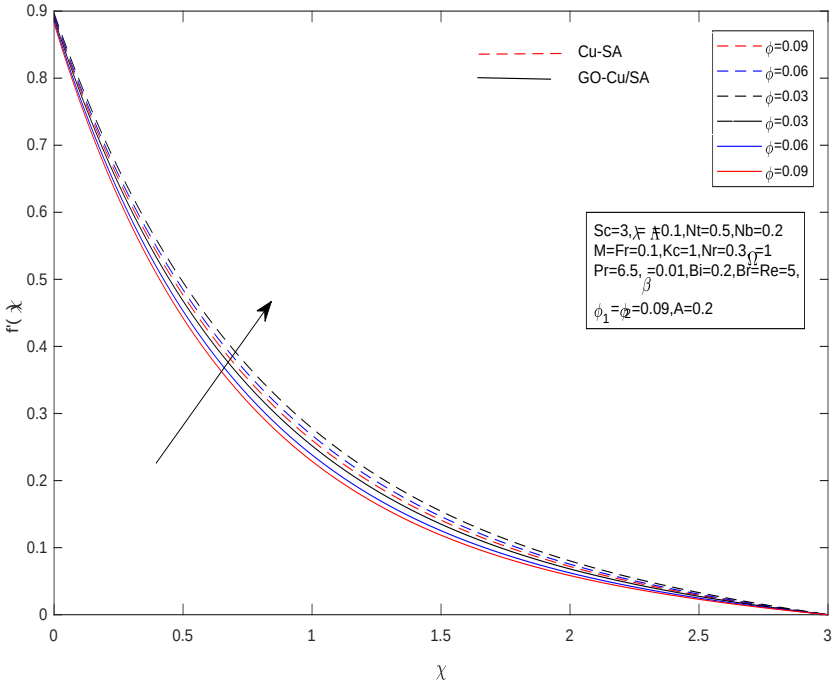

FIGURE 4.3: Impact of ϕ on $f'(\chi)$

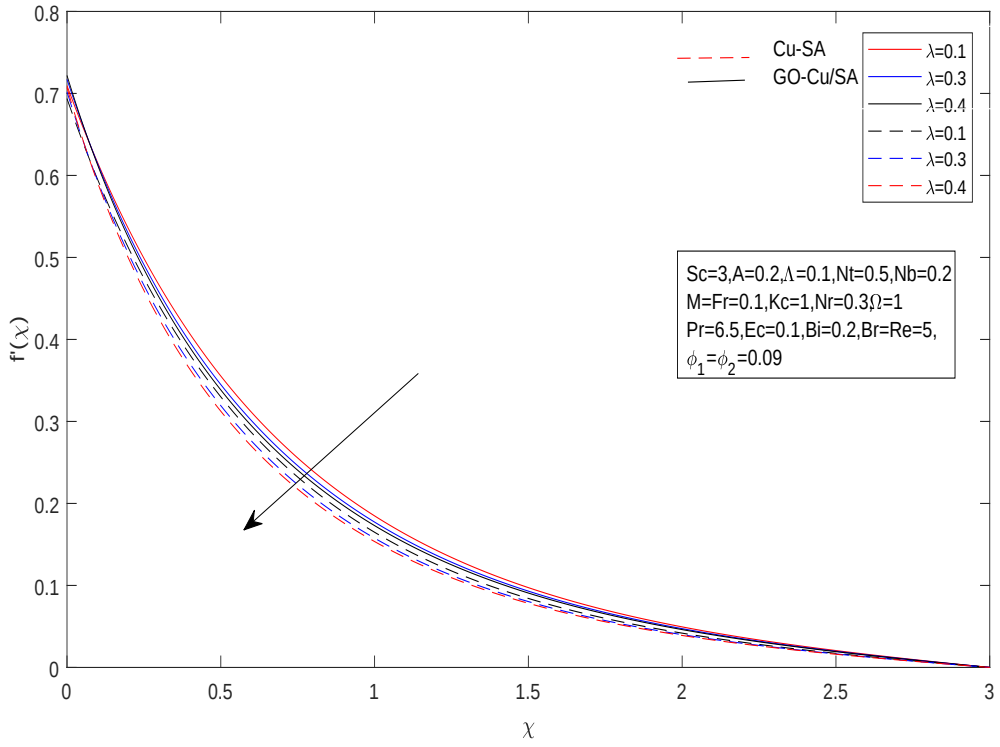

FIGURE 4.4: Impact of λ on $f'(\chi)$

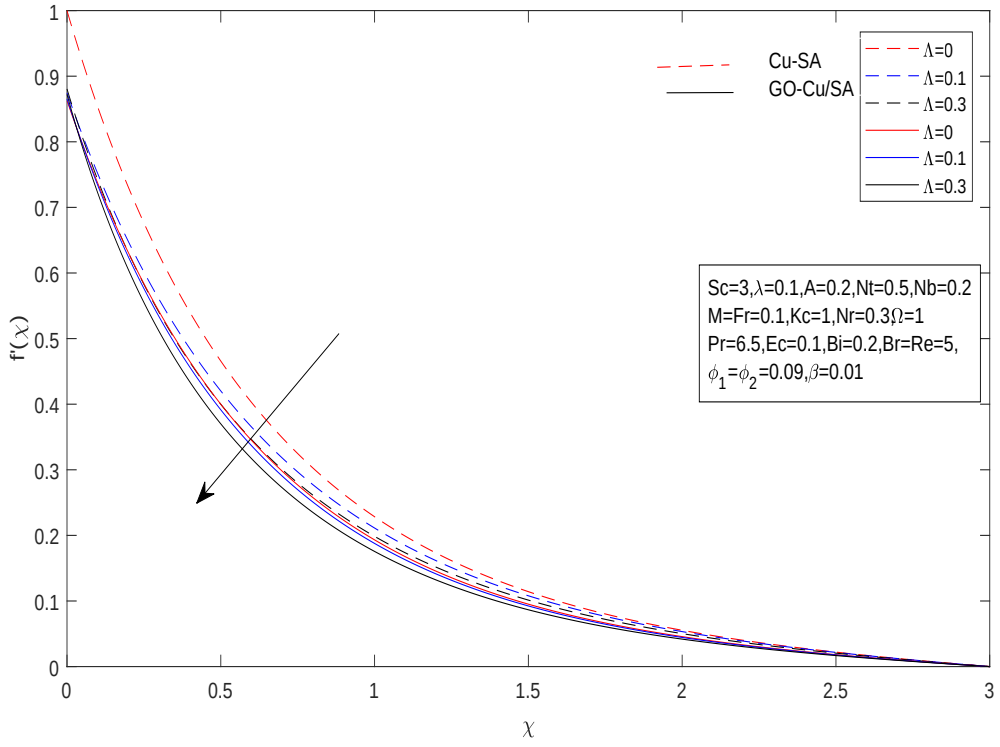

FIGURE 4.5: Impact of Λ on $f'(\chi)$

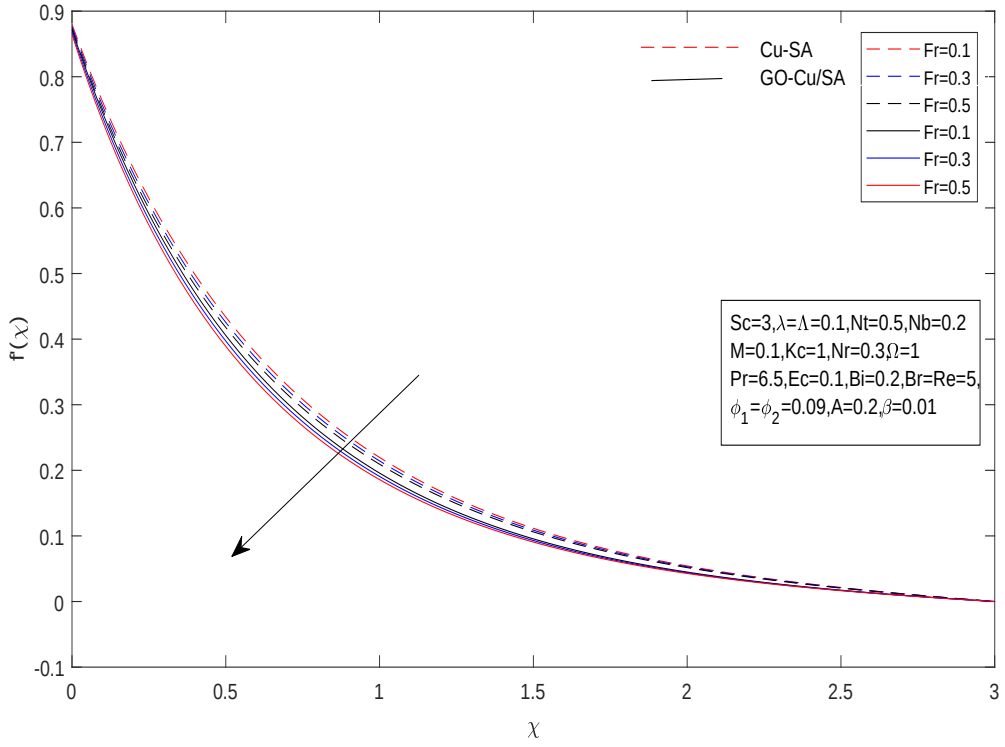

FIGURE 4.6: Impact of Fr on $f'(\chi)$

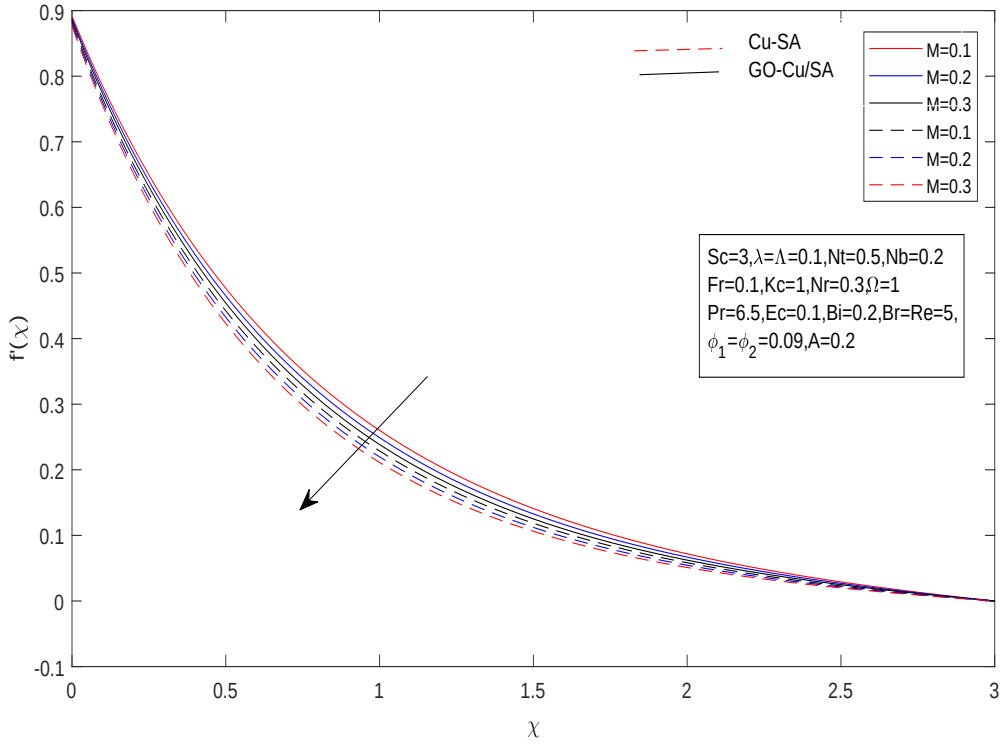

FIGURE 4.7: Impact of M on $f'(\chi)$

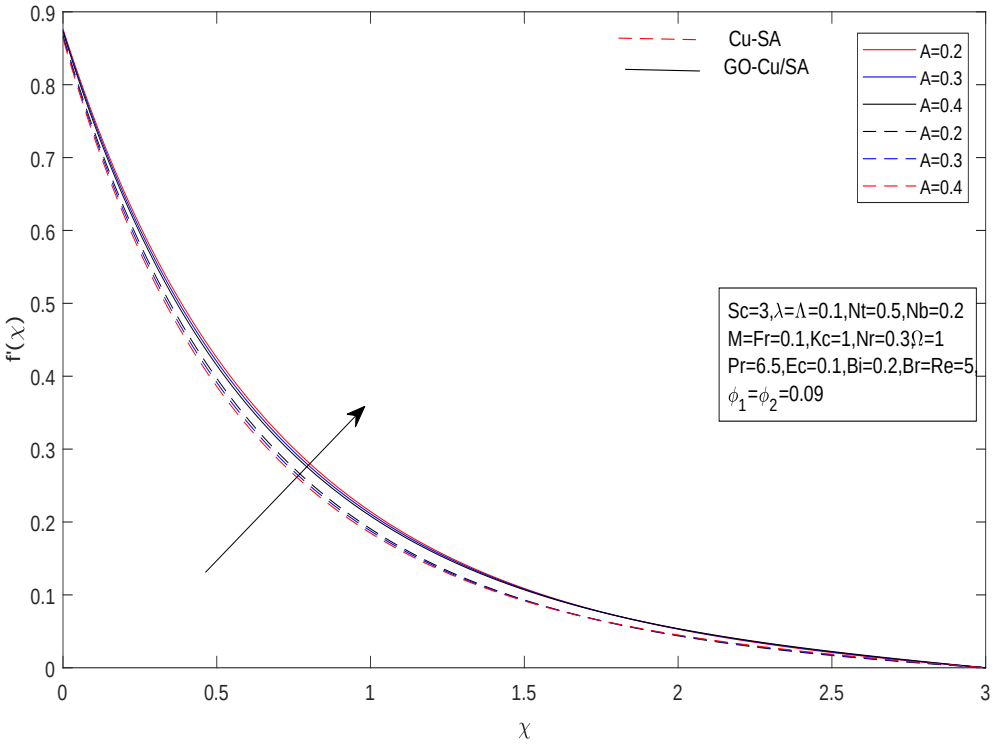

FIGURE 4.8: Impact of A on $f'(\chi)$

Temperature Profile, and entropy generation:

As the Eckert number rises, the temperature profile falls. The connection between kinetic energy and enthalpy change of flow is shown by the Eckert number, which falls as its value rises (Fig. 4.9). The growth of the entropy generation with increasing Eckert number value is seen in Figure 4.10. As we can see in Figures 4.11, 4.12, and 4.13, the temperature profile is affected by β, ϕ, and Λ. The temperature profile decreases as β, ϕ, and Λ increase. The effects of λ on the temperature profile and entropy generation are depicted in Figures 4.14 and 4.15. As can be shown in Figures 4.14 and 4.15, a rise in the value of λ causes an increase in the temperature profile and entropy generation. The effect of Bi on the temperature profile is shown in Figure 4.16. It is observed that the temperature profile rises with increasing Bi values.

The impacts of ϕ, Br, and Re are used to show the entropy generation in Figures 4.17, 4.18, and 4.19. Figures 4.17, 4.18, and 4.19 demonstrate that entropy generation increases with ϕ, Br, and Re levels.

The effect of the thermal radiation parameter Nr on the temperature profile is shown

in Figure 4.20. The relationship between the production of q entropy and the thermal radiation parameter Nr is shown in Figure 4.21.

The thermal radiation parameter Nr represents the effect of thermal radiation on heat transmission. An increase in Nr values indicates that heat radiation is having a greater impact or intensity.

Thermal radiation is the process by which electromagnetic waves transfer heat, and higher Nr values indicate more effective radiation-induced heat transfer. In Figure 4.22, the effect of Λ on entropy generation is illustrated. Figure 4.22 illustrates how the generation of entropy decreases as Λ increases.

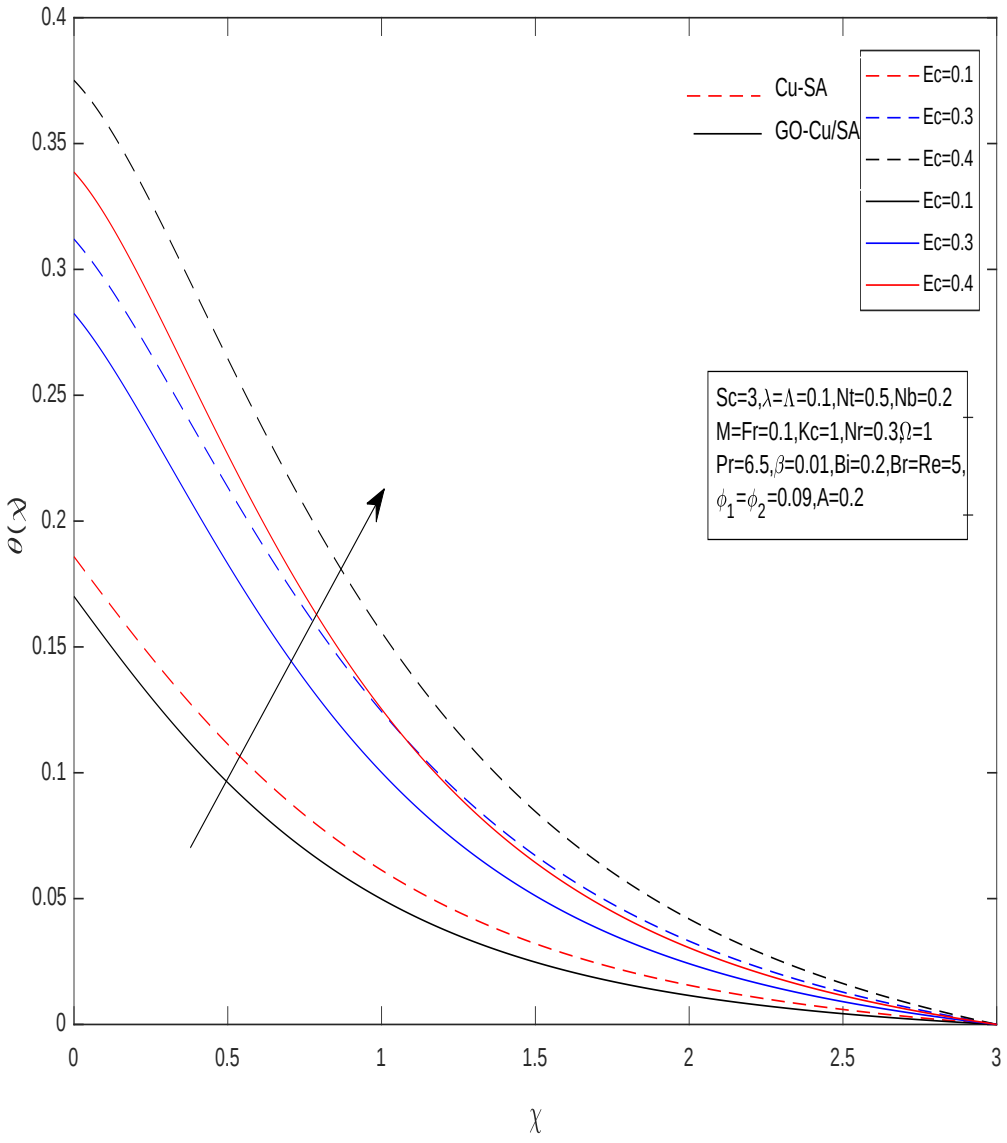

FIGURE 4.9: Impact of Ec on $\theta(\chi)$

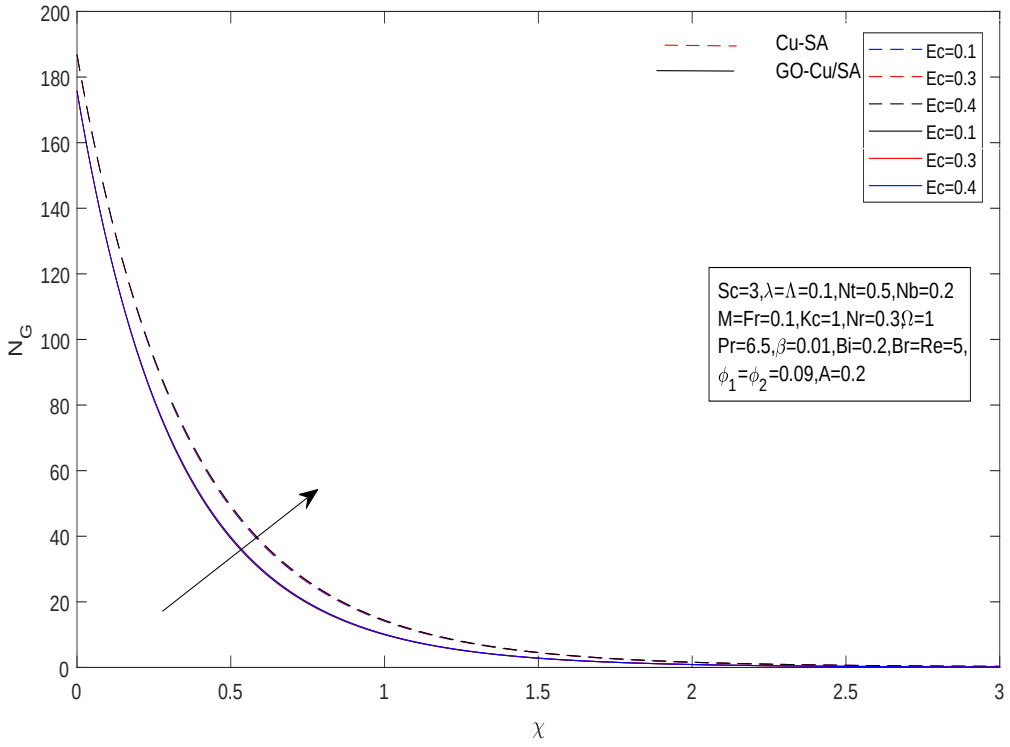

FIGURE 4.10: Impact of Ec on N_G

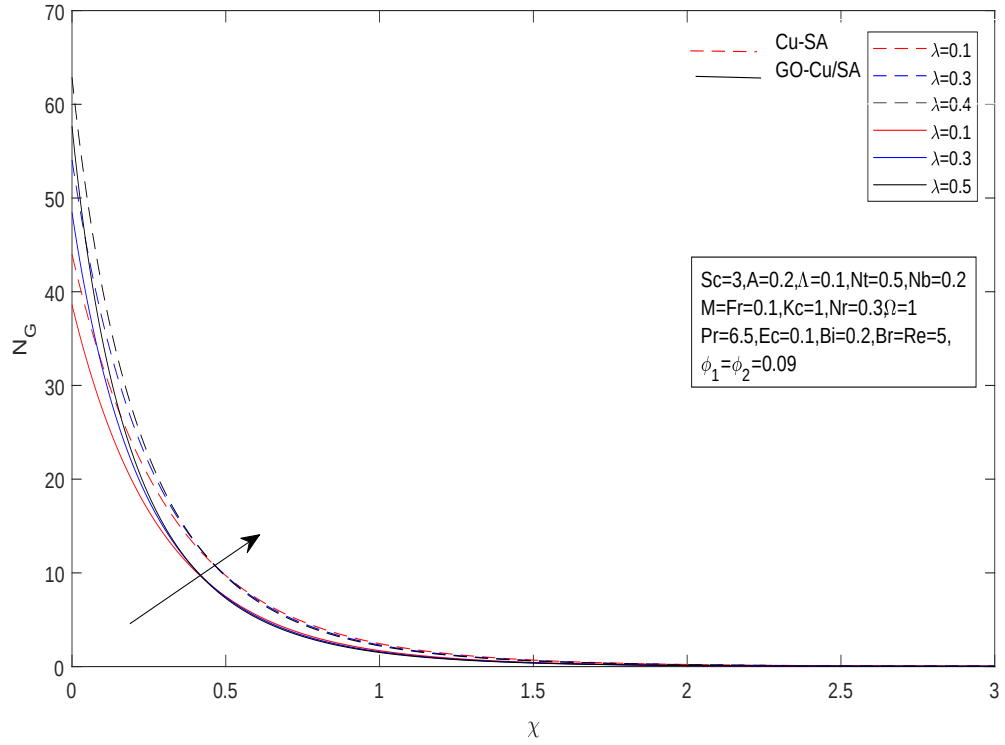

FIGURE 4.11: Impact of β on $\theta(\chi)$

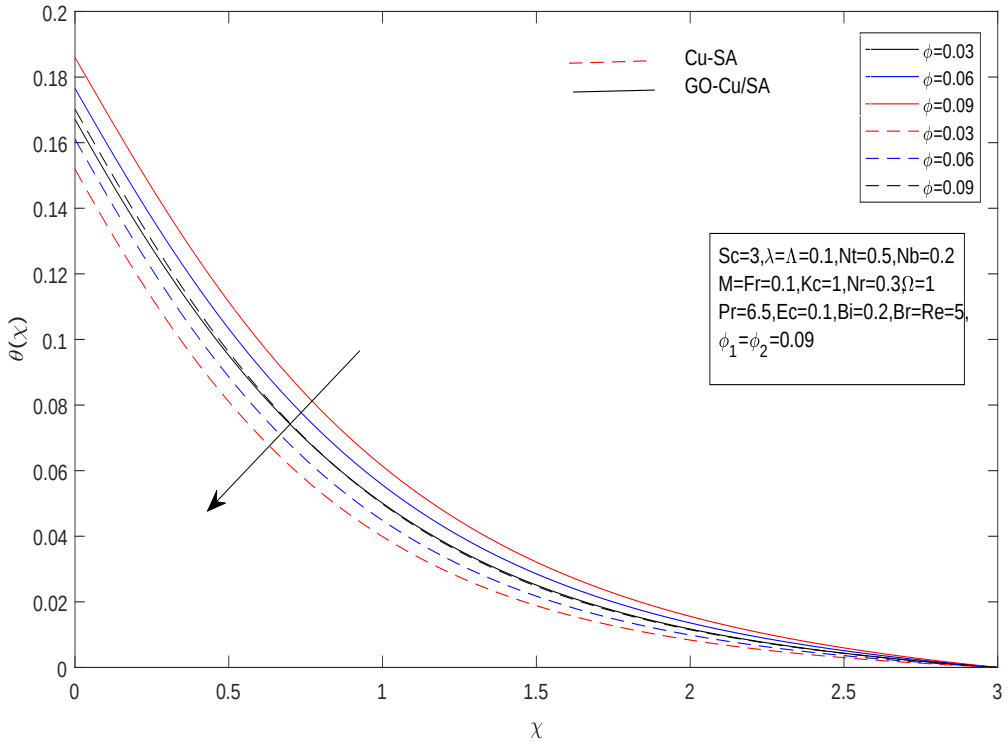

FIGURE 4.12: Impact of ϕ on $\theta(\chi)$

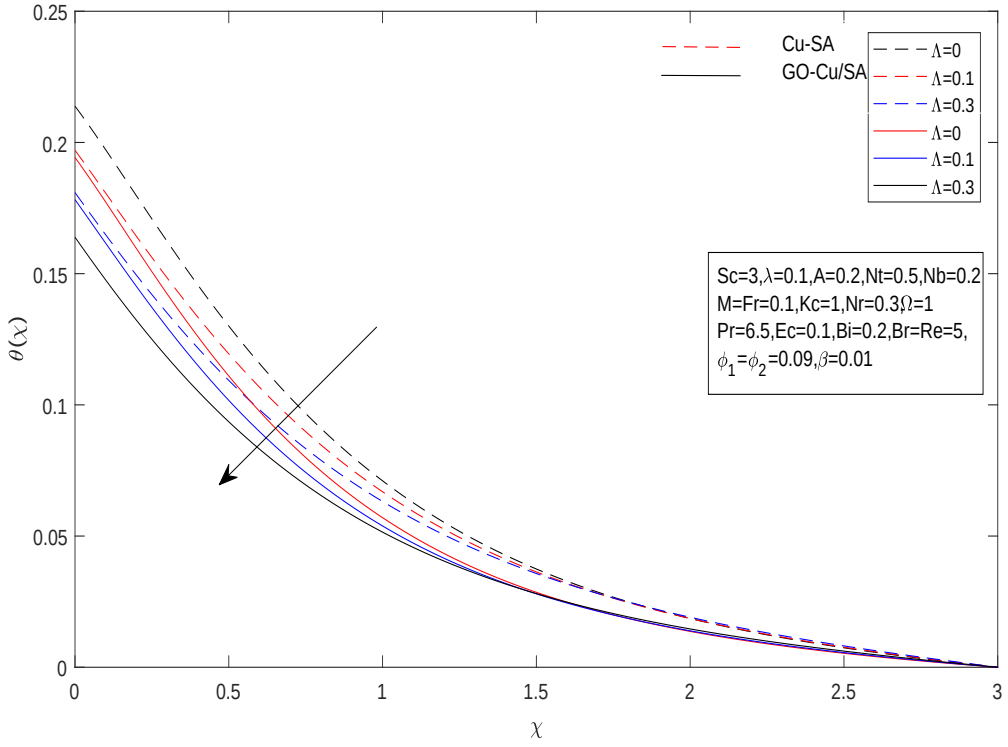

FIGURE 4.13: Impact of Λ on $\theta(\chi)$

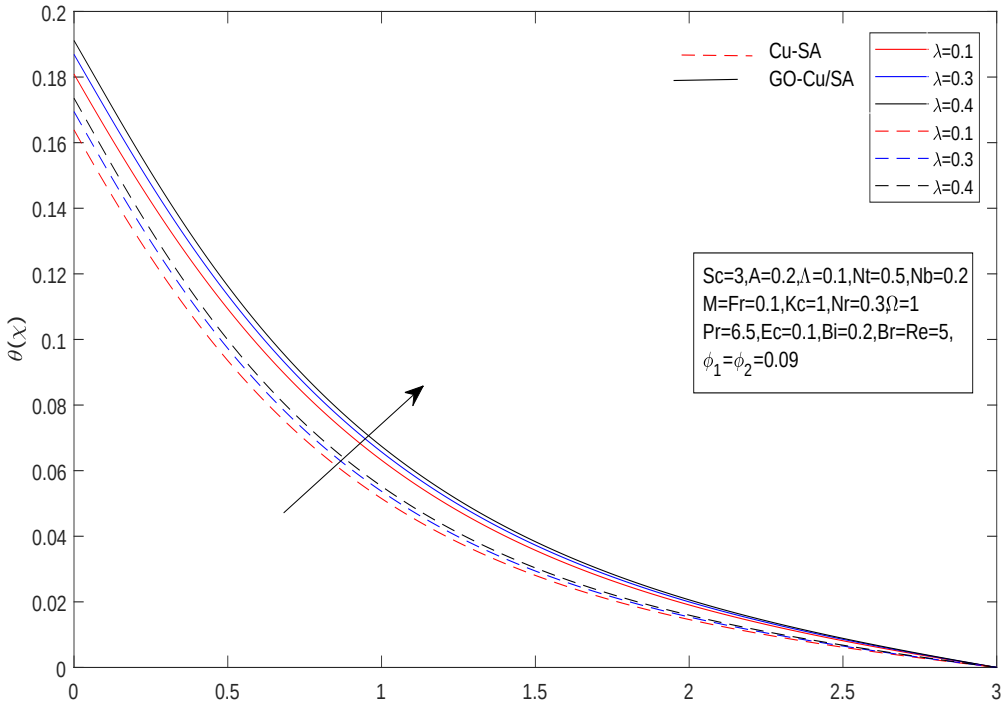

FIGURE 4.14: Impact of λ on $\theta(\chi)$

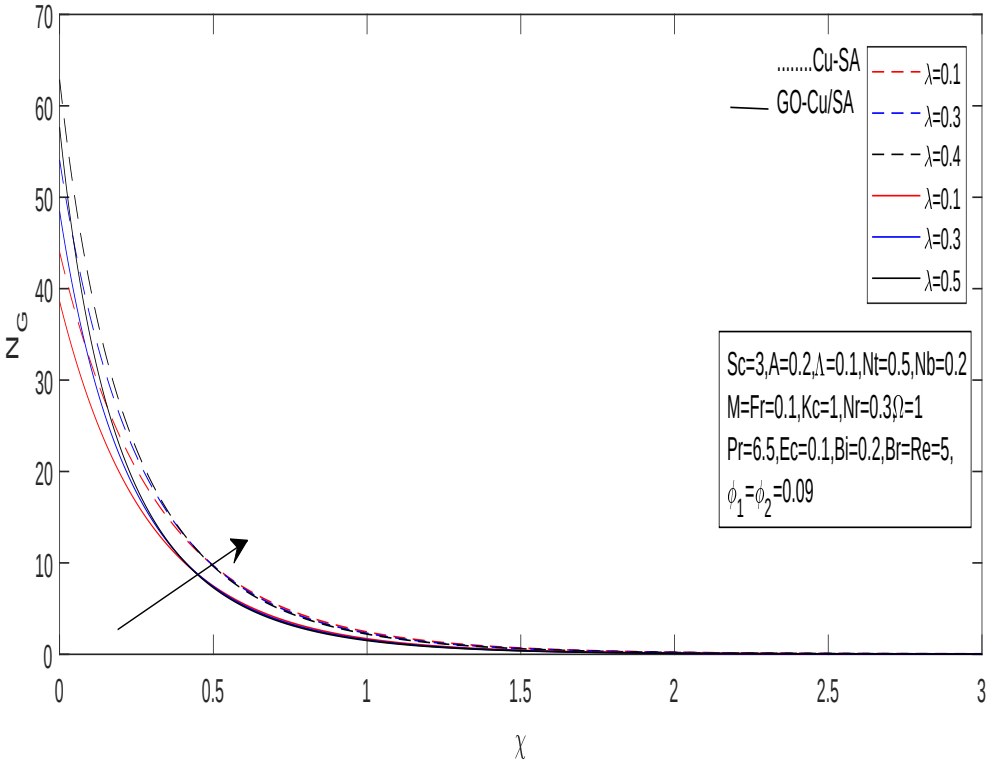

FIGURE 4.15: Impact of λ on N_G

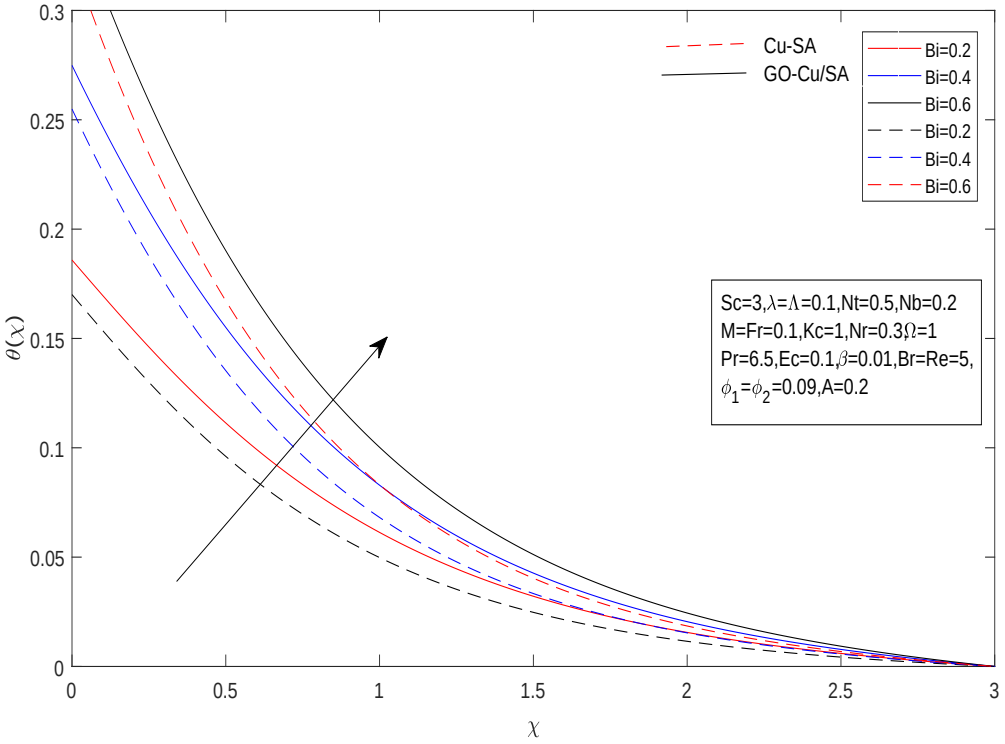

FIGURE 4.16: Impact of Bi on $\theta(\chi)$

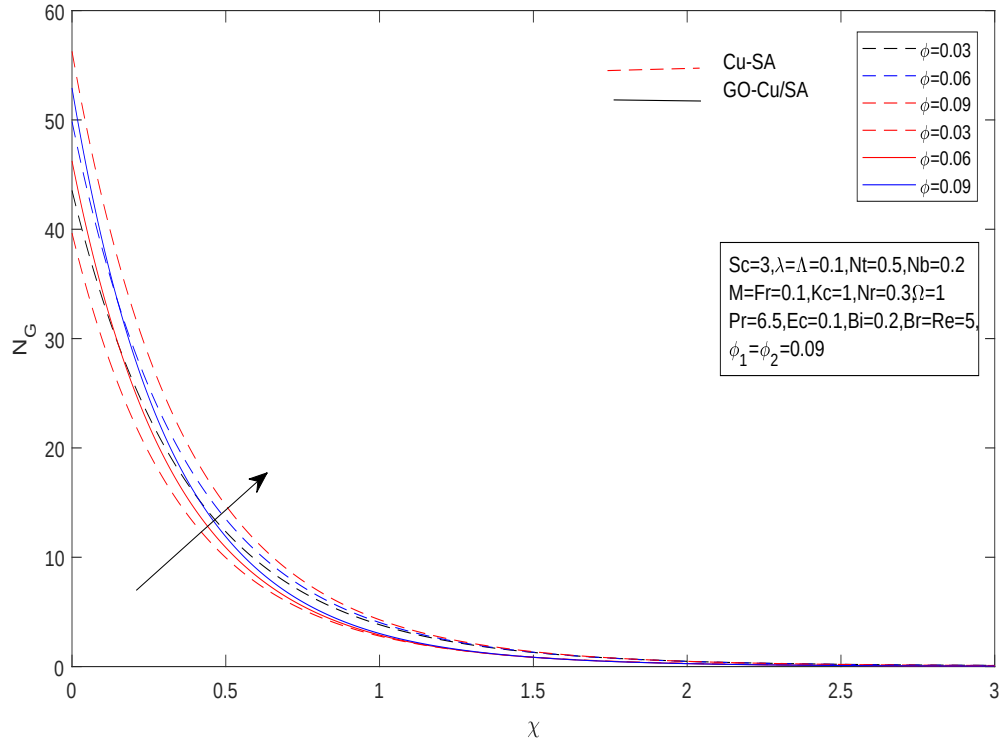

FIGURE 4.17: Impact of ϕ on N_G

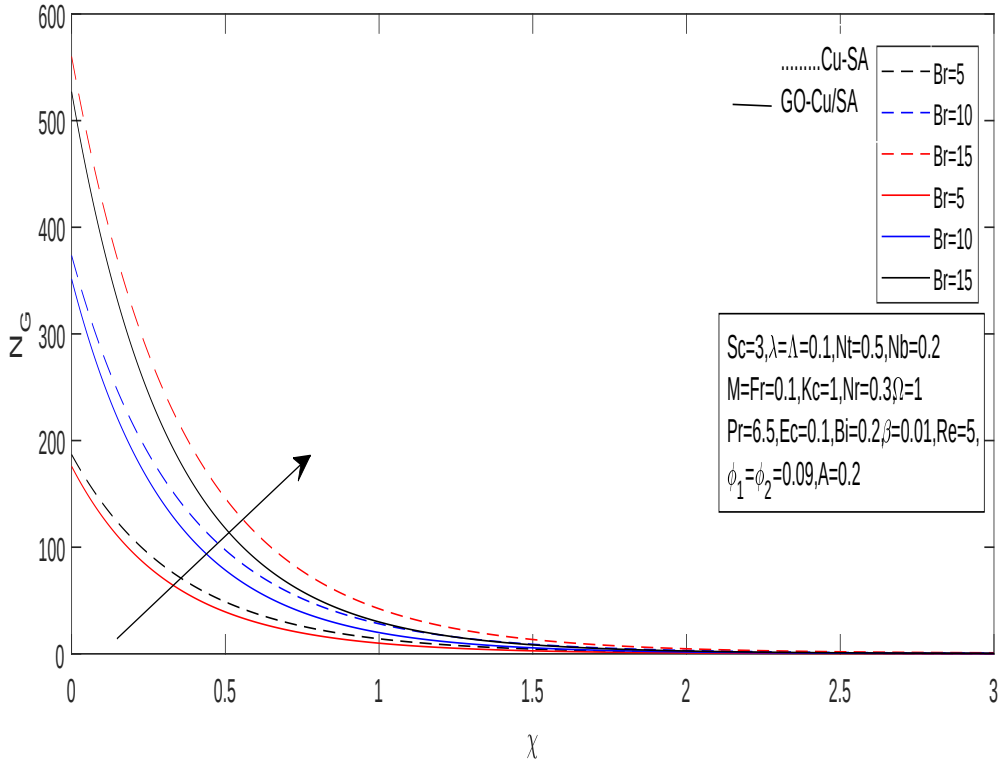

FIGURE 4.18: Impact of Br on N_G

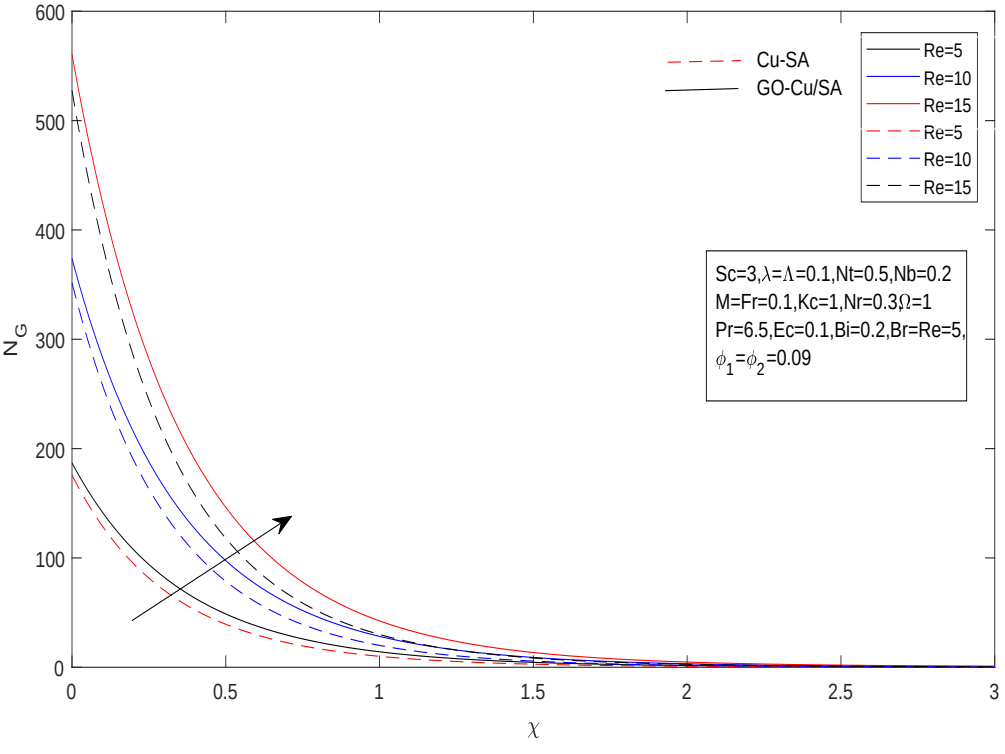

FIGURE 4.19: Impact of Re on N_G

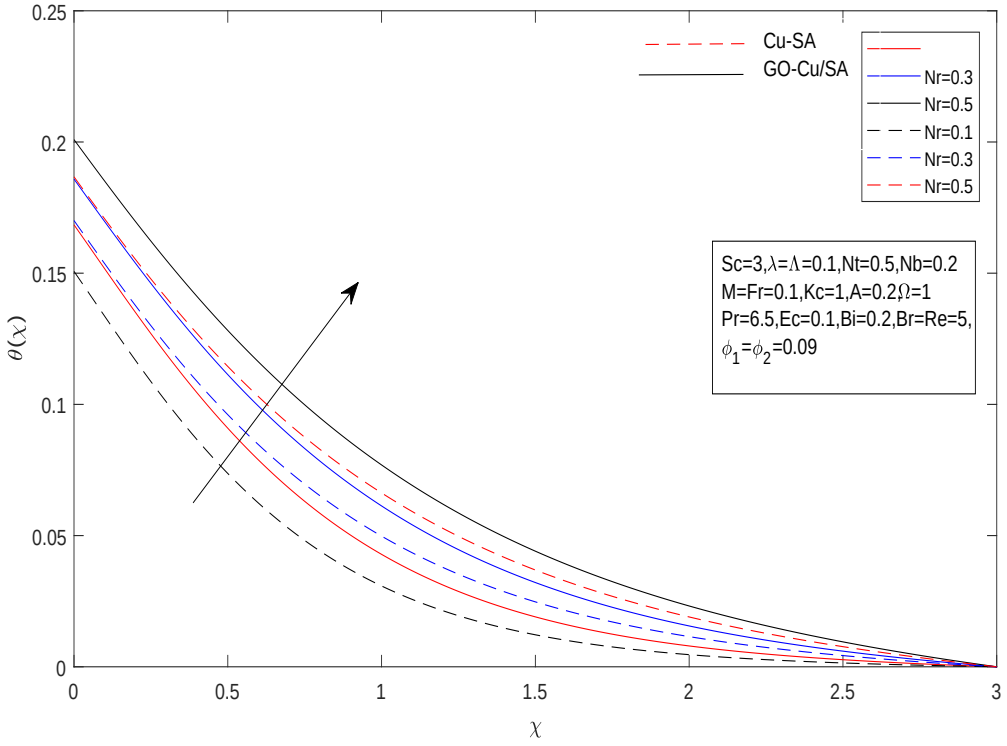

FIGURE 4.20: Impact of Nr on $\theta(\chi)$

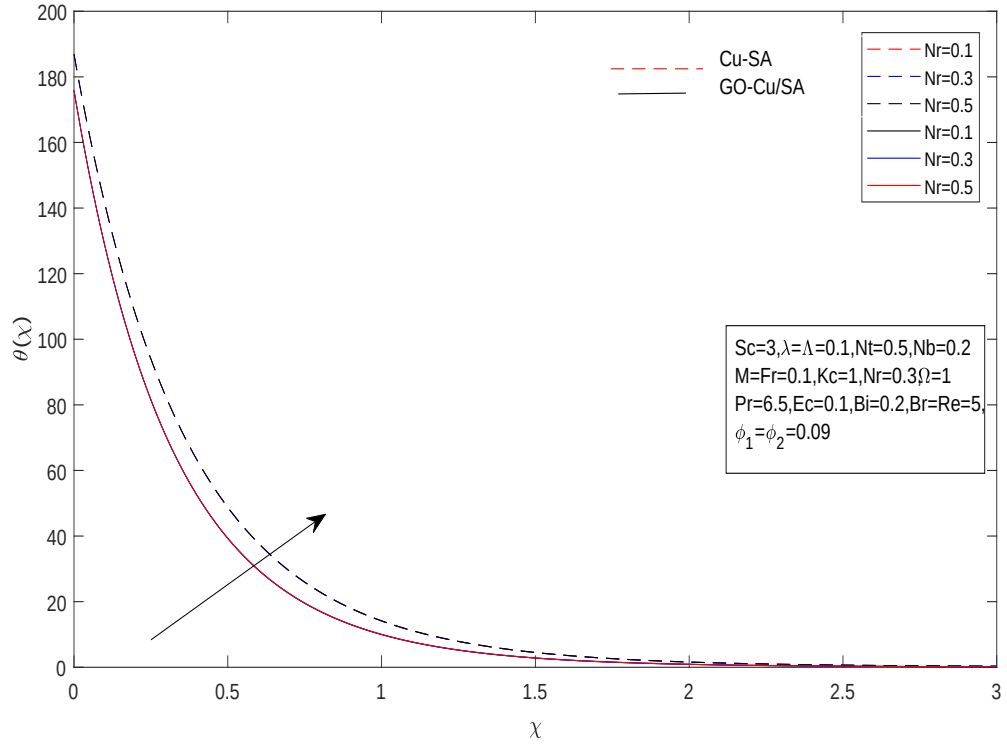

FIGURE 4.21: Impact of Nr on N_G

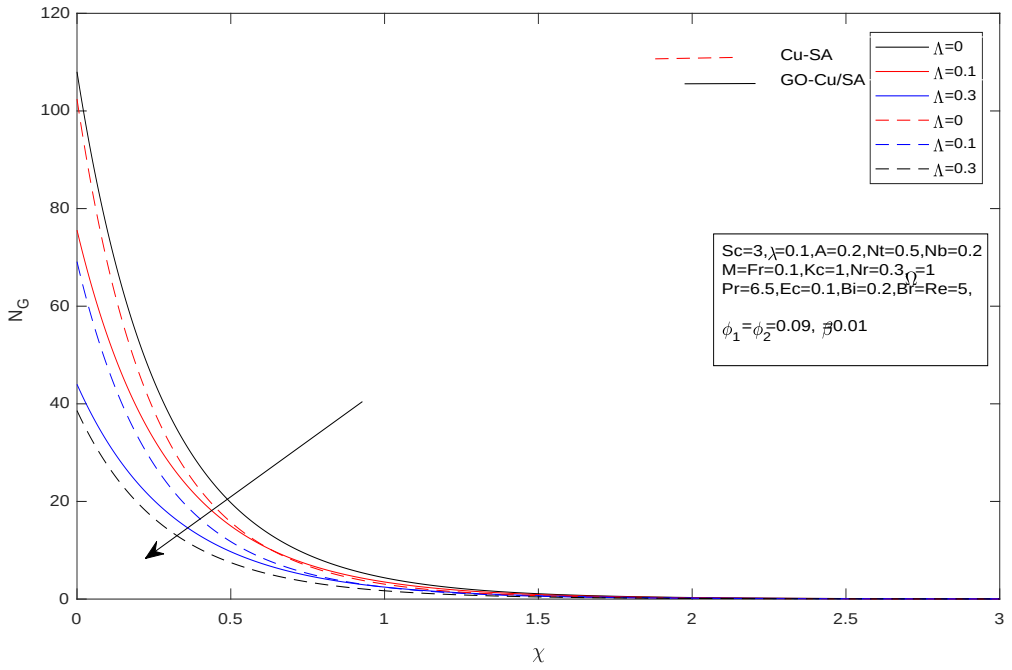

FIGURE 4.22: Impact of Λ on N_G

Concentration profile:

In this section, the impact of different dimensionless parameters on the concentration profile has been briefly addressed. The following is a line-up of the concentration profile results from the graphs plotted against changes in various dimensionless parameters.

Figure 4.23 illustrates how the fluid's nanoparticle concentration distribution is affected by the Brownian motion parameter (Nb). An increase in Nb leads to a decrease in the concentration of nanoparticles. Brownian motion is the term used in physics to describe the random movement of nanoparticles in a fluid. An increase in the Brownian motion parameter allows for greater freedom of motion for nanoparticles in all directions. This initially results in an increase in the nanoparticle concentrations they spread uniformly throughout the fluid. However, heightened thermal diffusion effects, influenced by factors such as thermal radiation and thermophoresis, result in a constrained enhanced Brownian motion. As a consequence, there is a notable reduction in nanoparticle concentration upon reaching a specific height above the wall. The impact of the chemical reaction parameter (Kc) on (ϕ is depicted in Figure 4.24. An inverse relationship appears with an increase in the chemical reaction parameter, which lowers the concentration of nanoparticles. It's crucial to remember that the concentration of nanoparticles behaves erratically at first. In physical terms, the chemical reaction parameter signifies the rate of chemical reactions occurring within the fluid, potentially impacting the behavior of nanoparticles.

Naturally, changes in the concentration profile result from variations in the chemical reaction parameter. The effect of the thermophoresis parameter (Nt) on the concentration distribution (ϕ) is shown in Figure 4.25. With an increase in the value of Nt, there is a subsequent rise in ϕ. Notably, in the initial stages, the concentration of nanoparticles (ϕ) demonstrates a decreasing trend. Physically, thermophoresis involves the movement of nanoparticles in response to temperature variations within the fluid. When the thermophoresis parameter is heightened, nanoparticles exhibit enhanced motion from warmer to cooler regions, resulting in an initial decline in their concentration in specific areas as they migrate towards colder regions. Nevertheless, as the thermophoresis effect intensifies, more nanoparticles accumulate in areas with favorable temperature gradients, increasing the total concentration of nanoparticles (ϕ) in the fluids. The influence of Schmidt number (Sc) on the fluid's nanoparticle concentration distribution is shown in Figure 4.26. Nanoparticle concentration falls with increasing Schmidt number. The Schmidt number (Sc), a dimensionless quantity, is used to express the relative importance of momentum diffusion and mass diffusion in fluid dynamics and mass transfer processes. This initially results in an increase in the nanoparticles concentration. As a consequence, there is a notable reduction in nanoparticles concentration upon reaching a specific height above the wall.

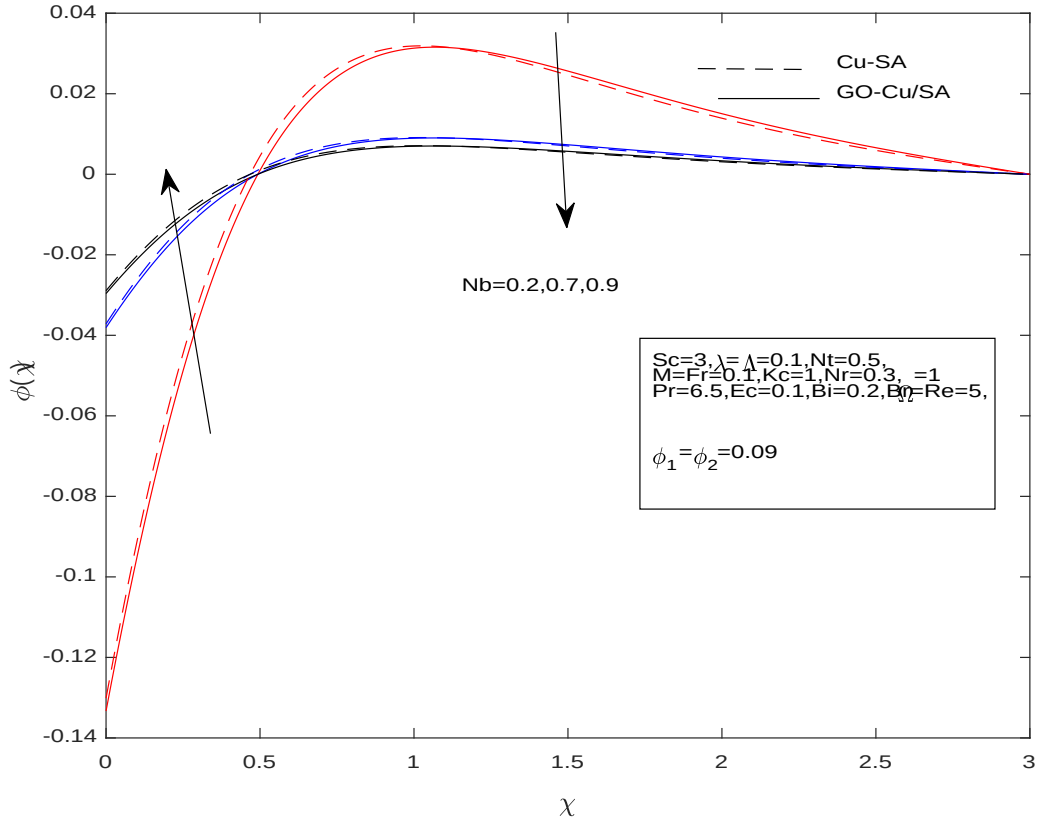

FIGURE 4.23: Impact of Nb on $\phi(\chi)$

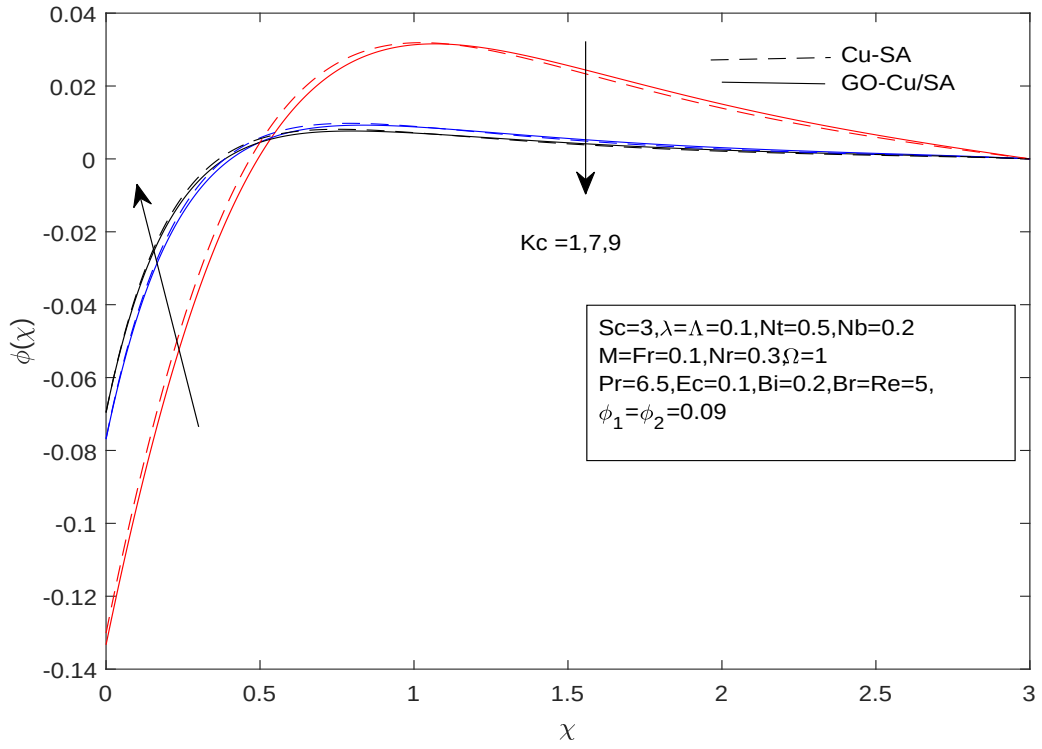

FIGURE 4.24: Impact of Kc on $\phi(\chi)$

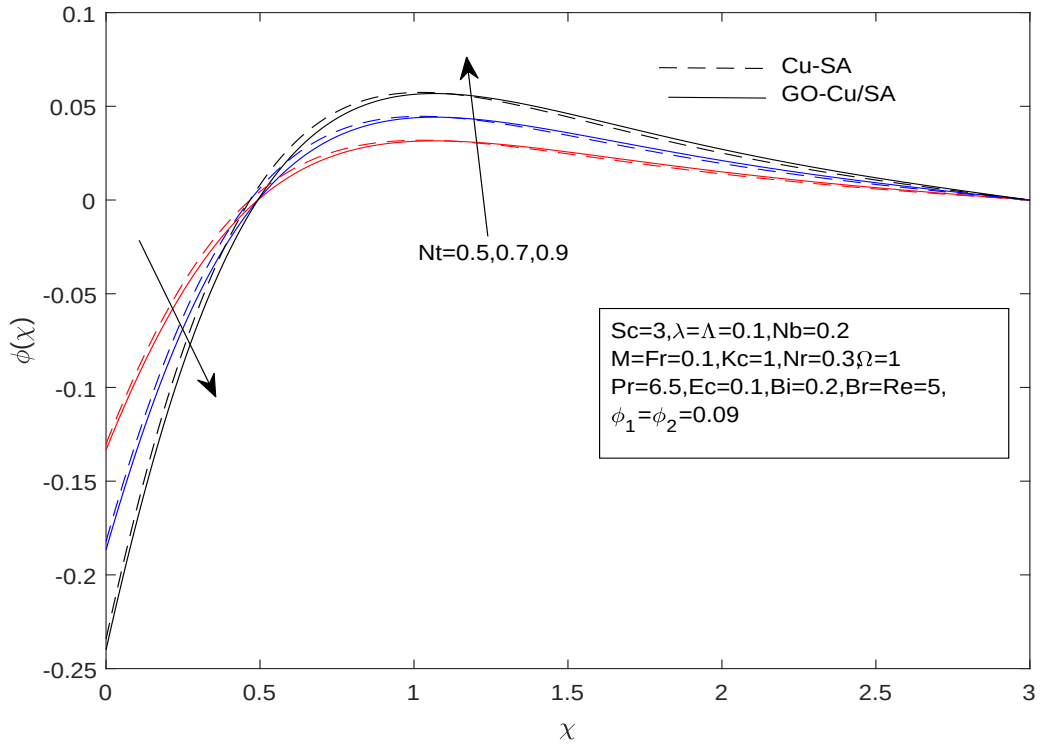

FIGURE 4.25: Impact of Nt on $\phi(\chi)$

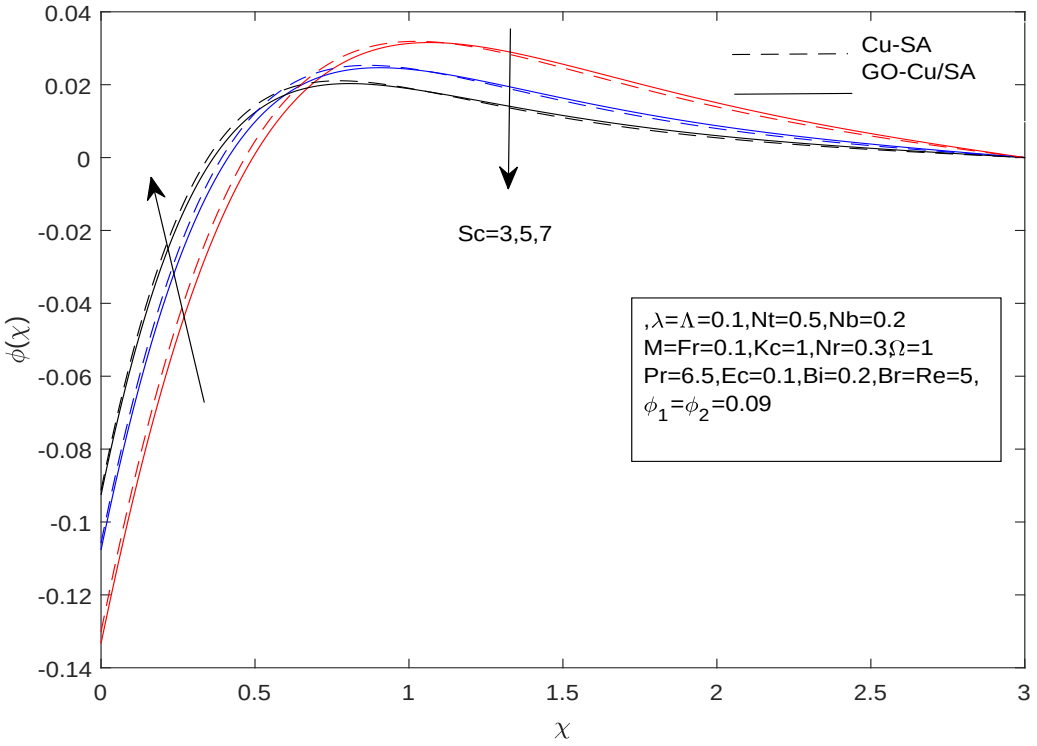

FIGURE 4.26: Impact of Sc on $\phi(\chi)$

Chapter 5

Conclusions

The temperature, velocity, and concentration profiles of nanoparticles in two different fluids—the hybrid nanofluid ($GO-Cu/SA$) and the nanofluid (Cu/SA)—were examined in this thesis in relation to several physical parameters. Williamson fluid model served as the foundation for our investigation. Forchheimer number (Fr), nonlinear thermal radiation parameter (Nr), thermophoresis parameter (Nt), Brownian motion parameter (Nb), chemical reaction parameter (Kc), Schmidt number (Sc), Eckert number (Ec), and magnetic field coefficient (M) were among the parameters that were examined.

- Non-Newtonian Williamson parameter (λ) and Forchheimer number (Fr) inversely affected the fluid velocity, leading to reduced flow rates. Magnetic field parameter (M) caused a decrease in the fluid velocity due to Lorentz force.
- An increment in the Cattaneo-Christov heat flux, Eckert number (Ec), volume fraction (ϕ), and velocity slip (Λ) leads to a decay in the temperature profile.
- For the positive variation in Brinkman number (Br), Reynolds number (Re) and thermal radiation parameter (Nr), entropy generation rises.
- The thermophoresis parameter (Nt) affects the concentration profile and causes the concentration to increase.
- Brownian motion parameter (Nb), chemical reaction parameter (Kc) and Schmidt number (Sc), led to a decrease in the nanoparticle concentration.

Bibliography

[1] Yunus Cengel, John Cimbala, and Robert Turner. *EBOOK: Fundamentals of Thermal-Fluid Sciences (SI units)*. McGraw Hill, 2012.

[2] Bin Xia and Da-Wen Sun. Applications of computational fluid dynamics (cfd) in the food industry: a review. *Computers and Electronics in Agriculture*, 34(1-3):5–24, 2002.

[3] Eric Paul Shipley. *Study of Natural Gas Vehicles (NGV) During the Fast Fill Process*. West Virginia University, 2002.

[4] R Vo Williamson. The flow of pseudoplastic materials. *Industrial & Engineering Chemistry*, 21(11):1108–1111, 1929.

[5] S Shaheen, MB Arain, Kottakkaran Sooppy Nisar, Ashwag Albakri, MD Shamshuddin, and Fouad Othman Mallawi. A case study of heat transmission in a Williamson fluid flow through a ciliated porous channel: A semi-numerical approach. *Case Studies in Thermal Engineering*, 41:102523, 2023.

[6] Sanju Jangid, Ruchika Mehta, and Manoj Kumar Sharma. Williamson fluid flow and heat transfer analysis over a stretched sheet along with Newtonian heating in the existence of thermal radiative, buoyancy, and viscid dissipative impression. 22: 1209–1229, 2023.

[7] Moeen Taj and T Salahuddin. A three dimensional frictional flow study of Williamson fluid with chemical reaction. *Materials Science and Engineering: B*, 291:116305, 2023.

[8] Syed M Hussain. Dynamics of radiative Williamson hybrid nanofluid with entropy generation: significance in solar aircraft. *Scientific Reports*, 12(1):8916, 2022.

[9] Wasim Jamshed, M Prakash, Syed M Hussain, Mohamed R Eid, Kottakkaran Sooppy Nisar, and Taseer Muhammad. Entropy amplified solitary phase relative probe on engine oil based hybrid nanofluid. *Chinese Journal of Physics*, 77:1654–1681, 2022.

[10] Shihao Han, Liancun Zheng, Chunrui Li, and Xinxin Zhang. Coupled flow and heat transfer in viscoelastic fluid with Cattaneo-Christov heat flux model. *Applied Mathematics Letters*, 38:87–93, 2014.

[11] Bagh Ali, Rizwan Ali Naqvi, {Za/Dildar Hussain, Omar M Aldossary, and Sajjad Hussain. Magnetic rotating flow of a hybrid nano-materials hybrid base fluid over an extending surface involving activation energy: FE simulation. *Mathematics*, 8(10): 1730, 2020.

[12] M Subhas Abel, N Mahesha, and Jagadish Tawade. Heat transfer in a liquid film over an unsteady stretching surface with viscous dissipation in presence of external magnetic field. *Applied Mathematical Modelling*, 33(8):3430–3441, 2009.

[13] Muhammad Mubashir Bhatti and Mohammad Mehdi Rashidi. Effects of thermo-diffusion and thermal radiation on Williamson nanofluid over a porous shrinking/stretching sheet. *Journal of Molecular Liquids*, 221:567–573, 2016.

[14] Syed Modassir Hussain, J Jain, GS Seth, and MM Rashidi. Effect of thermal radiation on magneto-nanofluids free convective flow over an accelerated moving ramped temperature plate. *Scientia Iranica*, 25(3):1243–1257, 2018.

[15] SRR Reddy, H Thameem Basha, and Prakash Duraisamy. Entropy generation for peristaltic flow of gold-blood nanofluid driven by electrokinetic force in a microchannel. *The European Physical Journal Special Topics*, 231(11-12):2409–2423, 2022.

[16] Syed M Hussain, Rohit Sharma, Gauri S Seth, and Manas R Mishra. Thermal radiation impact on boundary layer dissipative flow of magneto-nanofluid over an exponentially stretching sheet. *International. Journal. Heat Technol*, 36(4):1163–1173, 2018.

[17] MR Mishra, Syed Modassir Hussain, R Sharma, and GS Seth. Effect of heat absorption on cu-water based magneto-nanofluid over an impulsively moving ramped temperature plate. *Bul. Chem. Commun.*, 50(4):621–630, 2018.

[18] Syed Modassir Hussain, HJ Joshi, and GS Seth. Radiation effect on mhd convective flow of nanofluids over an exponentially accelerated moving ramped temperature plate. In *Applications of Fluid Dynamics: Proceedings of ICAFD 2016*, pages 31–43. Springer, 2018.

[19] Rohit Sharma, Syed Modassir Hussain, and Garima Mishra. Soret and Dufour effects on viscoelastic radiative and heat absorbing nanofluid driven by a stretched sheet with inclined magnetic field. In *Defect and Diffusion Forum*, volume 388, pages 223–245. Trans Tech Publ, 2018.

[20] Syed M Hussain, Rohit Sharma, Manas R Mishra, and Sattam S Alrashidy. Hydromagnetic dissipative and radiative graphene Maxwell nanofluid flow past a stretched sheet-numerical and statistical analysis. *Mathematics*, 8(11):1929, 2020.

[21] R Sharma, Syed Modassir Hussain, CSK Raju, GS Seth, and Ali J Chamkha. Study of graphene Maxwell nanofluid flow past a linearly stretched sheet: A numerical and statistical approach. *Chinese Journal of Physics*, 68:671–683, 2020.

[22] Syed M Hussain, Rohit Sharma, and Sattam S Alrashidy. Numerical study of Casson nanofluid flow past a vertical convectively heated Riga-plate with navier's slip condition. In *AIP Conference Proceedings*, volume 2435. AIP Publishing, 2022.

[23] Aamir Hamid, Masood Khan, and Umair Khan. Thermal radiation effects on Williamson fluid flow due to an expanding/contracting cylinder with nanomaterials: dual solutions. *Physics Letters A*, 382(30):1982–1991, 2018.

[24] H Thameem Basha, R Sivaraj, A Subramanyam Reddy, and AJ Chamkha. SWCNH/diamond-ethylene glycol nanofluid flow over a wedge, plate and stagnation point with induced magnetic field and nonlinear radiation–solar energy application. *The European Physical Journal Special Topics*, 228:2531–2551, 2019.

[25] Sami Ullah Khan, Usman, Kamel Al-Khaled, Syed Modassir Hussain, Abuzar Ghaffari, M Ijaz Khan, and M Waqar Ahmed. Implication of Arrhenius activation energy and temperature-dependent viscosity on non-newtonian nanomaterial bio-convective flow with partial slip. *Arabian Journal for Science and Engineering*, pages 1–12, 2022.

[26] H Thameem Basha and R Sivaraj. Numerical simulation of blood nanofluid flow over three different geometries by means of gyrotactic microorganisms: applications to the flow in a circulatory system. *Proceedings of the Institution of Mechanical Engineers, Part C: Journal of Mechanical Engineering Science*, 235(2):441–460, 2021.

[27] Aimad Koulali, Aissa Abderrahmane, Wasim Jamshed, Syed M Hussain, Kottakkaran Sooppy Nisar, Abdel-Haleem Abdel-Aty, IS Yahia, and Mohamed R Eid. Comparative study on effects of thermal gradient direction on heat exchange between a pure fluid and a nanofluid: employing finite volume method. *Coatings*, 11 (12):1481, 2021.

[28] A Bhattacharyya, R Sharma, SM Hussain, AJ Chamkha, and E Mamatha. A numerical and statistical approach to capture the flow characteristics of Maxwell hybrid nanofluid containing copper and graphene nanoparticles. *Chinese Journal of Physics*, 77:1278–1290, 2022.

[29] Edward J Shaughnessy, Ira M Katz, and James P Schaffer. *Introduction to Fluid Mechanics*, volume 8. Oxford University Press New York, 2005.

[30] RK Bansal. *A Textbook of Fluid Mechanics and Hydraulic Machines:(in SI units)*. LAXMI Publications, Ltd., 2005.

[31] R.K. Bansal. *A Textbook of Fluid Mechanics and Hydraulic Machines*. Laxmi Publications, 2010. ISBN 9788131808153. URL https://books.google.com.pk/books?id=0clZbfwgiyUC.

[32] Sarit K Das, Stephen U Choi, Wenhua Yu, and T Pradeep. *Nanofluids: Science and Technology*. John Wiley & Sons, 2007.

[33] Hafiz Muhammad Ali. *Hybrid Nanofluids for Convection Heat Transfer*. Academic Press, 2020.

[34] Sergei S Molokov, René Moreau, and H Keith Moffatt. *Magnetohydrodynamics: Historical evolution and trends*, volume 80. Springer Science & Business Media, 2007.

[35] SK Som. *Introduction to Heat Transfer*. PHI Learning Pvt. Ltd., 2008.

[36] Junuthula Narasimha Reddy and David K Gartling. *The Finite Element Method in Heat Transfer and Fluid Dynamics*. CRC Press, 2010.

[37] Yunus Cengel and John Cimbala. *Ebook: Fluid Mechanics Fundamentals and Applications (si units)*. McGraw Hill, 2013.

[38] J Kuneš. Thermomechanics. *Dimensionless Physical Quantities in Science and Engineering. Elsevier, Oxford*, pages 173–283, 2012.

[39] Josef Kunes. *Dimensionless Physical Quantities in Science and Engineering*. Elsevier, 2012.